DISSERTATION

SUBMITTED TO THE

COMBINED FACULTIES FOR THE NATURAL SCIENCES AND MATHEMATICS

OF THE RUPERTO-CAROLA-UNIVERSITY OF HEIDELBERG, GERMANY

FOR THE DEGREE OF

DOCTOR OF NATURAL SCIENCES

PUT FORWARD BY

ROSALIND EUGENIE SKELTON

BORN IN: JOHANNESBURG, SOUTH AFRICA

ORAL EXAMINATION: FEBRUARY 25^{th}, 2010

THE EFFECT OF MERGERS ON GALAXY FORMATION AND EVOLUTION

REFEREES: PROF. DR. HANS-WALTER RIX
PROF. DR. ERIC F. BELL

To my granny Pat,
a constant source of inspiration and love

Summary

This thesis explores the effect of galaxy mergers on the evolution of galaxies over the last 8 billion years using the merger trees from a semi-analytic model (SAM) of galaxy formation. The SAM produces reasonable agreement with the distribution of mass, luminosity and colour at low redshifts, as well as the observed merger fractions. I revisit two apparent contradictions between the standard hierarchical model of galaxy formation and observations of early-type galaxies, using the galaxy merger trees as the basis for further modelling. The observed colour–magnitude relation from the Sloan Digital Sky Survey has a change in slope and smaller scatter at the bright end. A simple toy model shows that dry mergers produce similar characteristics. Contrary to previous claims, the small scatter in the observed CMR thus cannot be used to constrain the amount of dry merging. I incorporate stellar population synthesis modelling into this framework to explore the evolution of early-type galaxies since $z = 1$. There is strong evolution in colour and magnitude if no mergers occur after this time. Dry mergers and the recent addition of younger populations onto the red sequence reduce the evolution, mimicking that of an ancient passively-evolving population. Early-type galaxies can therefore appear to have evolved passively even though significant merging activity continues to recent times.

Zusammenfassung

Diese Arbeit untersucht die Auswirkungen des Verschmelzens von Galaxien auf die Evolution der Galaxien in den vergangenen 8 Milliarden Jahren unter Zuhilfenahme von *merger trees* (die baumartige Struktur, die das Verschmelzen innerhalb einer Anzahl Galaxien beschreibt) aus einem halbanalytischen Modell (*semi-analytic model*, SAM) der Galaxienentstehung. Dieses Modell stimmt gut mit der Verteilung von Masse, Leuchtkraft und Farbe bei niedriger Rotverschiebung, so wie auch mit dem beobachteten Anteil an Verschmelzungen, überein. Die *merger trees* werden im folgenden als Basis für weitere Modelle benutzt, um zwei scheinbare Widersprüche zwischen dem hierarchischen Standardmodell der Galaxienenstehung und den Beobachtungen früher Galaxientypen neu zu beleuchten. Die gemessene Farb-Helligkeitsbeziehung aus dem Sloan Digital Sky Survey verändert am hellen Ende ihre Steigung und hat dort eine geringere Streuung. Mit einem einfachen Sandkastenmodell kann ich demonstrieren, dass sogenannte *dry merger* (Verschmelzungen von Galaxien, die kein Gas enthalten) ähnliche Merkmale im Farb-Helligkeitsdiagramm erzeugen. Im Gegensatz zu früheren Behauptungen, kann die beobachtete geringe Streuung des Farb-Helligkeitsdiagramms nicht benutzt werden, um die Zahl der *dry mergers* festzulegen. Um die Entwicklung früher Galaxientypen ab einer Rotverschiebung $z = 1$ zu untersuchen, binde ich Sternpopulationssynthese-Modelle in diesen Rahmen ein. Ohne Verschmelzungen später als $z = 1$ findet man eine starke Entwicklung der Galaxien in Farbe und Leuchtkraft. *Dry mergers* und das kürzliche Hinzufügen jüngerer Populationen zur *red sequence* verlangsamen die Entwicklung, und ahmen so eine sich passiv entwickelnde, ältere Population nach. Frühe Typen können daher erscheinen, als hätten sie sich passiv entwickelt, obwohl Verschmelzen bis in die jüngste Vergangenheit stattgefunden hat.

Abstract

This thesis explores the effect of galaxy mergers on the evolution of galaxies over the last 8 billion years (since $z \sim 1$) using the merger trees from a semi-analytic model (SAM) of galaxy formation. I compare the predictions of the SAM to the distributions of galaxy mass, luminosity and colour in the local Universe and out to $z \sim 1$. The SAM matches the local observations well but there is too little evolution in the mass function compared to observations, indicating that the low mass galaxy population builds up too early. I investigate how the merger fraction and rate vary with redshift for galaxies of different mass and gas content. The fraction of galaxies involved in mergers increases with mass. Gas-poor mergers become increasingly important with decreasing redshift, particularly for high mass galaxies, as the mass on the red sequence builds up. I test the predicted merger fraction against the results of two recent observational studies that use different methods to identify mergers, finding satisfactory agreement. The fraction of recent merger remnants with $M_\star \geq 2.5 \times 10^{10}\mathrm{M}_\odot$ evolves mildly from 3 – 10% from $z = 0.2$ to $z = 1$. Major mergers contribute 1.5 – 4.5% over this period. The fraction of galaxies with $M_\star > 5 \times 10^{10}\mathrm{M}_\odot$ involved in mergers ranges from 2.8 to 3.3% for $0.2 < z < 1.2$.

I revisit two apparent contradictions between the standard hierarchical model of galaxy formation and observations of early-type galaxies. I develop a simple toy model that assumes gas-rich major mergers are effective at quenching star formation and moving galaxies onto the colour–magnitude relation (CMR) of early-type galaxies. Subsequent dry mergers build up mass but do not change galaxy colours. More massive galaxies undergo more dry merging, resulting in a change in slope and decrease in scatter at the bright end of the relation. The amount of dry merging predicted by a hierarchical model results in a CMR that matches well with the observed relation from the Sloan Digital Sky Survey, averaged over all environments. Contrary to previous claims, the small scatter in the observed CMR cannot be used to constrain the amount of dry merging. I incorporate stellar population synthesis modelling into this framework to explore the evolution of early-type galaxies. The observed CMR at $z = 1$ can be reproduced either by the recent formation ($z_f = 2$) and subsequent passive evolution of a galaxy population or by the recent quenching of star formation in galaxies that formed earlier ($z_f = 4$). If no mergers occur after $z = 1$ there is too much evolution in colour and magnitude compared to observations. Dry mergers and the recent addition of younger populations onto the red sequence after $z = 1$ result in bluer colours and a smaller change in magnitude. This slower evolution mimics that of an ancient passively evolving population. Early-type galaxies can therefore appear to have evolved passively even though significant merging activity continues to recent times.

Contents

List of Figures

List of Tables

Chapter 1

Introduction

Humankind has been curious about the nature and origin of our world and the Universe beyond as far back as historical records can show. As with any unchartered territory, the quest to understand the heavens began with mapping what could be seen with the naked eye from earth. This year, internationally recognised as the Year of Astronomy, commemorates the 400th anniversary of the first telescope, which Galileo Galilei used to discover Jupiter's moons and study the moon and stars in more detail than had ever been possible before. This was a giant step forward, enabling us to begin exploring the solar system and outer space and slowly build up an understanding of our place in the Universe. Telescopes have dramatically increased in size over the centuries, improving our light-gathering power. Alongside this we have seen the development of instruments, cameras and computers that enable us to extract, store and analyse the information that arrives in ever-increasing amounts. When we train these telescopes on patches of sky that appear empty to the naked eye, we now see that there are countless distant galaxies beyond our own Milky Way. Observations have become both deeper and wider. We have entered the era of survey Astronomy, scanning the sky systematically to produce all-sky maps of millions of stars within our Galaxy and millions of galaxies beyond. By mapping the sky over the whole electromagnetic spectrum, ranging from the highest energy gamma rays and x-rays, through the visible to the near infrared and radio, we piece together parts of the puzzle of how the Universe and objects within it formed and evolved.

This thesis explores the formation and evolution of galaxies by investigating how galaxy mergers have affected the population. Although Astronomy can be said to be an ancient subject, the study of galaxies is relatively young. Because of the difficulty in establishing distances, galaxies recorded in the first deep sky catalogues – Sir John Herschel's Catalogue of Nebulae (1864) and the New General Catalogue of Nebulae and Clusters of Stars (Dreyer 1888), for example – were not distinguished from nebulous objects within our stellar system. Indeed, galaxies were only recognised as huge collections of stars outside of our own Galaxy, their own so-called "island universes", in the 1920s. Observations of Cepheid variable stars, which have a tight relation between period and luminosity, allowed Hubble (1925) to estimate distances to M31 (Andromeda) and M33. The determination of distances to a number of other galaxies and

the relation to their recession velocities (Hubble 1929; Hubble & Humason 1931) showed that the Universe is expanding , requiring a dramatic change in the cosmological views of the time. The relation between distance and velocity has become known as Hubble's Law. Soon after this, it was noted that many of the nebulae, as galaxies were often still called, seemed to occur in pairs or small groups (Holmberg 1940). In two classic papers, Holmberg explored the clustering of galaxies and its consequences for the cosmological model (Holmberg 1940) and carried out one of the first N-body simulations, making use of the $1/r^2$ dependence of the decrease in the intensity of light with distance to represent the gravitational force (Holmberg 1941). He showed that the tidal forces between interacting stellar systems may lead to loss of orbital energy and possible capture of one system by another. In the first of these papers he speculated a link between interactions and the morphologies of galaxies, a concept that arose again prominently only in the 1970s. A beautiful paper by Toomre & Toomre (1972) entitled "Galactic bridges and tails" demonstrated that many of the unusual galactic configurations, such as the Mice (NGC 4676 or Arp 242) and the Antennae (NGC 4038/9 or Arp 244) (see Fig. 1.1), can be reproduced as the result of a merger between two disk galaxies. Toomre (1977) proposed that elliptical galaxies may be the end result of collisions between disk galaxies, an evolutionary link that has since been confirmed by a number of simulations (e.g., White 1978; Barnes & Hernquist 1996; Cox et al. 2006). There are still many unanswered questions on the transformation of galaxies by mergers. *To what extent do mergers play a role in the quenching of star formation in gas-rich disk galaxies and subsequent build up of the colour–magnitude relation on which spheroidal galaxies lie? How are the most massive ellipticals on this relation formed? How important are mergers for the growth of stellar mass?*

To address these questions, I use a combination of observations from large surveys and semi-analytic modelling techniques. Data on the low redshift galaxy population is from the Sloan Digital Sky Survey (SDSS, York et al. 2000). The final data release (DR7, Abazajian et al. 2009) covers an area of approximately 10 000 square degrees over the Northern sky, resulting in spectroscopic data for almost a million galaxies and photometry for many more. Look-back surveys with the Hubble Space Telescope (HST) such as Galaxy Evolution from Morphology and SEDs (GEMS, Rix et al. 2004), DEEP2 (Davis et al. 2003) and the NOAO Deep Wide-Field Survey are used to study the evolution of the galaxy population out to redshifts of approximately 1. This corresponds to about 8 billion years - more than half of the Universe's history. To investigate how mergers affect the evolution of galaxies I use galaxy merger trees from the Somerville et al. (2008) semi-analytic model (SAM), set in the currently favoured Λ cold dark matter (CDM) cosmology. These are combined with stellar population synthesis models (Bruzual & Charlot 2003) to obtain magnitudes and colours.

I begin by giving an overview of the cosmological background (Section 1.1) and theory of galaxy formation (Section 1.2), including some of the most important observational results showing how the galaxy population has changed with time. A more detailed description of our theoretical understanding, as modelled by SAMs, is given in the introduction to Chapter 2. A

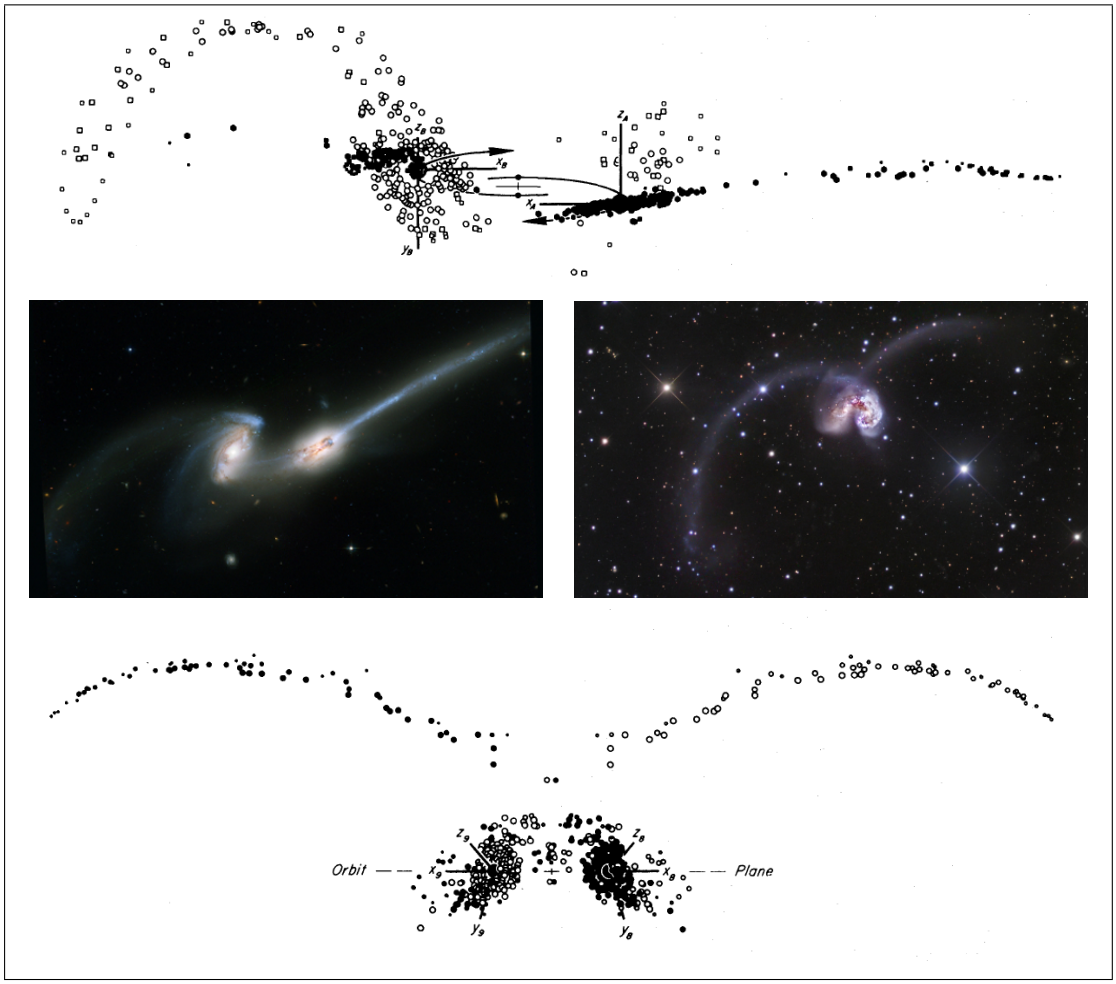

Figure 1.1: Observations and simulations of two merging systems. The central panel shows images from the STSci Archive: The Mice (NGC 4676) photographed with the Advanced Camera for Surveys (ACS) on the Hubble Space Telescope (Credit: NASA, H. Ford (JHU), G. Illingworth (UCSC/LO), M.Clampin (STScI), G. Hartig (STScI), the ACS Science Team, and ESA) are shown on the left, and a ground-based image of The Antennae (NGC 4038/9) is shown on the right (Credit: Robert Gendler). In the top and bottom panels, the simulations of these systems from the Toomre & Toomre (1972) paper are shown. This was the first paper to simulate mergers and demonstrate convincingly that the bridges and tails observed in some systems are tidal features caused by galaxy encounters.

cosmology with $\Omega_M = 0.3$, $\Omega_\Lambda = 0.7$, and $H_0 = 100h$ km s^{-1} Mpc^{-1} with $h = 0.7$ is used throughout this thesis.

1.1 Cosmological paradigm

The theory of General Relativity describing the gravitational force was worked out by Albert Einstein in the early 20th century. This provided the framework upon which modern cosmology could develop. The Einstein field equations link the geometry of the Universe with its matter

and energy content, and solutions to these equations describe the dynamics of model universes. Finding solutions to the field equations is greatly simplified in the case of a homogeneous (the same everywhere) and isotropic (the same in every direction) matter distribution. A set of solutions, now known as the Friedman world models, was determined by Aleksander Friedman in the 1920s (Friedman 1922, 1924) and independently by Georges Lemaître a few years later (Lemaître 1927). These included both static and expanding universes. Einstein's own attempt to find a stable solution lead to him to include the now famous "cosmological constant" as an additional term in the field equations. When the expansion of the Universe was discovered a decade later, he apparently regretted this means of forcing a static solution; however, the cosmological constant has resurfaced as an important parameter in modern cosmological models.

The Robertson-Walker metric given by

$$ds^2 = -c^2dt^2 + a^2(t)\left[\frac{dr^2}{1-kr^2} + r^2(d\theta^2 + sin^2\theta d\phi^2)\right], \tag{1.1}$$

represents the space-time metric for all expanding, isotropic and homogeneous models. $a(t)$ is a time-dependent scale factor and r is a time-independent comoving coordinate. k describes the curvature of the universe and can take the values 0, +1 or -1, representing flat, closed and open universes, respectively. The scale factor is usually normalised to have a value of one at the present time, i.e. $a(t_0) = 1$. In an expanding Universe, the wavelength of light is stretched between emission and observation, with the ratio of wavelengths at the two epochs equal to the ratio of the scale factors. The relative change in wavelength is termed redshift and is thus given by

$$z = \frac{\lambda_o - \lambda_e}{\lambda_e} = \frac{1}{a(t_e)} - 1, \tag{1.2}$$

where the subscripts o and e represent the epochs of observation and emission, respectively. Redshift is thus a measure the scale factor at the epoch when the light was emitted.

The so-called Hubble function is given by $H(a) = \frac{\dot{a}}{a}$. Its value at the present day gives the rate of expansion of the Universe and is known as the Hubble constant, $H_0 = \dot{a}(t_0)$ (the subscript 0 indicates the present day value throughout this work). Hubble's constant is thus the constant[1] of proportionality in Hubble's Law, relating the distances of galaxies to their recession velocities. Hubble's constant has proved very difficult to measure. Although there are many ways of estimating distances to galaxies, with different techniques appropriate for galaxies of different distances, the uncertainties involved are large. A "distance ladder" is built up using local relations to calibrate measurements of galaxies further away. Cepheid variable stars and Type Ia supernovae are two of the most useful distance indicators, because their intrinsic luminosities can be inferred relatively straight-forwardly. Such objects are known as "standard candles". The determination of recession velocities is complicated because local over- and underdensities in the distribution of galaxies cause galaxies to have large peculiar velocities. As

[1] Hubble's constant is not constant with time; neither has it maintained anything like a constant value over the course of its history. Estimates have ranged from values of 50 to more than 500 km s^{-1} Mpc^{-1}.

the distance increases, the recession velocity increases and thus the contribution from peculiar velocities to the total velocity decreases. It is thus important to measure the distances and velocities of galaxies well beyond the range of influence of the Local Supercluster, a large association of nearby galaxy groups and clusters centered on the Virgo cluster, as well as other structures and voids. The best estimate of the Hubble constant is now $H_0 = 72 \pm 8$ km s^{-1} Mpc^{-1} from the HST Key Project, which determined accurate distances to 26 galaxies, with 5 nearby galaxies used for calibration and testing (Freedman et al. 2001). This agrees well with other constraints, such as those from the Wilkinson Microwave Anisotropy Probe (WMAP, see below) combined with Baryon Acoustic Oscillations and Type Ia supernovae measurements, for example ($H_0 = 70.5 \pm 1.3$ km s^{-1} Mpc^{-1}, Komatsu et al. 2009). The uncertainty in H_0 is usually parametrised by including the dimensionless factor $h = H_0/100$ km s^{-1} Mpc^{-1} when quoting values that depend on H_0, such as masses, luminosities and distances.

With the assumptions of isotropy and homogeneity, the field equations can be reduced to a pair of differential equations known as the Friedman equations. These can be combined to form

$$H^2(a) = H_0^2 \left[\frac{\Omega_{m,0}}{a^3} + \frac{\Omega_{r,0}}{a^4} + \Omega_\Lambda + \frac{1 - \Omega_{m,0} - \Omega_{r,0} - \Omega_\Lambda}{a^2} \right]. \tag{1.3}$$

Here the subscripts m, r and Λ denote the contributions to the density parameter Ω_0 from mass, radiation and the vacuum energy density, represented by the cosmological constant, Λ. The density parameter is the ratio of the density of each component to the so-called "critical density", given by $\rho_c = \frac{3H_0^2}{8\pi G}$. The Friedman equation thus describes how the dynamics of the Universe depend on the densities of matter and the vacuum. The relative dependencies of each term on the scale factor show that at early times the Universe was radiation dominated, while it is matter dominated today. The density parameter for matter has contributions from baryonic matter ($\Omega_{b,0}$) in the form of hot gas, cold gas and stellar material, as well as dark matter ($\Omega_{DM,0}$), the nature of which is as yet unknown. From the Friedman equations, the curvature of the Universe, which depends only on the total matter density at the epoch of interest and the deceleration parameter, q_0, giving the present day acceleration of the Universe, can be determined. Current measurements of the deceleration parameter show that the expansion of the Universe is accelerating (Riess et al. 1998; Perlmutter et al. 1999; Riess et al. 2007), rather than slowing down due to the influence of gravity, as expected if the Universe contains only the known forms of matter and radiation (see Frieman et al. 2008, and references therein).

The Big Bang theory is based on the idea that extrapolating an expanding Universe back in time leads to a hotter, denser state. The name arises from following this extrapolation as far as possible - all of space and time burst into existence at a singular point of infinite density - though the singularity itself is beyond the reach of theory. In the early years of cosmology, following the development of Hubble's Law, there was strong competition between this model and the so-called "Steady State" universe, in which matter is continuously created in order to maintain a static universe. In the mid 1960s a strong theoretical argument in favour of the Big Bang model

arose. It was realised that the measured abundances of light elements are too high to have been created only by nuclear processes in stars, and detailed calculations by Hoyle & Tayler (1964) showed that the observed abundance ($\sim 25\%$) is exactly what is expected from primordial nucleosynthesis. Remaining doubts about the Big Bang model were largely resolved in 1965 by Penzias & Wilson's serendipitous discovery of the Cosmic Microwave Background (CMB) radiation, a relic from the Universe's early hot phase. When the Universe was approximately 1000^{th} of its current size, the temperature was about 4000 K, sufficiently high that all the hydrogen was ionised. Photons were strongly coupled to the ionised gas through Thomson scattering, but as the Universe expanded, the temperature dropped and protons and electrons were able to combine to form neutral hydrogen. This is known as the era of recombination. Thereafter photons were able to stream freely, and thus it is an imprint of this "surface of last scattering" that we see as the CMB today. The expansion of the Universe causes a stretching of the photons to microwave frequencies. The CMB, with a mean temperature of $\sim 2.73K$, has been shown to be perfectly black-body in nature (Mather et al. 1990; Fixsen et al. 1996) and remarkably uniform over the whole sky (Bennett et al. 1996). The large-scale uniformity of the CMB strongly supports the assumptions of homogeneity and isotropy required by the standard models.

The distribution of galaxies is also remarkably uniform on very large-scales. The distribution on smaller scales is far from uniform, however, with groups and clusters of galaxies in turn grouping together to form superclusters arranged in filamentary and wall-like structures. Sheets of galaxies surround voids that contain very little matter, so that the overall impression is that the galaxy distribution is sponge-like (e.g., Geller & Huchra 1989; Gott et al. 1986, and see Fig. 1.2). To proceed from a homogenous model for the early universe to the structured distribution of matter we see today, the background model must be perturbed by small fluctuations in density. These perturbations are thought to arise from quantum fluctuations in the early Universe and grow under the influence of gravity during a period of rapid inflation. When the gravitational force exceeds the outward pressure they collapse to form bound virialized structures. This picture of structure growth was strongly confirmed by the detection of temperature perturbations of the order of 10^{-5}K in the CMB by the Cosmic Background Explorer (COBE) satellite (Smoot et al. 1992). More recently, the WMAP satellite mapped the CMB over the whole sky with 13 arcminute resolution, enabling the power spectrum of fluctuations to be determined to unprecedented accuracy over a wide range of scales (Fig. 1.2). Such detailed observations have made it possible to pin down the parameters of the cosmological model to very high accuracy, firmly establishing the standard cosmological paradigm in which current galaxy formation models are embedded.

The most recent results from the CMB (WMAP5, Komatsu et al. 2009) as well as the HST Key Project, supernovae Type Ia (see for e.g., Astier et al. 2006; Riess et al. 2007) and Baryon Acoustic Oscillation (Eisenstein et al. 2005; Percival et al. 2007) observations have considerably narrowed the parameter space in which our Universe could lie. The favoured model estimates the matter content of the Universe to be 74% dark energy, 23% dark matter and 3%

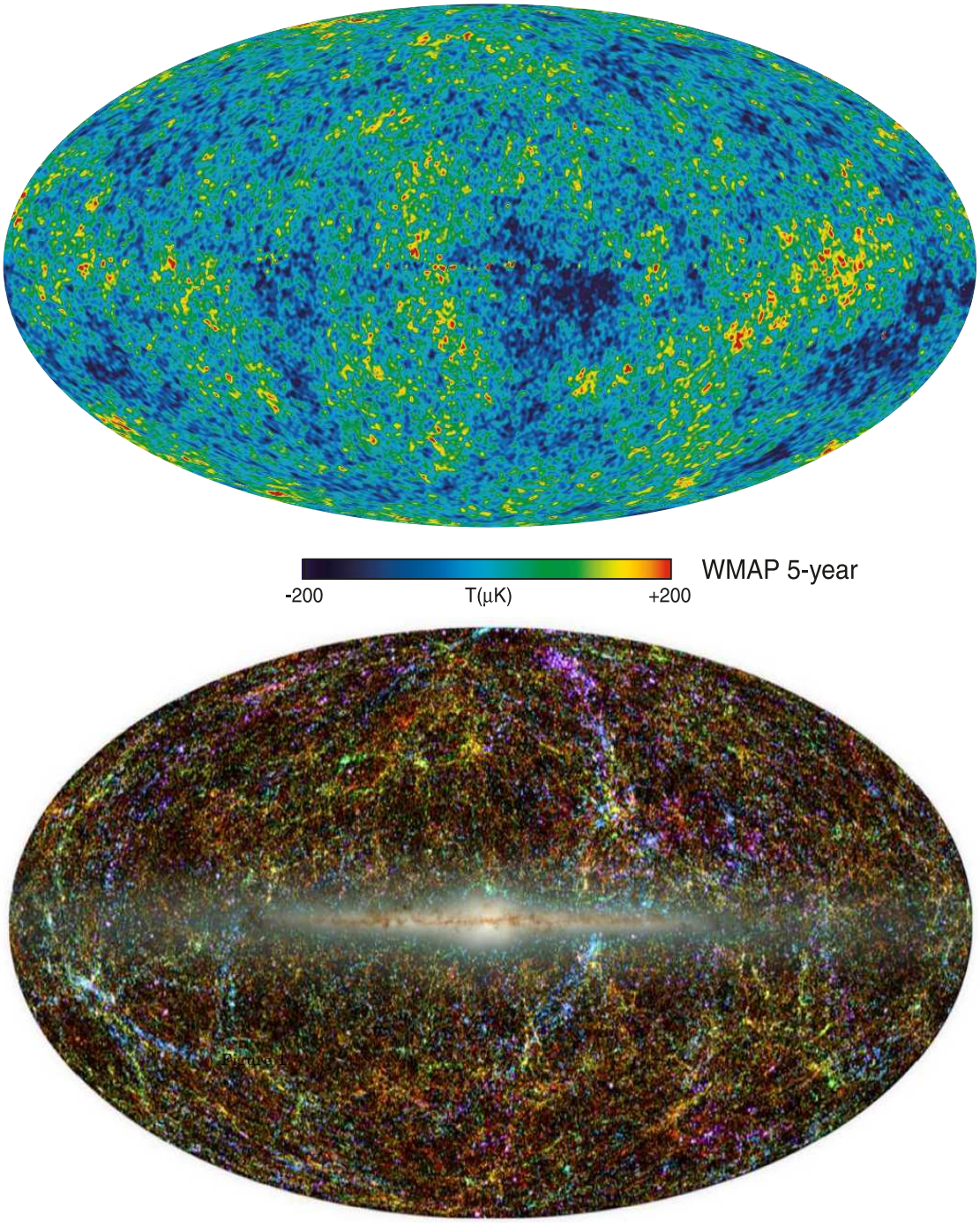

Figure 1.2: All-sky maps showing the structure in the microwave background and large-scale galaxy distribution. The top panel shows temperature perturbations in the CMB from the 5^{th} year WMAP data release (Credit: NASA / WMAP Science Team). Note that in this image the foreground emission from the Milky Way has been subtracted. The distribution of galaxies in the near infrared, from the Two Micron All Sky Survey (2MASS Jarrett 2004), is shown in the bottom panel. Galaxies are colour-coded by their redshifts, with blue representing the nearest sources ($z < 0.01$), green intermediate distances ($0.01 < z < 0.04$) and red the highest redshift galaxies resolved by 2MASS ($0.04 < z < 0.1$).

baryonic matter. The Universe is thus remarkably flat, with $\Omega_{b,0}+\Omega_{DM,0}+\Omega_{\Lambda,0} = 0.99 \pm 0.01$ (Komatsu et al. 2009). The nature of dark energy and dark matter are still unknown, however. The upper limit of the density of baryons from primordial nucleosynthesis arguments is low, requiring a different form of "unseen" matter to fit the observations. Further evidence for dark matter comes from dynamical measurements of the masses of galaxies and galaxy clusters, using rotation curves for spiral galaxies and the virial theorem to calculate the mass from velocity dispersions for ellipticals and rich nearby clusters such as Coma (Merritt 1987), for example. There is generally good agreement between such kinematic mass estimates and masses determined from the X-ray emission of gas or from strong lensing in clusters. A form of dark matter that was non-relativistic at the time of decoupling, so-called "cold" dark matter (CDM), is currently preferred.

Despite the success of this model at matching the observations, there are a number of unknowns, some of which can be resolved by invoking a period of exponential expansion in the early Universe. In this phase, known as inflation, small regions expanded very rapidly, moving nearby particles far apart. Regions which would otherwise not be causally connected thus started out close together, creating the required initial conditions for isotropy on large scales. In addition, inflation solves the flatness problem: $\Omega = 1$ is an unstable equilibrium point, thus any deviation from an initial value of 1 would cause it to change very quickly, making it impossible to have a value close to this to the present day.

Advances in cosmology over the past few decades have thus led to the adoption of a "concordance" cosmology with strong observational backing. This can be summarised as a ΛCDM model, with the cosmological constant or dark energy and cold dark matter the dominant components. The establishment of this standard model has enabled the study galaxy formation to proceed on a firm foundation, giving us much greater confidence in quantities such as distances, upon which estimates of intrinsic galaxy properties such absolute magnitudes rely.

1.2 Galaxy formation and evolution

In the cold dark matter scenario, the low level density fluctuations imprinted on the dark matter distribution of the early Universe are thought to have grown with time as the attractive gravitational force caused more and more matter to accumulate in slightly overdense regions. Gas pressure prevents the baryons from clumping at this stage. After the era of recombination, baryonic matter is no longer coupled to radiation and also begins to fall into the gravitational potential wells generated by the dark matter. Where the inward gravitational force becomes greater than the outward gas pressure, stability can no longer be maintained and the matter collapses to form bound structures. The condition for stability, known as the Jeans Stability Criterion, determines when objects form. This applies to both dark matter and baryonic matter and is therefore important for the formation of dark matter halos as well as stars. The smallest structures collapse first and grow through a process of hierarchical merging. The densest regions in the primordial

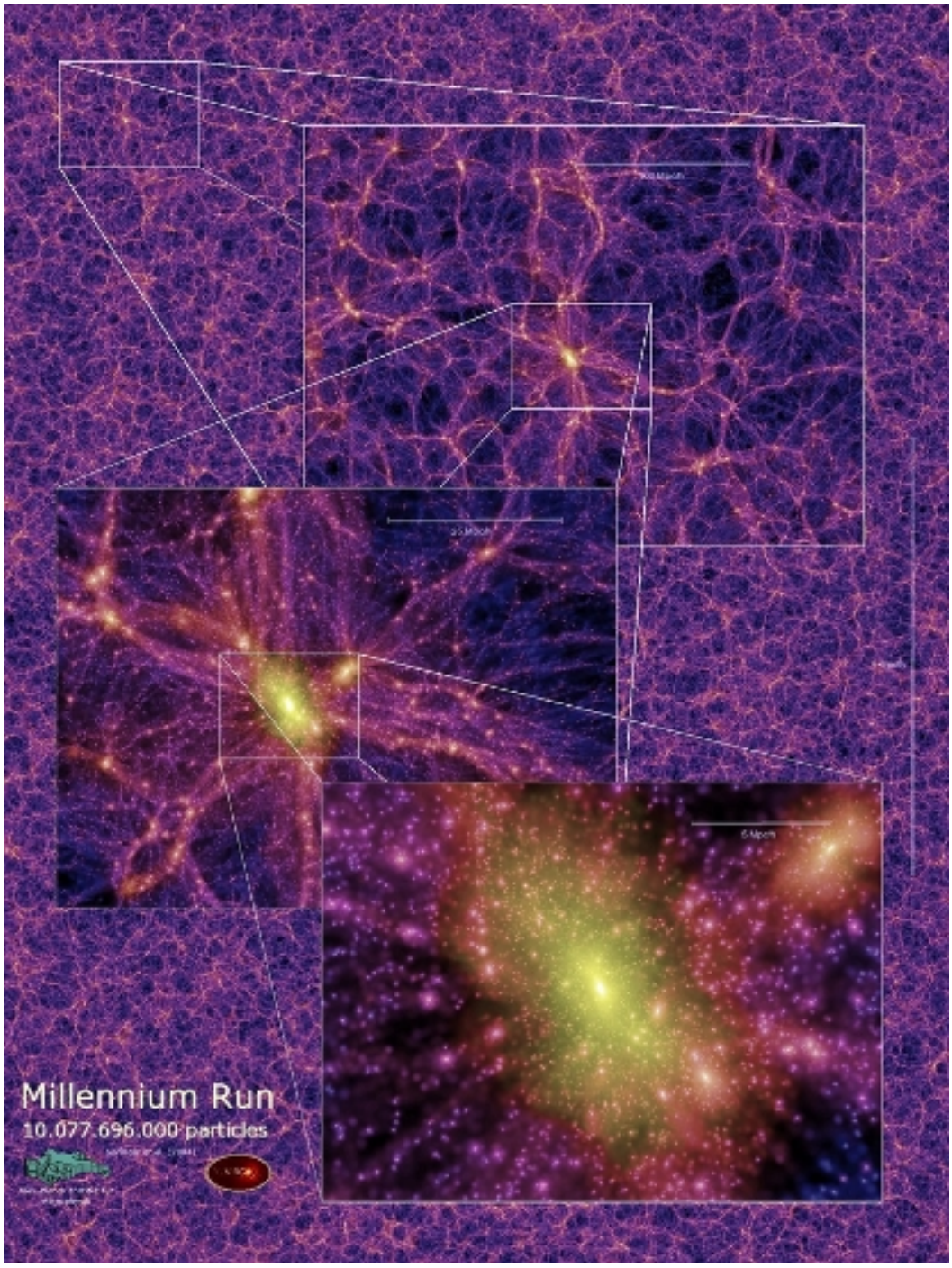

Figure 1.3: The $z = 0$ density distribution of dark matter within a 15 h^{-1} Mpc slice from the Millenium Run simulation (Springel et al. 2005b), illustrating the filamentary nature of structures produced in a ΛCDM hierarchical universe and large amount of substructure. Each overlaid panel zooms in by a factor of 4 to reveal a cluster formed at the intersection of many filaments.

matter distribution grow into the largest structures we see in the Universe today - clusters and superclusters.

The growth of the initial perturbations can be calculated analytically, however once the process becomes non-linear, numerical simulations are required to follow the build-up of structures. Cold dark matter particles are only affected by the gravitational force, making it possible to simulate the formation of CDM structures relatively straight-forwardly. The increase in computational power in recent years has provided the means to run cosmological simulations for large volumes with ever-increasing resolution. Figure 1.3 shows the dark matter "cosmic web" at $z = 0$ from the Millenium Run simulation (Springel et al. 2005b), which used 10 billion particles in a cube of 500 h^{-1} Mpc per side. Although numerical simulations are required to determine the spatial distribution of the dark matter structures, the mass distribution can be approximated analytically (see Chapter 2).

Within the bound dark matter structures, known as halos, galaxies form as the gas begins to cool and settle into exponential disks where star formation can occur. The resultant galaxies are made up of large amounts of gas, stars and dust, and contain approximately 50 times more dark matter than baryonic matter (Heymans et al. 2006). Bulges are thought to form later via disk instabilities or through the randomization of stellar orbits during galaxy mergers. The galaxy formation process appears to be inefficient in both the smallest and most massive halos, resulting in differently shaped mass distributions for galaxies and their dark matter hosts. The discrepancy between the mass functions of dark matter and galaxies is shown in Fig. 1.4, from Moster et al. (2009). Stars form with greatest efficiency in halos with masses of approximately $10^{12}\mathrm{M}_{\odot}$, corresponding to a galaxy mass of $\sim 3 \times 10^{10}\mathrm{M}_{\odot}$. The reason for this preferred mass scale is not yet well understood.

It is thought that star formation in small halos (with circular velocities $v_c \lesssim 50$ km s^{-1}) is suppressed by a background of photoionizing UV radiation (e.g., Efstathiou 1992, Thoul & Weinberg 1996, Somerville 2002) or supernovae feedback (Macciò et al. 2009). In intermediate mass halos ($50 \lesssim v_c \lesssim 130$ km s^{-1}) feedback processes that expel gas from the galaxy and prevent further star formation are dominant. The currently preferred mechanism for suppressing gas cooling in the most massive galaxies ($v_c \gtrsim 130$ km s^{-1}) involves the release of energy from the central supermassive black hole (SMBH) of active galactic nuclei (AGN), to remove material from the surroundings (so-called "AGN feedback", see, e.g., Springel et al. 2005a; Schawinski et al. 2006; Somerville et al. 2008, and references therein). This is modelled in two variations - the "bright mode", where high accretion rates power quasar activity for short periods, after a merger for example, and the "radio mode", with low accretion rates producing strong radio jets in the more commonly observed radio-loud galaxies. The latter prevents star formation from recurring over longer periods, keeping the galaxy "red and dead". All spheroidal galaxies are thought to contain SMBHs at their centres, although the period for which they are active may only be a short fraction of the galaxy's lifetime. The strong correlation between the mass of the black hole and the mass of the stellar spheroid (e.g., Kormendy & Richstone

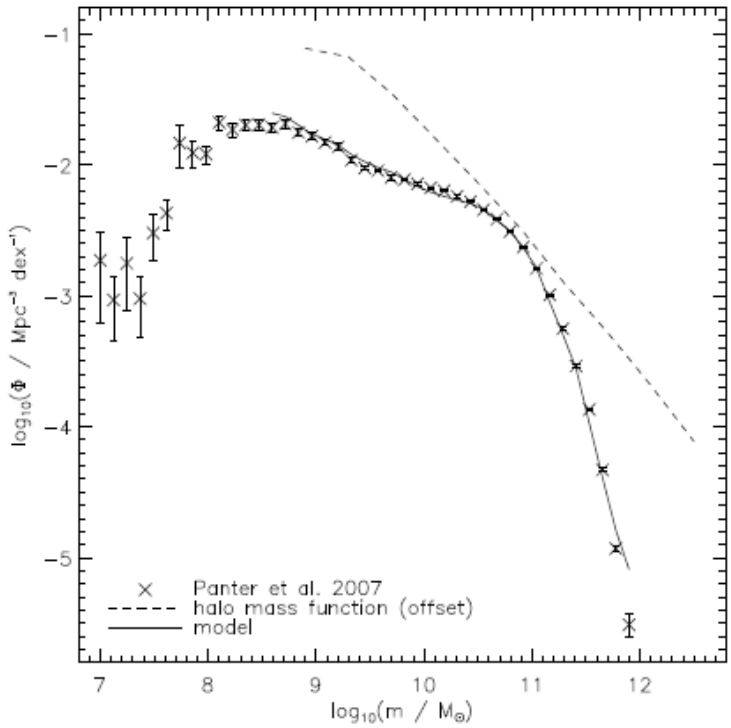

Figure 1.4: A comparison of the dark matter halo mass function with the stellar mass function from Moster et al. (2009). The data points represent the observed stellar mass function from the SDSS 3rd data release (Panter et al. 2007). The dashed line is the halo mass function multiplied by a constant stellar to halo mass ratio of 0.05. This indicates the under-efficiency of galaxy formation at the high and low mass ends. The solid line shows a 4-parameter model for a stellar to halo mass ratio that varies as a function of mass.

1995; Marconi & Hunt 2003; Häring & Rix 2004) suggests an evolutionary link between the formation of galaxies and the black holes at their cores.

Galaxies are found in a bimodal distribution in colour–magnitude space (see Fig. 2.3), with the two populations of galaxies having very different properties (e.g., Strateva et al. 2001; Baldry et al. 2004). Disk-like, star-forming galaxies form a broad distribution known as the blue cloud. They have large amounts of gas available to fuel further star formation, and are blue in colour as much of their light is contributed by massive, young O- and B-stars. The second population of galaxies forms a tight colour–magnitude relation (CMR) known as the red sequence. Most of the galaxies on the red sequence are early-type galaxies with spheroidal morphologies and low or negligible levels of star formation. With no new star formation, their colours can be accounted for by the substantial reddening of stellar populations that evolve off the main sequence. The brightest or most massive galaxies on the red sequence have redder colours than fainter galaxies. This relation between colour and luminosity arises primarily from a correlation between mass and metallicity, with more massive galaxies having higher metal content (Kodama & Arimoto 1997; Gallazzi et al. 2006), possibly due to their ability to retain

metals more easily within their deeper potential wells. There may also be a contribution from age, as older populations also have redder colours. The larger scatter at lower masses is caused mainly by spread in age, but scatter in metallicity also contributes to the width of the relation (Gallazzi et al. 2006).

The colour bimodality persists out to redshifts greater than one (e.g., Bell et al. 2004). With the advent of large look-back surveys in the last decade, appreciable numbers of galaxies have been observed out to high redshifts, allowing the distribution of galaxy luminosities and colours to be mapped out as a function of time. By splitting the luminosity function from the Combo-17 survey into contributions from galaxies on the red sequence and blue cloud, Bell et al. (2004) showed that the mass of galaxies on the red sequence has approximately doubled over the last 8 billion years, while the mass of galaxies in the blue cloud has remained approximately constant over the same period. This has since been confirmed by other studies (e.g., Faber et al. 2007, using the DEEP2 survey, and Brown et al. 2007 using the NOAO Deep Wide-Field Survey). These results apply to galaxies near the knee of the luminosity function ($\sim L^*$) where the number densities can be reliably measured. The evolution of the brightest galaxies is still uncertain, and is the subject of Chapter 5 of this thesis. The star formation occuring in blue cloud galaxies since $z \sim 1$ can account for the increase in total mass, however this mass must be transferred from the blue cloud onto the red sequence in order to produce the observed distributions at low redshift (Bell et al. 2004, 2007).

A number of different transformation mechanisms operating at different mass scales and in different environments have been proposed. Very few galaxies occupy the so-called "green valley" between the red sequence and the blue cloud, suggesting that the transition is relatively rapid. Mergers of galaxies are a promising means of converting the morphologies of disk galaxies into those of spheroids on the red sequence. This has been convincingly demonstrated by numerical simulations (e.g., Barnes & Hernquist 1996; Cox et al. 2006). Reddening of the stellar populations follows if mergers are accompanied by a burst of star formation or feedback from an AGN. In addition to mergers, the reddening of galaxies may be caused by a number of other "environmental" effects (as opposed to the secular evolution of a galaxy in isolation). Galaxies may pass closely enough to affect each other tidally, without capture occuring. Mergers and tidal interactions are most likely to occur in isolated to group-sized halos ($M_{\rm halo} \sim 10^{13}$) where the velocity dispersions are relatively low (e.g., McIntosh et al. 2008). In denser cluster environments, galaxies have high velocity dispersions and are thus unlikely to merge, although accretions of satellites onto the central galaxy are thought to play an important role in building up the mass of brightest cluster galaxies (BCGs, e.g., Bernardi et al. 2007). Tidal disruption of satellites also contributes to the intracluster light, which can amount to $\sim 10\%$ of the total cluster luminosity within 500 kpc (Zibetti et al. 2005). Ram-pressure stripping of gas, and the resulting strangulation are likely to play a strong role in reddening satellite galaxies as they enter the cluster environment (e.g., Gunn & Gott 1972; Bekki 2009).

Gas-rich mergers are thought to be the main mode of growth for the red sequence at $\sim L^*$.

The most massive galaxies on the red sequence are unlikely to have formed in the same way, nor can they form directly from the fading of blue galaxies, as there are too few very massive disks observed at any redshift. In the hierarchical picture of galaxy formation, "dry" or gas-poor mergers are a natural mechanism for building up the mass of bright red sequence galaxies. Dissipationless mergers have been shown to result in boxy isophotes (Naab et al. 1999; Naab & Burkert 2003) and maintain the fundamental plane (Nipoti et al. 2003; Ciotti et al. 2007), though the properties of merger remnants depend sensitively on mass ratio as well as gas fraction. The variation of the properties of early-type galaxies with mass may be a consequence of the increasing role of dry mergers toward the massive end of the red sequence. Most intermediate mass early-types have disky isophotes and are rotationally dominated, while at high masses, galaxies tend to be rounder (van der Wel et al. 2009), have boxy isophotal shapes and less rotational support. These properties are also correlated with nuclear activity, black hole mass and inner luminosity profile (see, e.g., Kormendy et al. 2009; Pasquali et al. 2007, and references therein). Dry mergers have been observed in the local Universe (van Dokkum 2005; Tal et al. 2009) and out to higher redshifts (Bell et al. 2006a) but the merger rate for massive gas-poor galaxies has not be pinned down sufficiently to determine the rate of growth from mergers.

The degree to which massive early-types form hierarchically has been a contentious issue in the literature. The uniformity of early-type galaxy colours and the small scatter in the colour–magnitude relation of clusters were argued to show that the stars in these galaxies formed at high redshifts, with the growth from dry mergers after the colour–magnitude relation was put in place limited to a factor of 2–3 (Bower et al. 1998). The colours and magnitudes of early-type galaxies have evolved little over the last half of the Universe's history, consistent with the passive evolution of stellar populations that formed at high redshift (e.g., Tinsley 1968; Ellis et al. 1997; Wake et al. 2006; Cool et al. 2008). The lack of evolution at the bright end of the luminosity function has also been used as an argument against recent growth from mergers, despite the strong evidence that we live in a hierarchical universe (see for e.g., Cimatti et al. 2006; Cool et al. 2008). I will address these two arguments against the growth of massive red sequence galaxies through mergers in this thesis.

Many of the processes that influence galaxy evolution described above are included in semi-analytic models (SAMs) of galaxy formation. SAMs ambitiously attempt to model all the baryonic physics of galaxy formation within the dark matter framework, with varying success. They are useful for building intuition and examining particular aspects of galaxy evolution, although it is difficult for models to reproduce the extensive array of observed galaxy properties simultaneously. In this thesis, I use the Somerville et al. (2008) SAM as the basis for exploration into the effects of mergers on galaxy evolution, concentrating on the role gas-poor mergers play in early-type galaxy evolution. I elaborate on the theory of galaxy formation as implemented by SAMs, and compare the galaxy distribution predicted by the model to the observed distributions of mass, luminosity and colour in Chapter 2. I show that the SAM reproduces the mass and luminosity function at low redshift, as well as a bimodal colour–magnitude distribution, but

the evolution of key quantities, such as the mass function, does not match the observations. In Chapter 3 I examine the merger histories of galaxies and compare to the observed merger fraction measured with two different methods. The qualitative agreement between the model and observations suggests that the model merger trees are a fairly robust prediction of the model. To disentangle the effects of merging from the complexity of other processes modelled by the SAM, I create a simple toy model based on the SAM merger trees in Chapter 4. I use this model to test how dry mergers affect the red sequence. I find that the red sequence predicted by a hierarchical merging model has characteristics that match well with observations. In Chapter 5 I expand this model using stellar population synthesis models to explore the evolution of the red sequence population. I show that the slow evolution of early-type galaxy colours and luminosities over the last half of Cosmic history may result from hierarchical growth, rather than being supportive of a purely passive history.

Chapter 2

Galaxy Evolution in Semi-Analytic Models

2.1 Introduction

Over the last two decades, semi-analytic models (SAMs) have provided an important means of exploring the details of galaxy formation on a cosmological scale without the massive computational resources required for particle-based simulations. In general, they are based on the dark matter merger histories produced by N-body simulations or determined analytically using the extended Press-Schechter (EPS) formalism, as described below. Baryonic structures are assumed to develop within the potential wells created by the gravitationally dominant dark matter. Simple recipes are used to follow the conversion of cold gas into stars, enrichment of the interstellar medium, feedback of gas into the halo and intergalactic medium as stars reach the end of their lives, merging of small subunits into more massive systems and so on (see, e.g., Lacey & Cole 1993; Kauffmann et al. 1993; Baugh 2006; Bower et al. 2006; Croton et al. 2006; Somerville et al. 2008). At any epoch the galaxies' properties are determined using stellar population synthesis models to convert the mass in different components to flux, and account for the dust content

Although SAMs have been successful at matching some of the observations of galaxy properties, particularly at low redshift, this has not been without considerable effort. The models are often unable to produce a distribution of galaxies that agrees well with the observed distribution at more than one epoch, having been tuned to match a particular set of observations. They are useful for exploring specific questions on the galaxy formation process within a cosmological context (the spirit of the models in Chapters 4 and 5) but, due to the simplicity of the recipes used and the limitations of our understanding on the processes that can be included, they should not be expected to meet all observational constraints simultaneously.

In this thesis, I use the output of the Somerville et al. (2008, S08 hereafter) SAM, kindly provided to me by Rachel Somerville, to build understanding on how mergers affect the forma-

tion and evolution of galaxies. Detailed descriptions of the model can be found in Somerville & Primack (1999), Somerville et al. (2001) and S08. These papers examine particular aspects of galaxy formation, such as the properties of high-z Lyman break galaxies and AGN feedback processes, and show the general results of the model as a motivation of its usefulness. I will apply a similar approach, describing results of the model that have not been presented elsewhere, and comparing the model output to observations. The agreement between the observed and model merger fractions (Chapter 3) gives us confidence that the model merger trees can be used as the basis for further modelling in Chapters 4 and 5.

Overview of this chapter

In Section 2.2, I describe how galaxy formation and evolution is modelled in the SAM framework, focusing on the S08 implementation. This illustrates the complexity of baryonic processes included in the model. Some of these ingredients, particularly those related to mergers, will influence the modelling in later chapters. Section 2.3 compares the properties of the model galaxy population with results from look-back surveys, highlighting areas where the SAM is successful and others where the match can be improved. I examine the luminosity function and mass function (Section 2.3.1) as well as the colour–magnitude diagram (Section 2.3.1) of SAM galaxies in some detail, as these are the tools used to examine the evolution of galaxies in Chapters 4 and 5. Although I was not involved in the development of the model, I present here my own analysis of the results and comparisons to observations.

2.2 Description of the model

SAMs are built upon dark matter (DM) halo merger histories. In the S08 model, an analytic method is used to determine the evolution of the dark matter halos, rather than extracting the histories directly from an N-body simulation. The number of DM halos as a function of mass at any output redshift is determined using the Sheth & Tormen (1999) model, a modification of the Press-Schechter formula (Press & Schechter 1974). The Press-Schechter model describes the mass function of bound structures that have grown from an initial Gaussian random field in a hierarchical universe. It was extended to provide the conditional mass function - the probability that a particle in a halo of mass M_0 at redshift z_0 was in a progenitor of mass M_1 at an earlier redshift z_1 (Bond et al. 1991; Bower 1991). Realizations of the dark matter merger histories are constructed with a Monte-Carlo method that uses the extended Press-Schechter formalism (see, e.g., Kauffmann & White 1993; Lacey & Cole 1993; Somerville & Kolatt 1999). The method developed in Somerville & Kolatt (1999), modified slightly to agree better with simulations, is used in S08. In Fig. 2.1 I show a schematic representation of a dark matter halo's merger history from Lacey & Cole (1993). This illustrates the process of hierarchical growth, with time progressing from top to bottom and the size of the branches representing the amount of mass in each halo that merges to form the final dark matter halo at t_0.

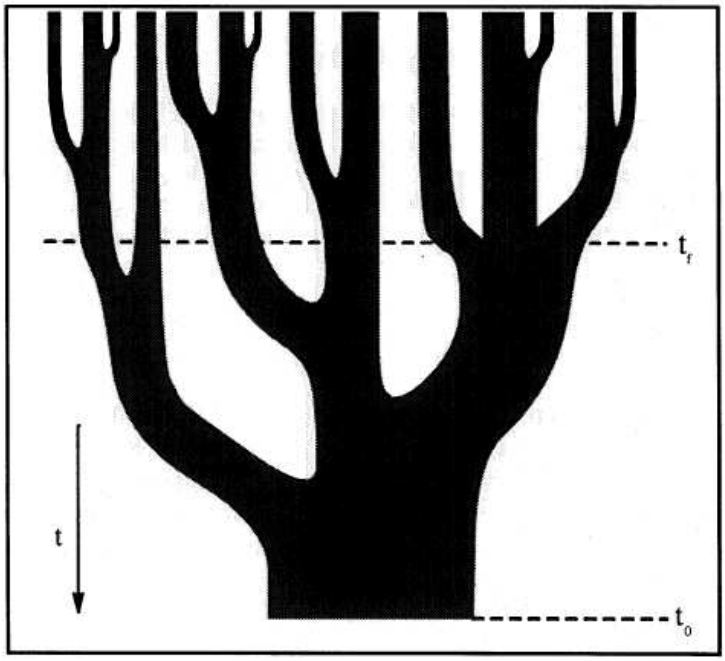

Figure 2.1: A schematic representation of a dark matter merger tree from Lacey & Cole (1993). The final dark matter halo at t_0 grows through the merging of smaller halos, with half the mass of the final halo in the largest progenitor at the formation time, t_f.

Each dark matter halo in the merger tree is assigned an angular momentum and a concentration. The dimensionless spin parameter, $\lambda = J_h|E_h|^{1/2}G^{-1}M_{\rm vir}^{-5/2}$ (Peebles 1969), where E_h is the energy of the halo and $M_{\rm vir}$ its virial mass, is used to represent the angular momentum. As halos merge, the spin parameter of the largest progenitor is passed onto the new parent halo. Halos are assumed to have Navarro-Frenk-White (NFW, Navarro et al. 1997) density profiles initially, with the concentration paramter $c_{\rm NFW}$ determined from a fitting formula based on numerical simulations (Bullock et al. 2001). The NFW profile is given by

$$\frac{\rho}{\rho_c} = \frac{\delta_c}{r/r_s(1+r/r_s)^2}, \tag{2.1}$$

where ρ_c is the critical cosmological density, δ_c is a dimensionless characteristic density, $r_{\rm vir}$ is the virial radius and r_s is a scale radius, defined as $r_s \equiv r_{\rm vir}/c_{\rm NFW}$. The scale radius is used to determine when a satellite is tidally destroyed, as well as setting the core radius within which the mass ratio during a merger is defined (see below).

The evolution of galaxies is modelled within this dark matter framework. In the traditional picture, gravitational pressure causes gas to collapse inwards until it reaches the virial radius, where it is shock heated, forming a hot halo of gas around a cooling core.[1] The gas has a density

[1] An alternative view that is gaining popularity proposes that cold gas flows inwards along filaments, forming stars in clumpy structures along the length of the filament. These eventually merge to form a galaxy at the core (Dekel et al. 2009). This has not yet been implemented in SAMs directly, although when the cooling time is less

profile given by that of a singular isothermal sphere, $\rho_g(r) = m_{\rm hot}/4\pi r_{\rm vir} r^2$. The rate at which the gas cools is given by

$$\frac{dm_{\rm cool}}{dt} = \frac{1}{2} m_{\rm hot} \frac{r_{\rm cool}}{r_{\rm vir}} \frac{1}{t_{\rm cool}}. \tag{2.2}$$

where the cooling time is chosen to be the dynamical timescale of the halo at the virial radius, $\tau_{\rm dyn}$. This is related to the circular velocity of the halo, $V_c(r_{\rm vir})$, by

$$\tau_{\rm dyn} \equiv \frac{r_{\rm vir}}{V_c(r_{\rm vir})} = \left(\frac{r_{\rm vir}^3}{G M_{\rm host}} \right)^{1/2}. \tag{2.3}$$

The cold gas accretes onto the central galaxy and is assumed to settle into a thin exponential disk, with the angular momentum assigned to the halo used to determine the radius of the disk.

Stars form within the region where the gas density is higher than a given threshold at the rate given by the Schmidt-Kennicutt law, with a Chabrier initial mass function (IMF). The Schmidt-Kennicutt law is an empirical relationship between the surface density of gas and the star formation rate: $\Sigma_{\rm SFR} = A \Sigma_{\rm gas}^{N_K}$, where A is an adjustable parameter in the model, with a fiducial value of 1.67×10^{-4}, $N_K = 1.4$, $\Sigma_{\rm gas}$ is the cold gas surface density in the disk (in units of $\mathrm{M_\odot pc^{-2}}$) and $\Sigma_{\rm SFR}$ is the star formation rate density per unit area (in units of $\mathrm{M_\odot yr^{-1} kpc^{-2}}$). The Chabrier IMF has a power-law slope of -1.3 between $1\mathrm{M_\odot}$ and $100\mathrm{M_\odot}$ and a log-normal distribution below this mass, centered on $0.08\mathrm{M_\odot}$ with a width of 0.69 (Chabrier 2003). As stars are formed, the metallicity of the cold gas available to form new stars is instantaneously increased, with the assumption that massive, short-lived stars rapidly inject enriched material into the interstellar medium. Subsequent stellar populations thus have higher metallicity. Winds from supernovae drive gas out of the galaxy into the hot gas halo or intergalactic medium beyond, with the allowance that it can settle back into the halo some time later and thereafter cool onto the disk once again.

Further bursts of star formation occur when galaxies merge. The efficiency of star formation during minor mergers has been shown to decrease with increasing bulge mass, as the presence of a bulge stabilises the galaxy (Mihos & Hernquist 1994; Cox et al. 2008). The efficiency of the burst thus depends on the mass ratio of the galaxies and fraction of mass contained in the bulge component. This dependency is parametrized as $e_{\rm burst} = e_{\rm burst,0}\, \mu^{\gamma_{\rm burst}}$, where μ is the merger mass ratio, defined to be the ratio of the total masses within twice the NFW scale radius:

$$\mu \equiv \frac{m_{\rm core,1} + m_{\rm baryons,1}}{m_{\rm core,2} + m_{\rm baryons,2}}, \tag{2.4}$$

with $m_{\rm core}$ the dark matter mass within $r_{\rm core} \equiv 2r_s$ and $m_{\rm baryons}$ representing the total baryonic matter contained in each galaxy (stars and gas). The less massive of the two galaxies is denoted by the subscript 1, so that $\mu \leq 1$. The scale radius for the halo of a Milky-Way sized galaxy ($M_{\rm vir} \sim 2 \times 10^{12}\mathrm{M_\odot}$) is $\sim$ 27 kpc, thus the core radius is approximately 60 kpc. The burst

than the free-fall time, the gas is assumed to have fallen in cold and is accreted onto the central galaxy.

efficiency $e_{\rm burst,0}$ is determined from numerical simulations (Robertson et al. 2006) and $\gamma_{\rm burst}$ is taken from Cox et al. (2008):

$$\gamma_{\rm burst} = \begin{cases} 0.61 & B/T \leq 0.085 \\ 0.74 & 0.085 < B/T \leq 0.25 \\ 1.02 & B/T > 0.25 \end{cases} . \tag{2.5}$$

B/T is the the ratio of the stellar mass within the bulge to the total stellar mass of the largest progenitor.

At any output redshift, luminosities are determined from the star formation histories of each galaxy by using the stellar population synthesis models of Bruzual & Charlot (2003) with a Chabrier IMF and the Padova 1994 library to synthesize a composite galaxy spectrum. Spectra are convolved with a filter response function to determine the luminosity in any of the commonly used wavelength bands. Dust attenuation has a strong influence on the luminosities and is modelled with two components, in a similar way to Charlot & Fall (2000). The first component accounts for the diffuse dust in the disk and is modelled as a standard "slab" after assigning a random inclination to each galaxy. The second component arises from dense clouds of dust surrounding young, star-forming regions. The free parameters in the dust model are set by requiring that the observed ratios of far-UV to far-IR in nearby galaxies are reproduced (see Gilmore et al. 2009, for details). Careful tuning is required in order to match observed luminosity and colour distributions.

When dark matter halos merge, the new halo formed is known as a parent halo. Each merged halo (now known as a subhalo) and the galaxy at its centre may remain intact for some time, slowly orbiting within the potential well of the parent until it becomes completely tidally disrupted or reaches the centre. The satellite galaxy will undergo deceleration due to the gravitational influence of the dark matter of the parent halo – a process known as dynamical friction. The Chandrasekhar formula relates the decrease in orbital velocity of a satellite (a point mass, in the simplest approximation) in a background "sea" of uniformly distributed mass to the orbital parameters and mass distribution, and is given by

$$\frac{d}{dt}\vec{v}_{\rm orb} = -4\pi G^2 \ln\Lambda M_{\rm sat}\, \rho_{\rm host}(< v_{\rm orb})\, \frac{\vec{v}_{\rm orb}}{v_{\rm orb}^3} , \tag{2.6}$$

where $\rho_{\rm host}(< v_{\rm orb})$ is the density of background particles with velocities less than the orbital velocity $v_{\rm orb}$ of the satellite, $M_{\rm sat}$ is the total mass of the satellite, and Λ is the Coulomb logarithm (see, e.g Chandrasekhar 1943; Binney & Tremaine 1987; Boylan-Kolchin et al. 2008). The Coloumb logarithm, which is related to the orbital parameters and masses of the satellite and background masses, is inherently uncertain, with much of the difficulty lying in the definition of the satellite mass. It is often approximated as $\Lambda = 1 + M_{\rm host}/M_{\rm sat}$ or $\Lambda = 1 + (M_{\rm host}/M_{\rm sat})^2$. The differential equation usually used by SAMs to calculate the time taken

for a satellite to orbit into the centre is

$$r\frac{dr}{dt} = -0.428 f(\epsilon)\frac{GM_{\rm sat}}{V_c}\ln\Lambda, \tag{2.7}$$

(Binney & Tremaine 1987; Somerville & Primack 1999), where $f(\epsilon)$ is a factor that depends on the circularity parameter ϵ, defined to be the ratio of the angular momentum of the satellite to that of a circular orbit with the same energy, and V_c is the circular velocity of the parent halo. Solving this equation with the initial radius equal to the virial radius of the host halo, $r_{\rm vir}$, results in a merger time of

$$\frac{\tau_{\rm merge}}{\tau_{\rm dyn}} = \frac{1.17}{f(\epsilon)\ln\Lambda}\frac{M_{\rm host}}{M_{\rm sat}}. \tag{2.8}$$

This equation underestimates the time taken for satellites to merge, as it does not account for the loss of satellite mass due to tidal stripping. Mass loss slows down the subhalo, since the orbital time increases as the mass ratio of the two bodies increases. The S08 SAM uses a variation of this formula, calibrated by Boylan-Kolchin et al. (2008) using a series of N-body simulations:

$$\frac{\tau_{\rm merge}}{\tau_{\rm dyn}} = A\,\frac{(M_{\rm host}/M_{\rm sat})^b}{\ln(1+M_{\rm host}/M_{\rm sat})}\exp\left(c\,\epsilon\right)\left[\frac{r_c(E)}{r_{\rm vir}}\right]^d \tag{2.9}$$

Here $A = 0.216$, $b = 1.3$, $c = 1.9$ and $d = 1$ are best-fitting parametrizations of the dependence on mass ratio, orbital circularity and orbital energy $r_c(E)$ from the simulations. The masses are taken to be the virial masses at the time when the satellite enters the host's virial radius. This simple prescription takes into account the tidal effects and the dependence on the angular momentum and energy of the orbit, resulting in much longer merging timescales than found using Equation 2.8, that agree better with numerical predictions.

Subhalos are considered destroyed by tides once their mass drops below that contained within the NFW scale radius. The stripped stars are added to a diffuse stellar component surrounding the central galaxy. If the subhalo reaches the centre of the parent halo before being tidally destroyed, the galaxies are assumed to merge. Some fraction of stars are scattered into the intergalactic medium, contributing to the intracluster light or stellar halo of the newly-formed galaxy. The fraction of scattered stars is an adjustable parameter in the model. Mergers are assumed to occur only at the centres of the halo potential wells, so mergers between subhalos (satellite galaxies) are not considered. Recent work using a SDSS group catalogue (McIntosh et al. 2008) has shown that $\sim 2\%$ of mergers in groups and clusters are satellite-satellite mergers occurring on the outskirts of groups, however it is postulated that such mergers took place at the centres of neighbouring halos shortly before they were accreted into the group halo. Mergers between satellites that are already accreted into the halo are expected to be negligible because of their relatively large velocities and limited gravitational influence compared to that of the host halo.

Mergers are instrumental in shaping the morphology of the remnant galaxy. SAMs usually assume that bulges are created by major mergers with very high efficiency while minor mergers

result only in a thickening of the disk. These assumptions are motivated by numerical simulations (e.g. Cox et al. 2006). In the latest version of the S08 SAM, bulge formation is assumed to depend on the mass ratio of the merging pair, resulting in a more continuous distribution of remnant properties. A fraction of disk stars, given by

$$f_{\rm sph} = 1 - \left[1 + \left(\frac{\mu}{f_{\rm ellip}}\right)^8\right]^{-1}, \tag{2.10}$$

where μ is the mass ratio of the galaxies given by Equation 2.4 and $f_{\rm ellip} \simeq 0.25$–$0.3$, is thus transferred into the bulge component, in addition to the new stars from the burst of star formation caused by the interaction. The formation of bulges via disk instabilities is not included in the latest incarnation of the SAM.

The feedback processes described in 1.2 are also an integral part of SAMs. I defer to S08 for further details, but note that there is thought to be an important link between mergers, AGN activity and the shutting down of star formation. This has been extensively explored through numerical simulations (e.g., Di Matteo et al. 2005; Springel et al. 2005b; Cox et al. 2006, 2008; Robertson et al. 2006). Hopkins et al. (2005, 2006a,b, 2008, and other papers) analyse the implications of these simulations, developing a comprehensive picture for quasar growth and feedback in a hierarchical context. Gas-rich galaxy mergers are thought to be followed by intense bursts of star formation and the development of a quasar. The resulting stellar and AGN feedback removes gas, eventually forming a "red and dead" early-type galaxy.

There are a number of free parameters in the SAM. In previous versions of the model, these were set by requiring the properties of a Milky Way-sized reference galaxy with $V_c = 220$ km s^{-1} to match the average observed properties of galaxies with this circular velocity using the Tully-Fisher relation. S08 uses the relationship between halo mass and stellar mass (Moster et al. 2009) and the observed relation between stellar mass and gas fraction to set the main parameters. Many of the other parameters are suggested by numerical simulations or observations, as described above, while some can be adjusted depending on the goals of a particular model run or varied to test the influence of a process on the model results. The versions of the model I use in this thesis are those presented in S08. A summary of the parameters is provided in their Table 2. Note that this version of the model was not carefully tuned to match the luminosity function by adjusting the parameters of the dust, metallicity and star formation recipes (R. Somerville, private communication, 2009). Fundamental quantities, such as stellar mass, gas fraction and star formation rates were compared to observations and used to test the model in S08.

2.3 General results of the model

Historically, SAMs were tested against their ability to match the optical and near infrared luminosity functions, giving the number density of galaxies as a function of brightness, and the

Table 2.1: Summary of Cosmological Parameters

parameter	description	ΛCDM
Ω_m	Present day matter density	0.30
Ω_Λ	Cosmological constant	0.70
H_0	Hubble Parameter [km s^{-1} Mpc^{-1}]	70.0
f_b	Cosmic baryon fraction	0.14
σ_8	Power spectrum normalization	0.9
n_s	Slope of primordial power spectrum	1.0

I-band Tully-Fisher relation. The first generations of models produced promising qualitative agreement with a number of observables, but generally failed to match both relations simultaneously (e.g., Kauffmann et al. 1993). Large excesses at both the bright end and the faint end of the luminosity function (LF) demonstrated the need for feedback processes to reduce the efficiency of star formation in large galaxies, and photo-ionization squenching to prevent star formation in small halos. Somerville & Primack (1999) showed that both the LF and Tully-Fisher relation could be matched to their observational counterparts at low redshifts, largely due to improvements in the modelling of feedback processes. This paper also demonstrated that extinction due to dust must be taken into account in determining luminosities. The recent inclusion of prescriptions for feedback from AGN at the centres of galaxies in the models has further improved the results.

Improvements in technology over the last decade have enabled look-back surveys to measure the LF out to redshifts beyond one in volumes big enough to provide meaningful number statistics. Though SAMs have been able to approximately reproduce the low redshift LF for a number of years now, matching the LFs at two or more epochs simultaneously is challenging. As shown below, the most recent implementation of the model matches both the observed LF and the mass function (MF) well at $z = 0$ (Section 2.3.1), however there are discrepancies at higher redshifts (see Section 2.3.2).

The model can be run in two modes, outputting data either for all galaxies in a cosmological volume (box) or simulating a look-back survey covering a fraction of the sky. In the second mode a mock catalogue that can be directly compared to observations out to high redshifts is produced. The specific models I use in this thesis are a simulation box with a length of $120h$ Mpc per side termed "ΛCDM" as it uses the standard "concordance" CDM cosmology, and a mock catalogue with an area of 2700 arcmin^2. This is termed "GEMS mock" because it was designed to be compared to observations from GEMS and other surveys out to a redshift of approximately 1 (see Chapter 3). The mock catalogue extends over approximately three times the volume of GEMS survey and uses the same cosmological parameters as the ΛCDM box. The cosmological parameters are summarised in Table 2.1.

2.3.1 The low redshift galaxy distribution

2.3.1.1 The luminosity and mass functions

At low redshifts, I compare the distributions of $z = 0$ galaxies in the ΛCDM box model with data from the SDSS survey. The left panel of Figure 2.2 shows the comparison of the model and observed LFs in the r-band, with the observed data points given by Bell et al. (2003). A comparison of the model and observed mass functions is shown in the right hand panel. The observed mass function (MF) was derived from the g-band LF by Bell et al. (2003). The observed quantities are coverted to a Hubble parameter of $H_0 = 70$ km^{-1} Mpc^{-3} and the model luminosities are corrected for the effects of dust, as described in Gilmore et al. (2009). There is excellent agreement between the model and observations in both cases. The results are similar for other SDSS wavelength bands. Differences occur only at the massive end of the MF ($\log [M_\star/\mathrm{M}_\odot] \gtrsim 11$), where the model predicts more galaxies than observed. Note that the LF and thus the MF are least well determined at the bright end in the local Universe, due to the difficulty of estimating total magnitudes and determining the background accurately for bright galaxies with extended halos (e.g., Lauer et al. 2007). As a result, discrepancies here may not be a concern.

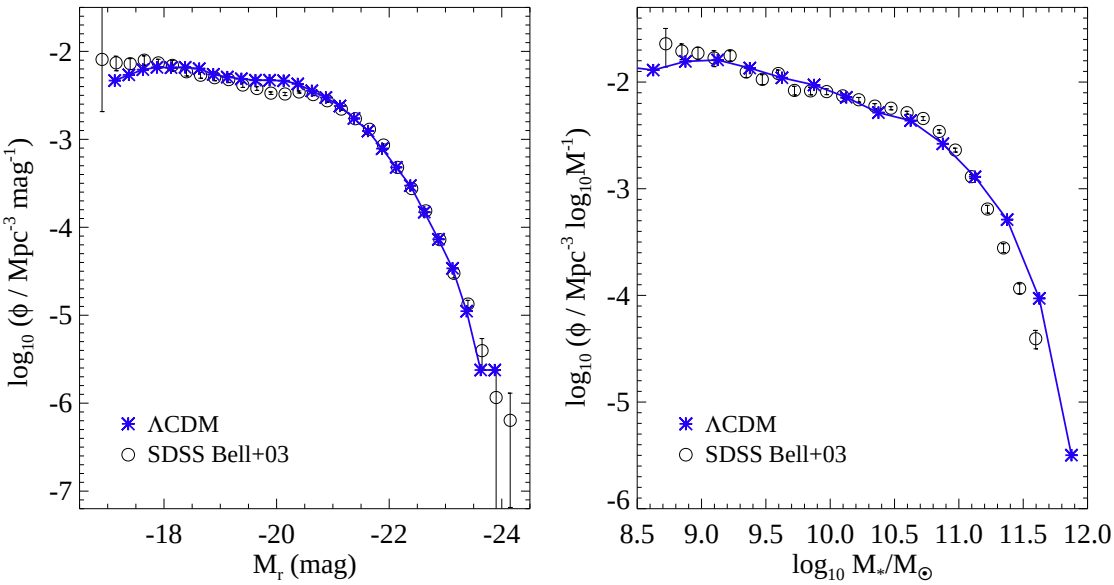

Figure 2.2: *Left panel:* The r-band LF at $z = 0$ in the ΛCDM model represented by stars, compared to the observed LF from the SDSS (Bell et al. 2003), shown by the circles and errorbars. *Right panel:* The MF at $z = 0$ for the model, in comparison to the MF determined from the SDSS g-band data (Bell et al. 2003).

2.3.1.2 The colour–magnitude diagram

A comparison of the observed and SAM galaxy distributions in colour–magnitude space is another important test of the model. Although there is also a bimodality in the model distri-

bution, the shape differs somewhat from the observations, particularly at higher redshifts (see Section 2.3.2). The colours of galaxies in the model depend strongly on the stellar population synthesis models used to determine the flux and a correction applied to account for dust. The dust prescription used in the S08 models is described in Gilmore et al. (2009), as discussed above.

In Fig 2.3 I compare the colour–magtitude diagram (CMD) for observed and model galaxies at $z \sim 0$. The top panel shows the distribution of 72,646 SDSS Data Release 6 (DR6; Adelman-McCarthy et al. 2008) galaxies in a thin redshift slice ($0.0375 < z < 0.0625$), selected from the New York University Value-Added Galaxy Catalog (NYU-VAGC; Blanton et al. 2005). This range in redshift provides a significant number of bright galaxies but is narrow enough to avoid the need for volume and evolution corrections. Galaxies are selected to have Petrosian magnitudes $m_r < 17.77$. The magnitudes are corrected for Galactic extinction using the dust maps of Schlegel et al. (1998) and k-corrected to rest-frame $z = 0$ bandpasses using `kcorrect_v4_1` (Blanton & Roweis 2007). Sérsic magnitudes are used as an estimate of total magnitude, and Model magnitudes, determined using a fixed convolution kernel in all bands based on the best-fit model (de Vaucoleurs or exponential) to the r-band image, are used to obtain colours. This choice is discussed in more detail in Section 4.2. The lower panels show the distributions of $z = 0$ model galaxies in the ΛCDM box, with (left panel) and without (right panel) a correction for dust. This gives some feeling for the uncertainties involved and how important it is to take dust extinction into account.

The distribution of colours is bimodal in both the observations and the model. There is a tight colour–magnitude relation for red galaxies extending to the bright end (the red sequence), and broader distribution of blue galaxies (the blue cloud). The model red sequence and blue cloud both have a peak at the faint end, below the completeness limit of the observations ($M_r \lesssim -19.5$ mag for the red sequence and $M_r \lesssim -19$ mag for the blue cloud). The peak of faint red objects in the SAM is populated by satellite galaxies, which are stripped of hot gas as they enter a larger halo. This stripping is assumed to be very efficient in SAMs and has been found to cause an excess of faint red galaxies compared to observations (Weinmann et al. 2006; Kimm et al. 2009, the "satellite overquenching problem"). Kimm et al. (2009) compare the CMDs of 5 SAMs (including S08) and find that models with AGN feedback seem to produce qualitative agreement with the colour distribution and fractions of red and passive galaxies for central galaxies, but not satellites.

In order to compare the model and observed distributions, I fit a double Gaussian given by Equation 2.11 to the distribution of colours in magnitude bins of 0.25 mag along the CMD,

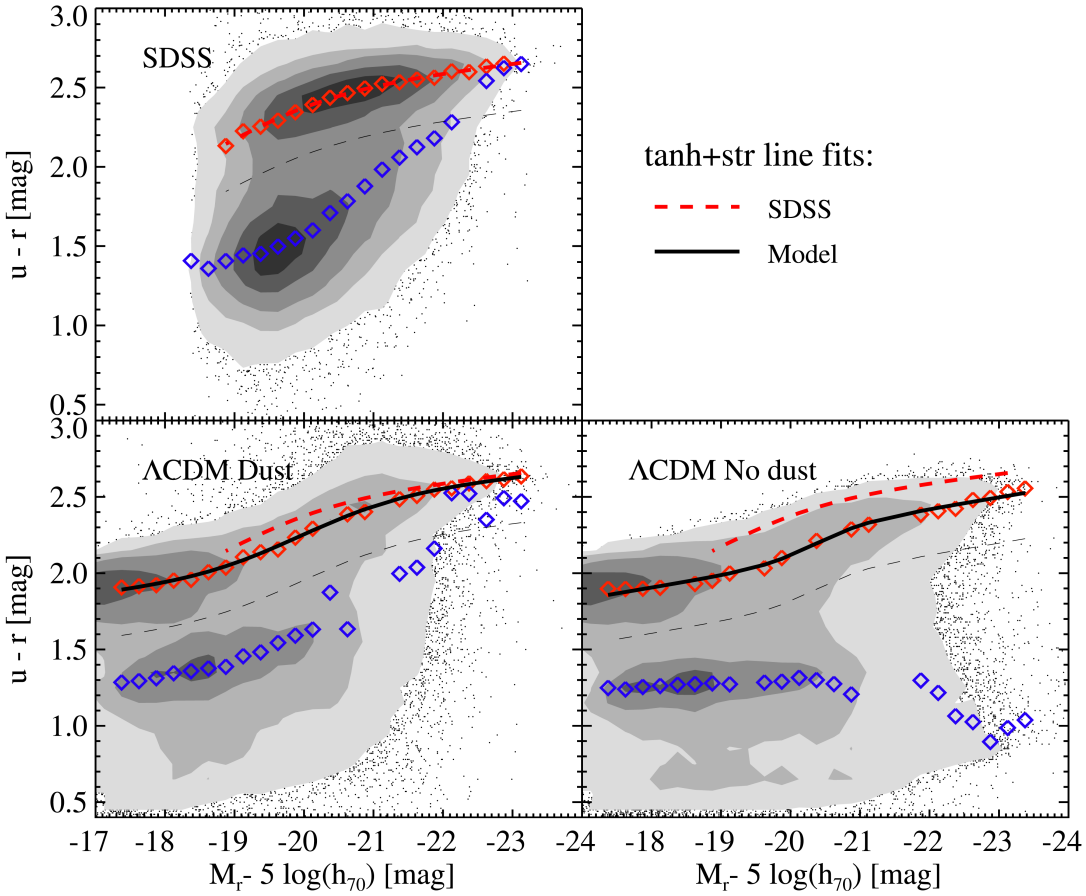

Figure 2.3: The CMD for galaxies in the SDSS survey (upper panel) compared to distributions of $z = 0$ galaxies in the ΛCDM box (lower panels). The contours enclose 2, 10, 25, 50 and 75% of the maximum value. For the model, the left panel shows the CMD after correcting for dust, while the right panel does not include a dust correction. In each panel the means of a double Gaussian fit are shown as blue and red diamonds for galaxies in the blue cloud and red sequence, respectively. A tanh plus straight line fit for the observed red sequence is shown in all panels as a red dashed line. Similar fits to the model red sequences are shown in black.

following Baldry et al. (2004).

$$\Phi(M_r, C) = \frac{\phi_{red}(M_r)}{\sqrt{2\pi}\sigma_{red}} \exp\left[-0.5\left(\frac{C-\mu_{red}}{\sigma_{red}}\right)^2\right] + \frac{\phi_{blue}(M_r)}{\sqrt{2\pi}\sigma_{blue}} \exp\left[-0.5\left(\frac{C-\mu_{blue}}{\sigma_{blue}}\right)^2\right]. \tag{2.11}$$

Here the subscripts red and $blue$ represent the contributions from galaxies in the red sequence and blue cloud, respectively. The normalisations of the two Gaussian functions, $\phi_{red}(M_r)$ and $\phi_{blue}(M_r)$, give the number density of galaxies as a function of magnitude, and thus represent the luminosity functions of the two types of galaxies. The variation with colour (C) in each magnitude bin is assumed to follow a normal distribution with mean μ and width σ. The

colour distributions and double Gaussian fits are shown in Fig 2.4 for the ΛCDM dust-corrected model. In each panel the single Gaussians fitted to the blue cloud and red sequence are shown as thin blue and red dashed lines, with the sum of the two shown as a black solid line. The means, μ_{red} and μ_{blue}, are shown by the vertical blue and red lines in each case and as diamonds on the CMDs in Fig. 2.3. In magnitude bins where a Gaussian cannot be reliably fitted, no point is shown. This occurs in bins where no bimodality is evident (see the $M_r = -20.375$ panel in Fig 2.4) or the distribution is relatively flat and no peak can be determined for one of the sequences (see the $M_r = -21.125$ panel in Fig 2.4), for example.

The effect of dust

The dust correction moves the whole distribution redward and alters the shape of both the blue cloud and the red sequence. The mean redward shift due to the dust correction is larger for the blue cloud than the red sequence, and particularly affects the bright end. It is surprising that the dust correction has a noticeable effect on the red sequence, as red galaxies are not expected to have much dust. Strongly star-forming galaxies contain large amounts of gas and dust, hence the dust correction has the greatest effect on the bright blue galaxies with high star formation rates. There is a dramatic decrease in the number density of bright blue objects after the correction. The means of the blue cloud are approximately constant with magnitude before the correction, but rise towards redder colours with magnitude after the correction, replicating the behaviour of the observed distribution. The red sequence moves upward by ~ 0.1 mag on average in the ΛCDM model. Although it appears from the points above the contours in the left-hand panel that the scatter of the relation increases at intermediate magnitudes, the measured scatter is larger in the uncorrected red sequence. The dust-corrected model shows much better agreement with the observations, and it is these corrected luminosities I use in further comparisons.

The red sequence

The red sequence, or colour–magnitude relation, results mainly from the relation between mass and metallicty, with a smaller contribution from age. Higher mass galaxies have deeper potential wells and are thus able to retain metals that may otherwise be expelled by winds, resulting in higher metallicities and thus redder colours (e.g., Faber 1973; Larson 1974; Kodama & Arimoto 1997; Gallazzi et al. 2006). The red sequence is usually assumed to be linear with magnitude, however the slope and shape depend somewhat on the filters used and the aperture within which photometry is done (Bernardi et al. 2003). In both the observed and model CMDs shown in Fig. 2.3 there is clearly variation of the slope with magnitude. The SAM red sequence is fairly flat at the bright end, steepening at intermediate magnitudes ($-19 \lesssim M_r \lesssim 21$). The observed relation seems to change slope more gradually and at slightly fainter magnitudes. In Chapter 4 we explore a possible explanation for the change in slope, attributing it to the increased numbers of dry mergers affecting the bright end. Bernardi et al. (2007) noted that other SAMs predict

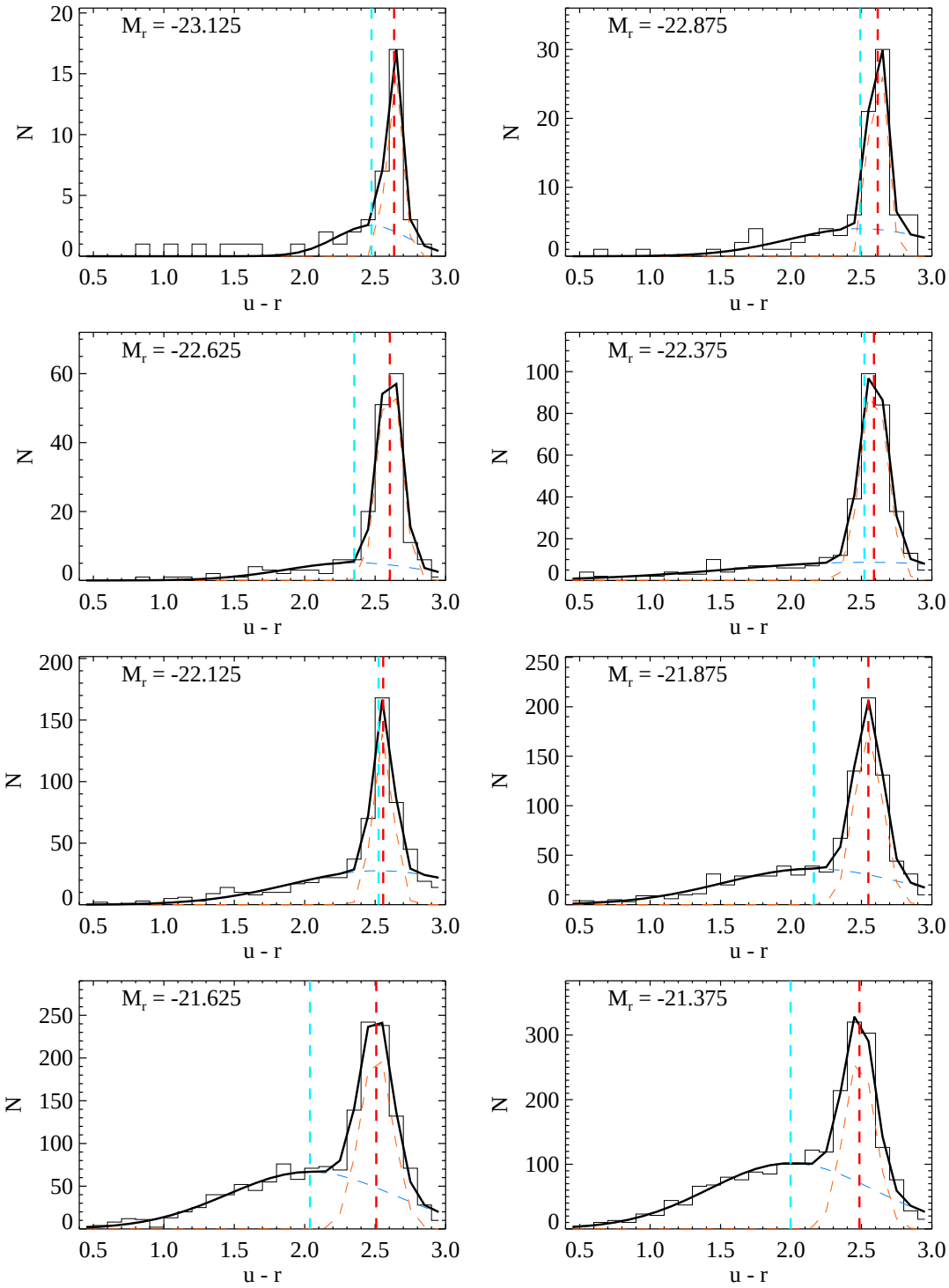

Figure 2.4: The colour distribution in each magnitude bin of 0.25 mag along the CMD of $z = 0$ galaxies in the ΛCDM box, with the dust correction applied. In each panel Gaussian fits to the blue cloud and red sequence are shown separately with thin dashed lines. The resulting double Gaussian is shown as a solid black line. The mean colours of the two Gaussian fits are shown as vertical dashed lines.

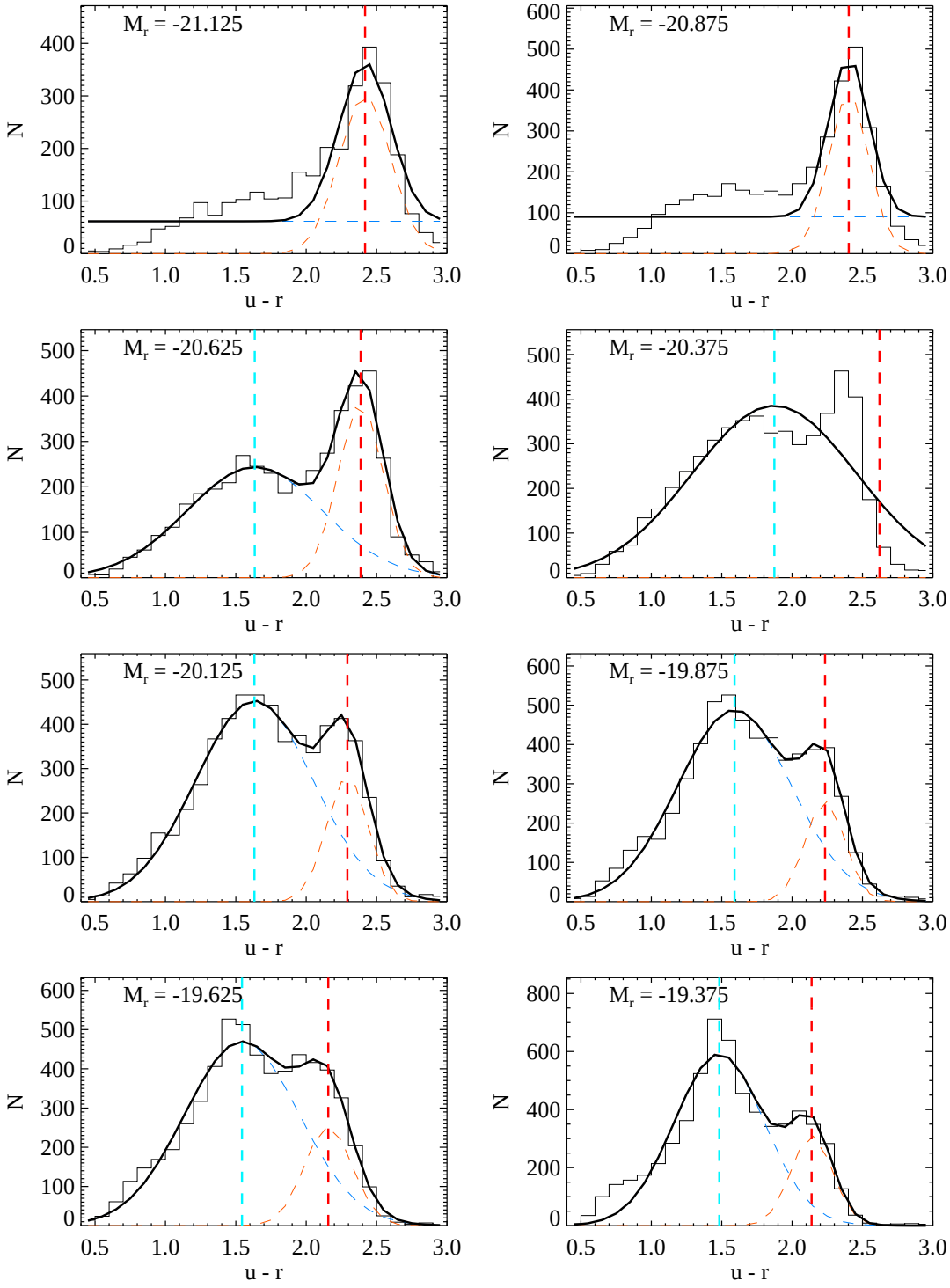

Figure 2.4: Continued from previous page.

Table 2.2: Parameters of tanh+straight line fit

	a	b	c_1	c_2	c_3
SDSS	1.117	-0.054	-0.295	-18.82	1.686
ΛCDM Dust	1.321	-0.046	-0.250	-19.94	1.573
ΛCDM No dust	0.629	-0.077	-0.104	-20.35	0.735
WMAP3 Dust	0.587	-0.081	-0.147	-19.41	2.163
WMAP3 No dust	0.116	-0.104	-0.060	-20.11	0.255

bluer than expected colours at the bright end (Bower et al. 2006; Croton et al. 2006). These earlier models did not reproduce the observed colour distribution very well, however.

Following Baldry et al. (2004), I have fitted the means of the red sequence with the combination of a hyperbolic tan and a straight line, given by

$$f(M_r) = a + bM_r + c_1 \tanh \frac{M_r - c_2}{c_3}. \tag{2.12}$$

The resulting fit parameters for the observations and four models are given in Table 2.2. The parameters a and b represent a straight line showing the general trend of increasing colour with brightness, while the parameters c_1, c_2 and c_3 parametrize the transition between the faint and bright ends. Such a function captures the change in slope along the relation fairly well, as can be seen in the figure, where the model fits are shown with a black line. For reference, the fit to the SDSS red sequence is shown with a red dashed line in each panel.

The red and blue LFs

The colours of galaxies correlate with their morphologies, gas fraction and star formation rate. There are thus a number of ways in which the luminosity and mass distributions can be separated to analyse the contributions from various populations. Observationally the split is often based purely on the bimodality in the colour-magnitude plane (see, e.g., Bell et al. 2004), since colours and magnitudes are directly measurable and such a cut is straight-forward to reproduce for other data sets and models. This avoids the subjectivity involved in visual morphological classification, differing definitions of concentration and different indicators used to measure star formation rate. From a model perspective, both the gas fraction and star formation rate are tracked for every galaxy and so either of these would be a natural choice. The amount of gas determines whether a merger is dissipative, influencing the morphology of the merger remnant, thus we use the gas fraction to distinguish between different types of mergers in Section 3.2. Galaxy morphology can also be estimated by assuming the fraction of stellar mass contained in the bulge component determines a galaxy's type. Previous work using semi-analytic models (e.g. Kang et al. 2007) has assumed that bulge-to-total mass ratios (B/T) above 0.6 correspond to early-type galaxies, $0.4 < B/T < 0.6$ to intermediate-type spirals and $B/T < 0.4$ to late-type disk or irregular galaxies. B/T depends directly on the merger history of the galaxy

through the model assumptions and so a comparison of morphological fractions determined this way can be a useful test of these assumptions. Since this is not our aim here, we avoid this somewhat artificial distinction and separate galaxies in colour-magnitude space, based on the double Gaussian fit to the distribution of colours in each magnitude bin along the relation shown above. At higher redshifts a simpler straight line cut at the estimated position of the "green valley" between the two sequences is used to separate the red and blue populations.

Fig. 2.5 shows the luminosity functions determined from the normalisation of the double Gaussian fits. The ΛCDM model results are shown by stars and the observed LFs from the SDSS by filled circles. The volume for the SDSS data is determined by assuming the spectroscopic survey has a completeness of 90%, based on the estimated tiling efficiency. There is good agreement for both red and blue galaxies over much of the magnitude range (as expected from the agreement between the total LFs in Fig 2.2). At intermediate magnitude ($M_r \gtrsim -20.5$) there appears to be an excess of blue galaxies and two few red galaxies. These differences compensate to produce the agreement in the total LF down to the faint end. The normalisation of the red sequence LF appears to rise again toward the faint end, where other works have shown there to be an excess of red satellites (Kimm et al. 2009).

2.3.2 The evolution of the luminosity and mass distributions

2.3.2.1 The colour–magnitude diagram

Figure 2.6 shows the CMD for galaxies in the GEMS mock in redshift slices of $0.2 \leq z < 0.4$, $0.4 \leq z < 0.6$, $0.6 \leq z < 0.8$ and $0.8 \leq z < 1.0$. Although a red sequence and blue cloud can be identified, the shape differs from the low-z CMD and there appear to be three peaks in the distribution - the blue cloud and two peaks of red galaxies, one at the faint end and one at intermediate brightness. As discussed above, the separation is likely to be caused by the feedback mechanisms operating at different mass scales and in different environments in the model – at low masses, galaxies are depleted of gas through stripping and stellar feedback, while AGN feedback is only effective in massive galaxies. Most of the galaxies at the faint end of the red sequence are satellites, while the bright end and blue cloud are dominated by central galaxies.

For comparison, the red sequence for galaxies in the NOAO Deep Wide-Field survey (solid red lines, Equation 2.13) and colour cut (dotted black lines) used to separate blue and red galaxies (Brown et al. 2007) are also shown in the figure. The observed red sequence is given by the fit to the evolution of the mean $U - V$ colour at $M_V = -20$,

$$U - V = 1.4 - 0.08(M_v - 5 * \log h + 20) - 0.42(z - 0.05) + 0.07(z - 0.05)^2 \qquad (2.13)$$

from Brown et al. (2007), with the cut 0.25 mag below this line. A very similar relation was found for the evolution of the red sequence in the Combo-17 survey (Bell et al. 2004). The comparison shows that the colours of galaxies in the model are bluer than observed, although

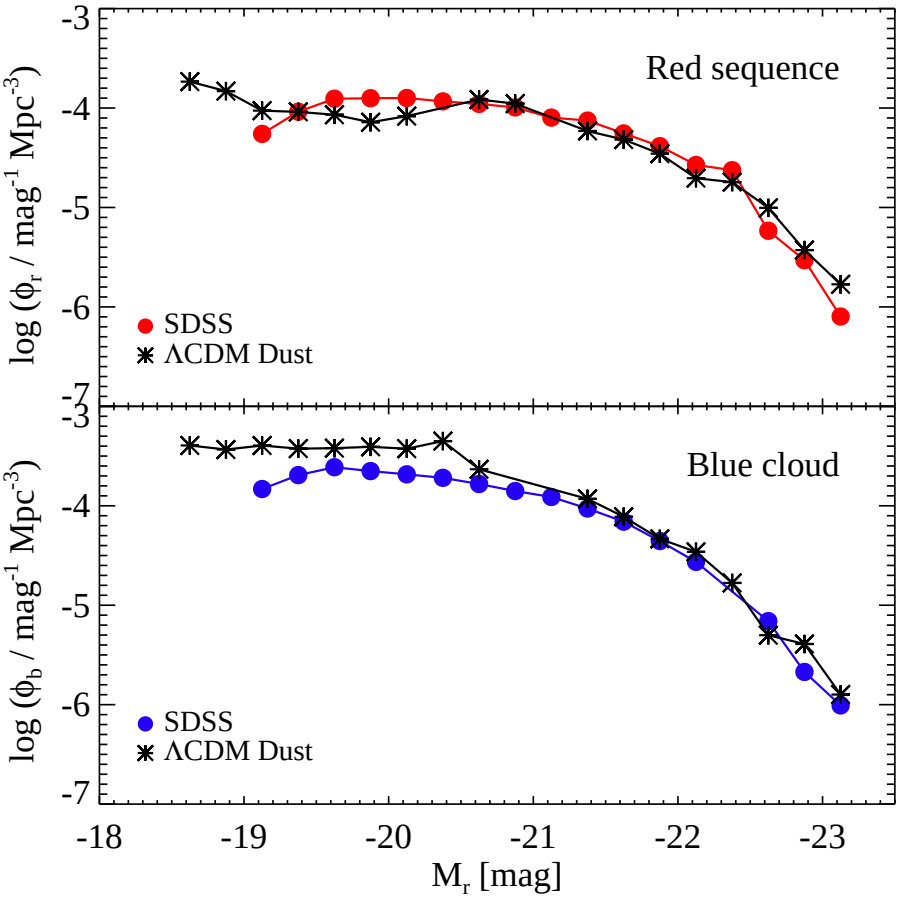

Figure 2.5: The r-band LFs of red sequence and blue cloud galaxies determined from a double Gaussian fit to the CMD. The dust-corrected ΛCDM model results are shown by the stars. Observations are from the SDSS DR6 (filled circles), as described in the text.

the observations are limited to magnitudes $M_V \gtrsim -20$ in the highest redshift bins, making it difficult to compare over the whole magnitude range. The peak of the red galaxy distribution in the model lies ~ 0.2 mag below the observed relation. In the highest redshift bins, the cut appears to include the majority of galaxies in the faint-end peak, but it passes through the centre of the densest region in the lowest redshift bin and will lead to an underestimate of the number of red galaxies. At high redshifts the bright-end has not yet developed into the tight colour–magnitude relation seen at low redshifts. It is also difficult to identify a clear green valley, which does appear to be present in the observations even at redshifts beyond one.

2.3.2.2 The luminosity and mass functions

The LFs in the Johnson B-band in redshift slices of $0.2 \leq z < 0.4$, $0.4 \leq z < 0.6$, $0.6 \leq z < 0.8$ and $0.8 \leq z < 1.0$ from the mock catalogue are shown in comparison to the Schechter

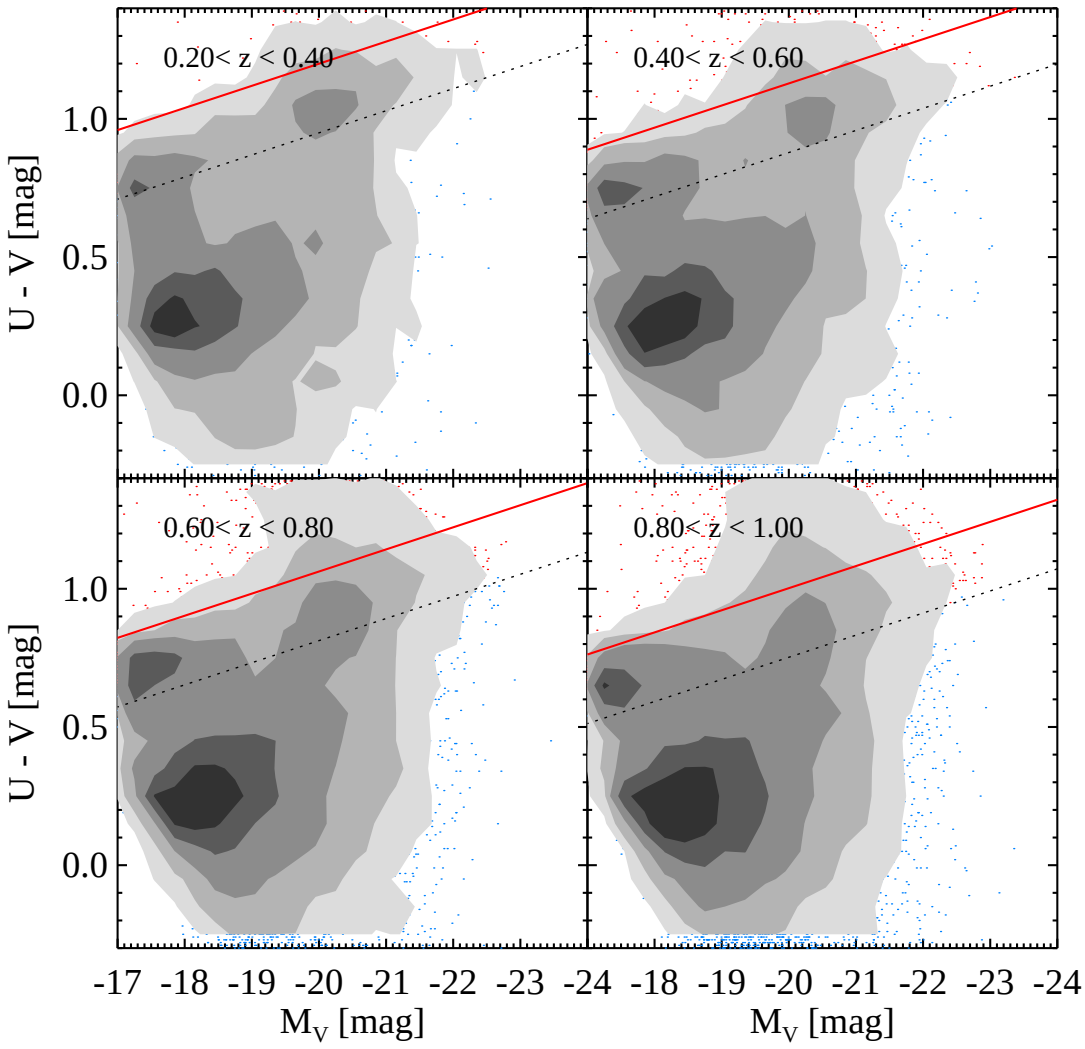

Figure 2.6: The evolution of the CMD in the GEMS mock model. The red sequence at the mean redshift of each bin from the NOAO Deep Wide-Field survey (Brown et al. 2007) is shown as a solid red line. The cut used to separate red and blue galaxies for the determination of the LFs is shown as a dashed line.

function fits from the Combo-17 survey (Wolf et al. 2003) in Fig. 2.7. The mock includes galaxies down to masses of $5 \times 10^8 \mathrm{M}_\odot$. There are ~ 6000 galaxies in the lowest redshift bin, increasing with the survey volume to ~ 32000 galaxies with $0.8 < z < 1.0$. The completeness begins to fall at $M_B \gtrsim -18$ mag for $z \lesssim 0.6$ and $M_B \gtrsim -18.5$ mag in the highest z slices. The total LF for the model is shown by the black dashed lines and diamonds. The solid black lines are the observed Schechter function fits. The normalisation of the LF agrees well with the observations at all redshifts, however there is a steeper drop than observed at the bright end, resulting in insufficient numbers of bright galaxies. The discrepancy becomes more severe in the higher redshift bins. For reference, the $0.8 \leq z < 1.0$ Schechter fit is repeated as a thin grey

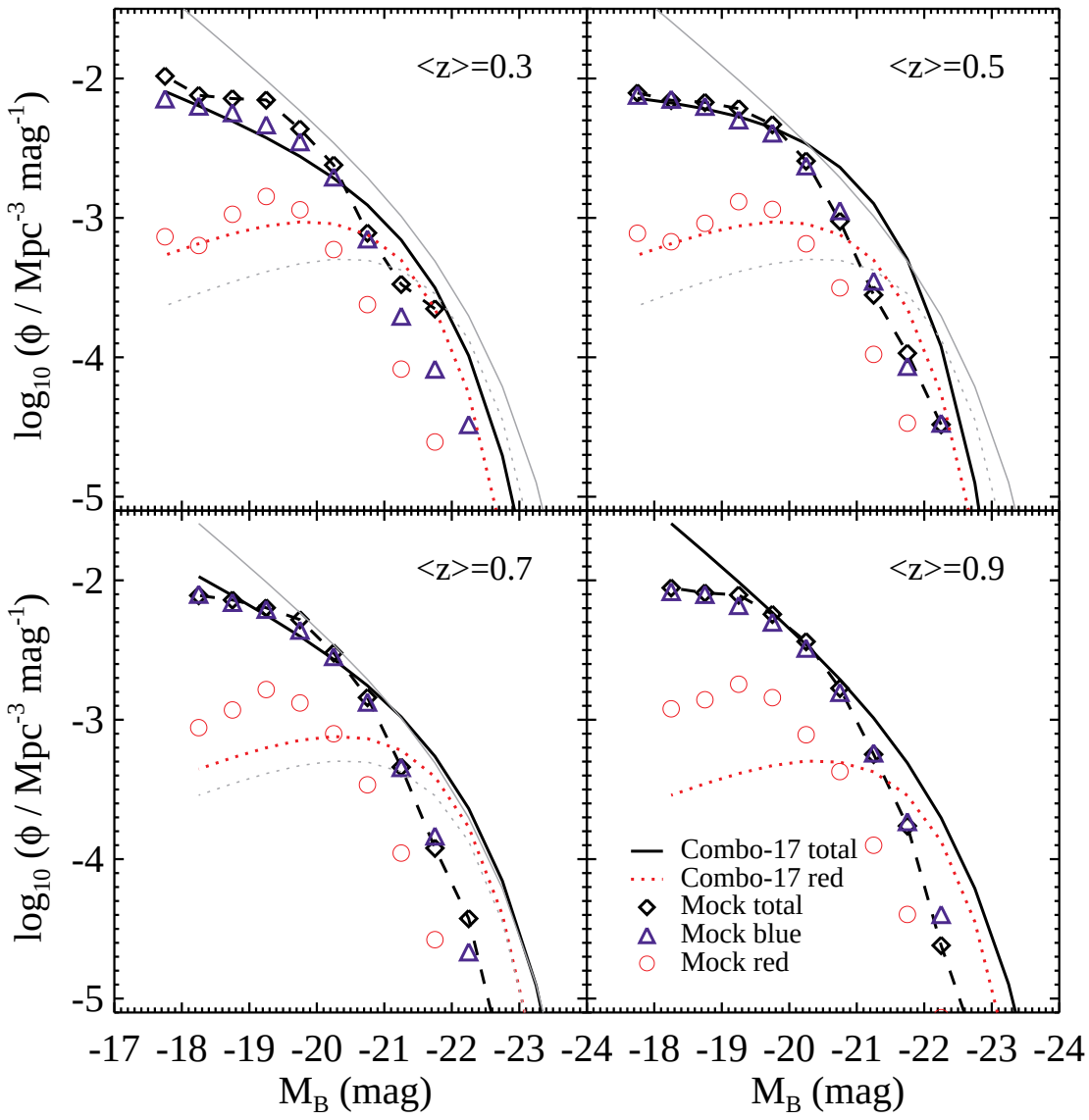

Figure 2.7: The B-band LF at different epochs derived from the GEMS mock model in comparison to the Schechter function fits to the observed LFs from the Combo-17 survey (Wolf et al. 2003). The total LF is given by the black diamonds and dashed lines for the model and solid black line for the observations. The contributions to the the model LF from red and blue galaxies are shown by the circles and triangles. The Schechter function fit to the red galaxy LF from Combo-17 is shown by the dotted red line. The $\langle z \rangle = 0.9$ observed Schechter functions are repeated as thin grey lines in all panels as a reference.

line in all the panels. Figure 2.7 also shows the LF split into contributions from galaxies on the red sequence and blue cloud. To compare directly with the observations, I apply the colour cut 0.25 mag below Equation 2.13 to separate red and blue galaxies. As shown above, this cut is too restrictive for the model and would better approximate the so-called green valley between the peaks of the red and blue distributions if it was shifted blueward by ~ 0.2 mag. The number density of faint red galaxies extends well above the Schechter fit in the highest redshift bins, despite the conservative cut. The space density of red galaxies measured by Brown et al. (2007) is higher than the Combo-17 measurement, with good agreement at the bright end, but still falls below the model LF at the faint end. The red galaxy population in the model undergoes very little evolution in both normalisation and magnitude. There are too few bright red galaxies at all redshifts. A colour cut with a shallower slope or shifted blueward would improve the agreement at the bright end but as the total number of galaxies at the bright end falls below the observations, this still cannot make up the difference. As noted in the introduction, the model parameters governing the luminosities were not carefully tuned and so it is possible that the agreement could be improved. In this sense, the mass function provides a more fundamental test of the model.

The mass function in the same redshift slices is shown in Fig. 2.8. The same cut in colour is used to determine the MFs for the red and blue galaxy populations. The observations shown here are also from the Combo-17 survey, in this case from Borch et al. (2006). The agreement of the total, red and blue MFs at the bright end is encouraging, however the model predicts many more galaxies than observed below masses of $M_\star \sim 6 \times 10^{10} \mathrm{M}_\odot$. This excess has contributions from both the red and blue populations in the high redshift bins, but is accounted for mainly by blue galaxies at low redshift. The difference between the model and observed MFs decreases toward lower redshift, as there is almost no evolution in the model MF (see Fig. 2.10).

The evolution of the total LF and MF are shown in Figs. 2.9 and 2.10. This highlights the problem mentioned above – while there is moderate luminosity evolution in the model, it is less than expected from the observations. The lack of evolution is even more severe for the distribution of mass, which undergoes almost no change since $z \sim 1$. As noted by Fontanot et al. (2009), this seems to be a difficulty for other SAMs too. In general, they show very little evolution in the mass function over the last half of the Universe's history. Since they are tuned to match the distribution at $z = 0$, they produce too many low mass galaxies at higher redshifts. The lack of evolution in mass is a serious problem for this SAM and possibly for SAMs in general, with no clear solution. It is beyond the scope of this thesis to investigate and resolve this issue.

2.4 Conclusions

I have described the formation and evolution of galaxies as modelled in the Somerville et al. (2008) SAM, which will be used as the basis for exploring the merger histories of galaxies and

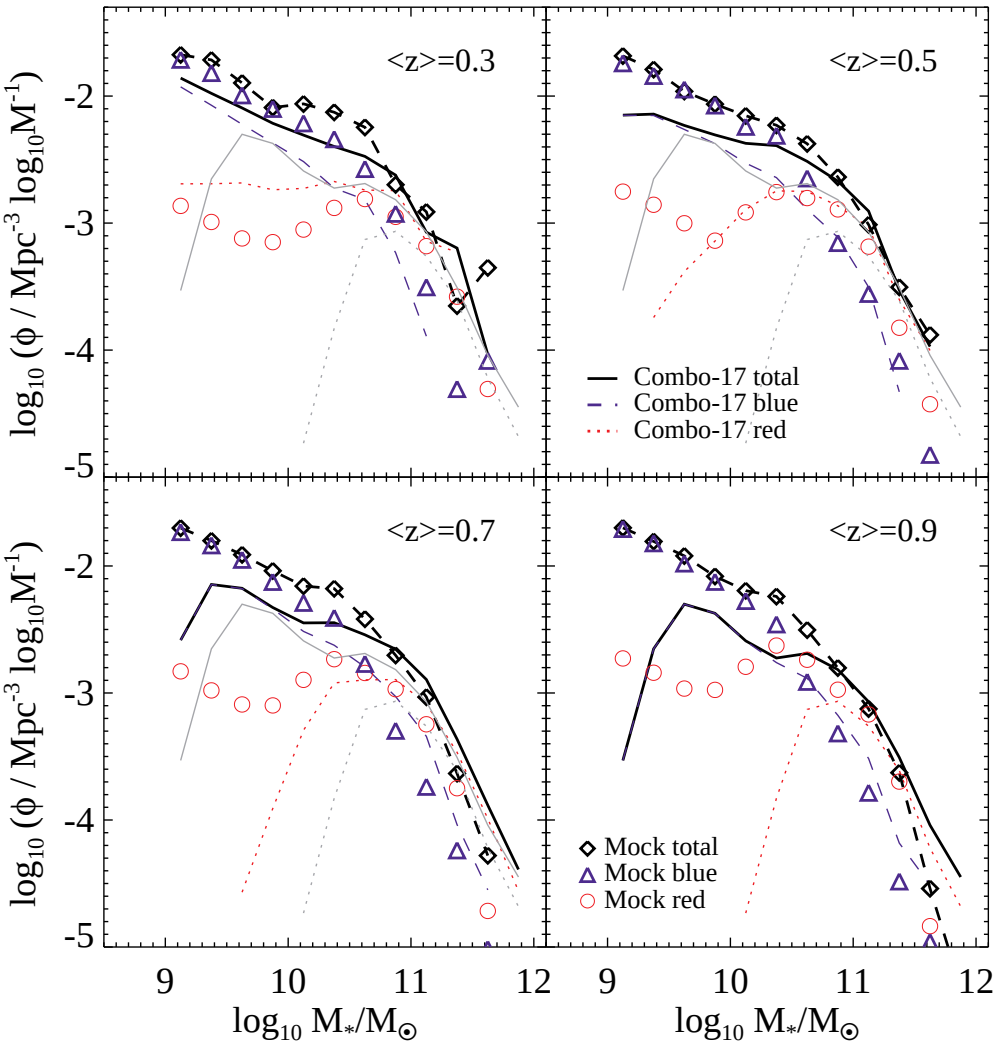

Figure 2.8: The model MF at different epochs derived from the GEMS mock model in comparison to the Schechter function fits to the observed LFs from the Combo-17 survey (Borch et al. 2006). The total MF is given by the black diamonds and dashed lines for the model and solid black line for the observations. The contributions to the the model MF from red and blue galaxies are shown by the circles and triangles. The observed MFs for red galaxies from Borch et al. (2006) are shown by the dotted red lines. The $\langle z \rangle = 0.9$ observed total and red MFs are repeated as thin grey lines in all panels as a reference.

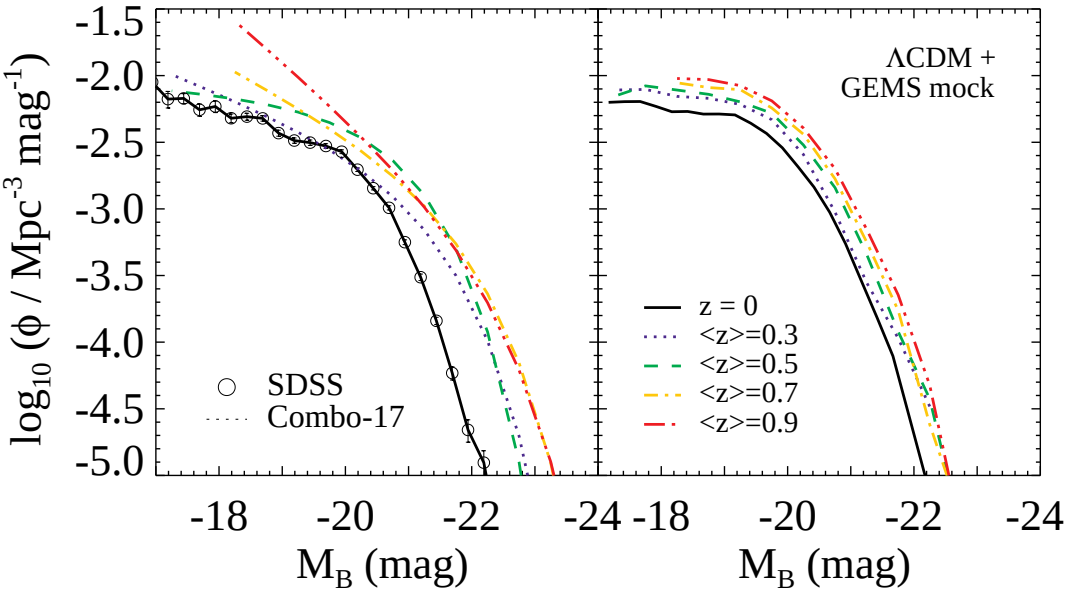

Figure 2.9: The evolution of the B-band LF derived from the GEMS mock model (right panel) in comparison to the observed LFs from the SDSS (Bell et al. 2003) and Combo-17 (Wolf et al. 2003) surveys (left panel).

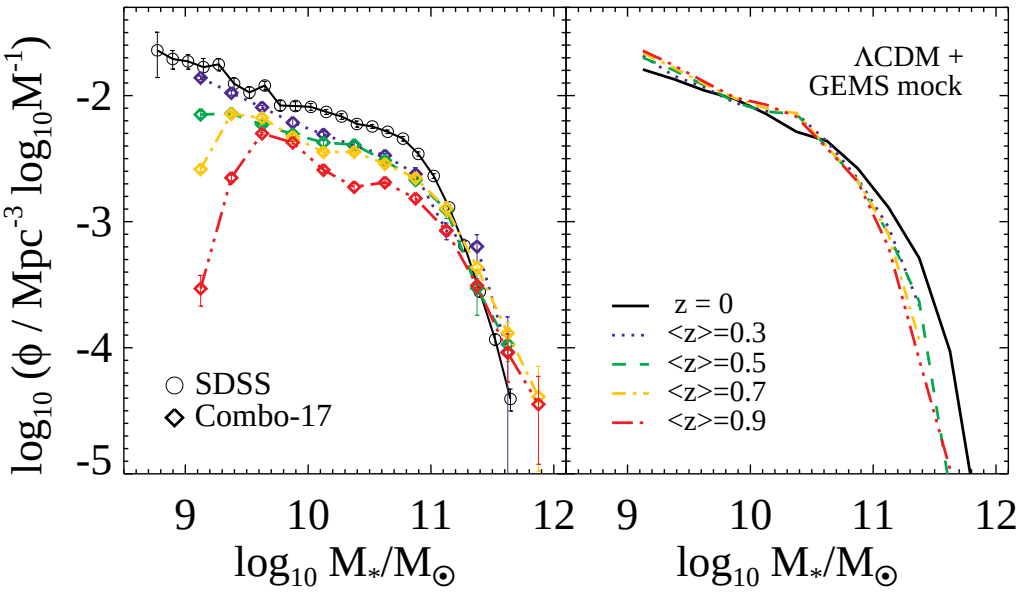

Figure 2.10: The MF evolution derived from the GEMS mock model in comparison to the observed LFs from the SDSS (Bell et al. 2003) and Combo-17 (Borch et al. 2006) surveys. There is much stronger evolution in the observations.

further modelling presented in this thesis. The model shows good agreement with the observed distributions of galaxy colours, masses and luminosities at $z = 0$. Galaxies are found in two distinct regions in colour–magnitude space, producing a bimodal distribution that matches well with observations from the SDSS. The slope of the red sequence changes with magnitude, flattening at the bright end. At all redshifts the model red sequence lies slightly blueward of the observed relation. At higher redshifts it becomes clear that there are discrepancies in the predicted number of red galaxies and the evolution of the mass function. The massive end of the MF agrees well with the observed distribution, both in terms of the total number density and relative contributions of red and blue galaxies. At intermediate and low masses, galaxies form too early in the model, resulting in very little evolution over the last half of cosmic history.

As I am particularly interested in the evolution of massive early-type galaxies that lie on the red sequence, it is reassuring that the massive end of both the total and red MFs are in the same range as the observations. The differences between the observed and model evolution are a nevertheless a serious concern. A toy model based on the galaxy merger histories that is independent of much of the SAM's complexity may provide useful insight into the effects of mergers on the galaxy population, despite these issues. In order to understand whether the galaxy merger trees from the model will be useful for further modelling, they need to be thoroughly tested against observations (see Chapter 3). As the galaxy merger histories follow relatively straight-forwardly from the dark matter merger histories, they are expected to be fairly robust.

Chapter 3

Mergers in the SAM

3.1 Introduction

In the currently favoured ΛCDM hierarchical picture of galaxy formation, galaxy mergers follow naturally from the mergers of the dark matter halos in which they are embedded. Although it is relatively straightforward to determine the merger rate for dark matter halos, the galaxy merger rate in models depends on how the halos are populated by galaxies and relative merger timescales. In SAMs, the main ingredients determining the relationship between halo and galaxy mergers are the dynamical friction and tidal stripping prescriptions (see Section 2.2). Once these are defined, the exact merger rate can be determined for the model. A comparison of the observed and predicted merger rates is an important test of our understanding of the way galaxies form and grow. In later chapters of this thesis, the consequences of merging on the red sequence galaxy population are investigated using the merger trees from the Somerville et al. (2008) SAM. In order to have some confidence in the predictions, it is necessary to test whether the amount of merging predicted agrees with observations. This is especially important in the light of the differences in mass function evolution shown in Section 2.3.2. Converting the model or observational results into the same system for a direct comparison can be difficult, however.

There are two main methods used to determine the fraction of galaxies involved in mergers observationally. The most robust method is to count the fraction of galaxies in close pairs (e.g., Patton et al. 2000; Le Fèvre et al. 2000; Patton et al. 2002; Lin et al. 2004; Bell et al. 2006b; Robaina et al. 2009a). The second method is to identify mergers by their morphologies, through either a visual or an automated classification scheme (e.g., Jogee et al. 2009; Conselice 2003; Lotz et al. 2008a). Each of these methods has both advantages and disadvantages, and is sensitive to different stages of the merger.

The fraction of galaxies in close pairs is measured using the two-point correlation function (see, e.g., Masjedi et al. 2006; Bell et al. 2006b; Li et al. 2008; Robaina et al. 2009a) or by counting the number of kinematic close companions per galaxy within a projected radius and line of sight velocity difference (e.g., Patton et al. 2000; Le Fèvre et al. 2000; Lin et al. 2004). Identifying galaxies in pairs before they merge has the advantage that it is a robust and repeat-

able measurement. To convert the measured close pair fraction into a fraction of galaxies that are likely to merge, the number of these pairs that are projected, rather than physical companions and the number that are unbound and will not merge must be estimated in some way. Such methodology can be used to study how the properties of galaxies are affect by interactions: the correlation function can be weighted by various galaxy properties (Skibba et al. 2006) to investigate the star formation enhancement due to interactions, for example (e.g., Li et al. 2008; Robaina et al. 2009a). Other means of identifying mergers, such as the visual classification described below, can complement the correlation function at small separations, to take into account very nearby pairs that are unresolved by ground-based observations and merger remnants (see Robaina et al. 2009a).

Interacting systems generally have asymmetric light distributions and bright regions offset from the centre. "Normal" galaxies, on the other hand, are usually symmetric and have concentrated light profiles with most of the light evenly distributed about the centre of the galaxy. These characteristics are exploited by both visual and automated classification schemes to identify galaxies of different types. The wide range of galaxy properties and uniqueness of each system makes this a challenging task, however. Galaxies with high star formation rates often contain numerous bright star-forming regions spread across the disk, while irregular galaxies do not have smooth light profiles. These classes of galaxies are particularly difficult to distinguish from merging systems. The ability to separate different classes will depend strongly on the wavelength band and signal-to-noise, which in turn depend on the redshift of the galaxy and details of the observational methodology.

The most commonly used automated classification schemes are the Concentration, Asymmetry and Smoothness (CAS, Bershady et al. 2000; Conselice et al. 2000; Conselice 2003) and Gini-M_{20} (Abraham et al. 2003; Lotz et al. 2004) methods. The CAS system uses the distribution of light to associate three parameters to each galaxy. Concentration is given by $C = 5\log(r_{80}/r_{20})$, where r_{80} and r_{20} are the radii in which 80% and 20% of the light within 1.5 times the Petrosian radius are contained, respectively. A measure of the asymmetry is obtained by subtracting an image of the galaxy rotated by 180 degrees from the original image and summing the residuals. The ratio of the residual sum to the total intensity is the asymmetry parameter, A. The clumpiness parameter, S, represents the fraction of a galaxy's light contained in high frequency structures. This is obtained by summing the residuals after subtracting a smoothed, low-resolution image of the galaxy from the original image. The criteria usually used to identify mergers are $A > 0.35$ and $A > S$ (Conselice 2003; Conselice et al. 2003; Conselice 2006). These were calibrated using a local sample with existing morphological classifications, exploiting correlations between colour and structure, as well as the equivalent width of Hα emission, to identify different galaxy types. As shown below, the CAS system has varying success in identifying mergers, with both contamination from non-merging galaxies and falsely identified mergers captured by these criteria. The Gini-M_{20} method uses the Gini coefficient, G, which is a measure of the relative distribution of flux values over the pixels of

a galaxy, and the second moment of the distribution of the brightest 20% of the pixels (M_{20}) to classify galaxies. Different classes of galaxies (major mergers, early- and late-type galaxies) fall into different regions within this parameter space. The regions of interest in this method are also calibrated using visually classified test samples. Lotz et al. (2004) argue that Gini-M_{20} is more effective at capturing merging systems than concentration and asymmetry measures and more robust at reduced signal-to-noise ratios.

The fraction of galaxies that are morphologically disturbed as the likely result of an interaction can be determined through visual identification of merger signatures – tidal tails and bridges, particularly for gas-rich interactions, and shells, ripples or common envelopes for gas-poor or well advanced mergers. The results of numerical simulations have been used to determine the types of morphologies that are identifiable at different stages of the interaction (e.g., Jogee et al. 2009, as presented here, or Bell et al. 2006a for dry mergers). Both merger remnants, where the individual progenitors are no longer separable, and pairs of interacting galaxies can be recognised visually. The eye is often able to distinguish features and recognise merger signatures at stages of the merger where the overall distribution is not perturbed enough to be noted by an automated scheme. Visual classification is naturally subjective, with large dispersion between classifiers.

In models, mock catalogues of galaxies within a lightcone, where the time between the last merger and the output redshift is recorded for each galaxy, provide a means of determining the merger fraction in an analagous way to the observational morphological classification. Alternatively, the merger rate can be directly determined by recording the time of each merger and the properties of the progenitor galaxies. In this chapter, I determine the merger rate and fraction for the S08 SAM using both these methods. "Snapshots" of simulated galaxies output at different redshifts can also be used to identify galaxies that were recently involved in mergers. This method is used in the comparison of the observational data with a number of different models in Section 3.3.

Each of the observational methods described above will be able to detect a merger for some fraction of the full time taken for the galaxies to merge. Knowledge of this visibility timescale is required to convert the measured merger fraction into a merger rate and to compare results from different methods. There is large uncertainty in assigning such a timescale. It depends strongly on the orbital parameters of the merger, the gas and dust fraction of the merging galaxies and the wavelength of observation. The simple assumption that the merger takes approximately one orbital period leads to a timescale of $t \sim 2\pi r/v_c$, where v_c is the circular velocity. Using $v_c = 1.4\sigma$, with σ the velocity dispersion, gives $t \sim 4r/\sigma$. Following Bell et al. (2006b), a typical galaxy with a velocity dispersion of 140 km s^{-1} at a radius of 15 kpc will have an orbital timescale of 0.4 Gyr. This is similar to the timescales used in the analyses of Patton et al. (2002) and Lin et al. (2004). It is also within the range expected from dynamical friction arguments, although here too, there is a wide range of possibilities (0.2 – 1 Gyr Lotz et al. 2008b). Gas-poor mergers are expected to be recognisable for shorter periods than gas-rich mergers (0.2

– 0.4 Gyr, Bell et al. 2006a). Lotz et al. (2008b) recently used a suite of N-body simulations to estimate the timescales that would be measured with different observational techniques for equal-mass gas-rich mergers with a variety of orbital parameters. The Gini-M_{20} method was found to have the shortest timescale of the morphological methods (0.2 to 0.6 Gyr). Asymmetry measures have timescales of 0.2 to 1.1 Gyr. The timescales for close pair measurements with projected radii of $10 < r_p < 30h^{-1}$ kpc were found to vary between 0.2 and 0.7 Gyr. It will be important to extend this work to unequal mass mergers and determine the appropriate mean timescale to use for each method. Kitzbichler & White (2008) calibrated the timescale taken for close pairs to merge as a function of mass and redshift using galaxy catalogues based on the Millenium Run simulation. They find relatively long timescales of 1.1 Gyr for $\sim M^*$ galaxies with line-of-sight velocity differences of up to 300 km s^{-1} and $\sim$ 1.6 Gyr for unconstrained velocity differences.

It is difficult to compare the merger fraction results based on different luminosity and mass selections directly, but a number of works using different methods seem to have converged on a major merger fraction for massive galaxies between 1 and 10% from $z = 0$ to $z = 1$. Within this range there is still discord and debate on the rate of evolution, as discussed below.

At low redshifts, an estimate based on the correlation function of 2dFGRS galaxies with $M_B \lesssim -20$ mag resulted in a pair fraction for $r_p < 30$ kpc of 0.3% (Bell et al. 2006b). As this is an extrapolation based on the correlation function at large scales (> 100 kpc) is is unlikely to be of much value, but at the time there were few low-z results to compare to. Since then Kartaltepe et al. (2007) have also found a very low fraction (0.7%) for $L_V \gtrsim L^*$ galaxies with $5 \lesssim r_p \lesssim 20$ kpc using the SDSS, but as a different distance and luminosity limit was applied and the pairs are taken from a catalogue of SDSS pairs with further selection criteria, it is difficult to compare this directly. To compare other results from the literature, I adjust the selection criteria to $M_B \lesssim -20$ mag and $r_p < 30$ kpc as far as possible following Bell et al. (2006b). Patton & Atfield (2008) find that over a fairly wide range in luminosity ($-22 < M_r < -18$) 2% of SDSS galaxies with $5h^{-1} < r_p < 20h^{-1}$ kpc and a relative velocity difference of < 500 km s^{-1} have a companion within a factor of two in luminosity ($\Delta M_r < 0.753$ mag). Adjusting for $H_0 = 70$ km s^{-1} Mpc^{-3} the distance criterion becomes $7 \lesssim r_p \lesssim 30$ kpc. Correcting for pairs within 7 kpc by multiplying by 4/3, and adjusting down by 65% for the fraction of projected pairs that are associated (in groups) but have real space distances of > 30 kpc (see Bell et al. 2006b), the fraction becomes 1.7%. This is still higher than other estimates at low-z, possibly as a result of the different luminosity selection. Adjusting the magnitude range of Patton et al. (2002) to $-23 \lesssim M_B \lesssim -20$ and applying the same corrections as above results in a consistent pair fraction of 1.7% for $0.12 < z < 0.55$, however. The bright sample of De Propris et al. (2005) corresponds to approximately the same luminosity range after adjusting for H_0. Correcting for pairs within 7 kpc by adjusting by 4/3, gives a pair fraction of 2.3% at a mean redshift of $z = 0.123$. Adjusting the pair fractions found by Le Fèvre et al. (2000) down by 65% results in values of 3.0, 5.3 and 12.6% at mean redshifts of 0.33, 0.63 and 0.91, respec-

tively. Bell et al. (2006b) find a fraction of 4% for $0.4 < z < 0.8$ using the selection criteria given above. Lin et al. (2008) select galaxies using $-21 < M_B^e < -19$ mag, corresponding to $0.4L^* < L < 2.5L^*$, with a passive evolution correction applied to select similar galaxies at all redshifts. Assuming an evolution correction of approximately 1 mag/z, this magnitude corresponds approximately to $-22 \lesssim M_B \lesssim -20$ mag, which can be directly compared with the results above. They require that pairs of galaxies have $10h^{-1} < r_p < 30h^{-1}$ kpc. This distance range should be roughly the same as requiring $r_p < 30$ kpc with $H_0 = 70$ km s^{-1} Mpc^{-3}. Making the same correction for projections in groups, their pair fraction ranges from 1.8% at $z = 0.014$ to 5.7% at $z = 1.08$. Their results are consistent with Lin et al. (2004) and De Propris et al. (2007).

To summarize these findings from close pair studies, there are conflicting estimates at $z \sim 0.1$ but the agreement seems to be slightly better at intermediate redshifts, where there are now good number statistics from a number of surveys. The pair fraction ranges from $\sim 2 - 6\%$ for $0.2 < z < 1.1$, with a higher estimate found by Le Fèvre et al. (2000) at $z = 0.9$ but with small number statistics. The discrepancies at low-z will need to be better understood to have confidence in the measured evolution of the merger rate. I do not compare directly to morphological estimates here, but note that recent results seem to be slightly higher (8–10% at intermediate redshifts) and almost constant (see Section 3.3 and Lotz et al. 2008a). This may be due to the inclusion of more minor mergers that can result in significant morphological distortions. The studies of Lotz et al. (2008a); Conselice et al. (2003); Cassata et al. (2005); De Propris et al. (2007) and Le Fèvre et al. (2000) are claimed to be consistent within the error bars. The range of results suggests that more work is needed on the observational side to clarify the role mergers play between $z = 1$ and $z = 0$. My aim in this chapter is to check that the SAM result lies within the fairly large range covered by the data, rather than resolving any of the differences between the observations. The comparison is aided by being able to apply the same selection criteria as the observational studies over the same range in redshift (Section 3.3 and 3.4).

The evolution of the merger fraction is often described as a power-law, with

$$f_m(z) = f_0(1+z)^m. \tag{3.1}$$

The halo merger rate has an exponent in the range of $2.5 \lesssim m \lesssim 3.5$ (e.g., Governato et al. 1999; Gottlöber et al. 2001) but most estimates for galaxies are lower than this. The difference can largely be resolved by the delay in time between the merger of the dark matter halos and the merger of the galaxies they contain (Berrier et al. 2006; Guo & White 2008). The measured values of m for galaxies span a wide range from $\sim 0 - 6$ (although most estimates are ≤ 4, see e.g., Table 2 in Kartaltepe et al. 2007 for a summary of previous results). The fit may be substantially altered when different estimates for the low-z anchor point are used (see, e.g., Kartaltepe et al. 2007; Lotz et al. 2008a), suggesting that tighter constraints on the local value are required. The redshift range over which the fit is made has a strong influence on the result,

but cosmic variance, small sample sizes and differences in method also play a role.

Very different conclusions on the average number of major mergers per galaxy and resulting mass growth have been drawn from the merger fraction results described above. The selection criteria, methods used to identify pairs, conversion from a pair fraction to a merger fraction and fraction to a rate, assumptions on the number density of the parent population and the uncertainty in the visibility timescale all contribute to the different estimates for how large a role mergers play in the evolution of galaxies since $z \sim 1$.

Overview of this chapter

In this chapter I present the merger rate and fraction for the Somerville et al. (2008) SAM as a function of mass, redshift and gas content (Section 3.2). We are able to make predictions of these quantities down to low masses, which are not yet possible to constrain observationally. In the mass range where observations exist, the results are broadly consistent. In Section 3.3 and 3.4, care is taken to use analogous methods and mass selections for the comparison of the model with observational results. The model predicts a merger rate and fraction that agree well with observations. These two sections present results from papers on which I am a co-author: Jogee et al. (2009) and Robaina et al. (2009b). In both cases I contributed the model prediction for comparison to the observational results.

3.2 The model merger rate and fraction

Definitions Numerical simulations have shown that the morphology of merger remnants depends sensitively on the mass ratio (e.g., Naab et al. 1999; Naab & Burkert 2003). The dynamics of the merger will be affected by the total mass in the central parts of the galaxies, rather than just the stellar mass. The mass ratio that has been used to determine morphology in the Somerville et al. (2008) SAM is therefore the ratio of the core masses at the time of the merger μ, where the core mass of each subhalo is defined as the total baryonic and dark matter mass within twice the NFW scale radius (see Section 2.2). This is approximately 60 kpc for a Milky Way-sized galaxy. To be consistent with this definition, I maintain the use of the core mass ratio to separate major and minor mergers, unless stated otherwise. Note that the stellar mass is used to determine the mass ratio and distinguish between major and minor mergers in observations. There can be a substantial difference between the two definitions.

Major mergers are defined to be those where the mass ratio is between 1:1 and 1:4 and minor mergers to be those where the mass ratio is between 1:4 and 1:10. Although this is a common choice there is wide variety amongst the different works on galaxy mergers and caution is required when comparisons are made. If the smaller of the two galaxies is less than $1/10^{th}$ of the mass of the larger, the mass is assumed to be accreted smoothly and no merger is recorded in the model.

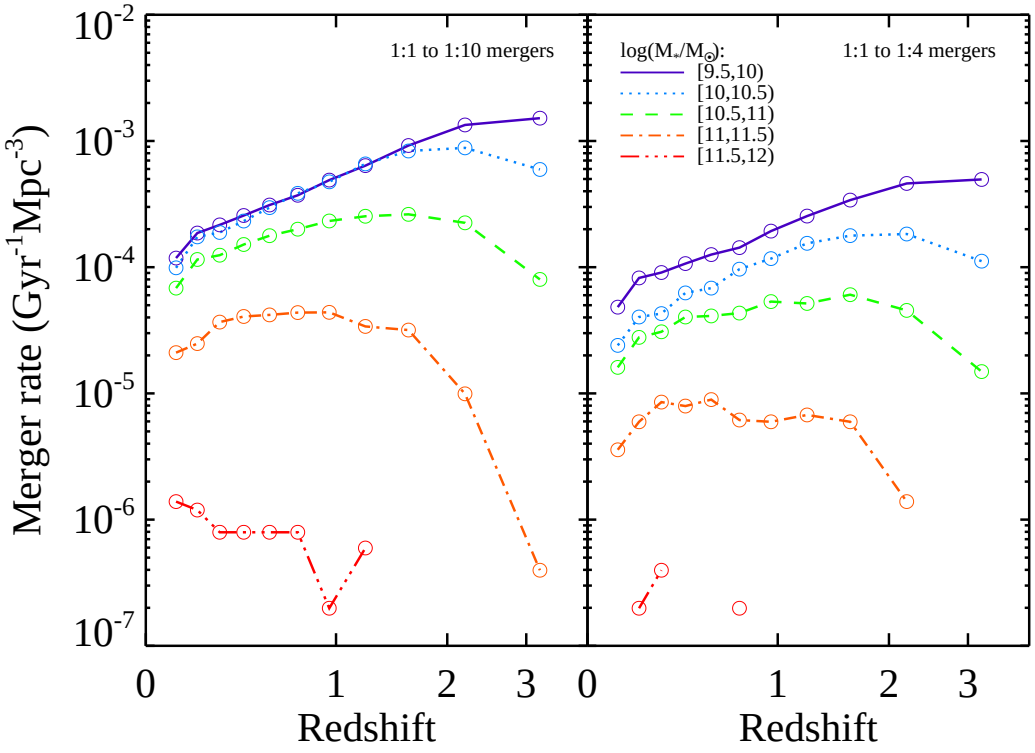

Figure 3.1: Model merger rate for progenitor galaxies in 5 mass bins, as a function of redshift. The left panel shows all mergers with mass ratios of 1:1 to 1:10, while the right panel shows the rate for major mergers, with mass ratios of 1:1 to 1:4.

The merger rate The model merger rate for galaxies above $3\times10^9 M_\odot$ is shown as a function of redshift in Fig. 3.1. The sample is complete to a mass 10 times smaller than the lowest mass bin boundary in order to include all major and minor mergers in each mass bin. The rate is determined by counting the number of merging pairs in the box simulation where the most massive of the two galaxies is within the mass bin under consideration. In this way, each merger is counted only once. The left hand panel of Fig. 3.1 shows the total rate of merging where the mass ratio can vary between 1:1 and 1:10. The right hand panel shows only major mergers, with mass ratios from 1:1 to 1:4. The rate in all but the highest mass bin increases from high redshift, as the number of galaxies of a particular mass grows, reaches a turnover point and declines toward lower redshifts. Galaxies in the highest mass bin have not yet reached the turnover point and have an increasing merger rate from $z \sim 1$ to the present day. The rates changes relatively slowly below a redshift of 1, particularly for galaxies with masses above $3\times10^{10} M_\odot$.

A measurement of the merger rate per volume for different mass bins convolves the number of mergers with the galaxy mass function. The highest mass galaxies have a much lower merger rate than low mass galaxies due to the small total number of galaxies at the massive end of the distribution. Each of the high mass galaxies is built up by multiple mergers, and undergoes

far more merging during its history than a low mass galaxy, however. The fraction of merging galaxies in each mass bin may be a more intuitive quantity to interpret.

The merger fraction The model mock catalogue, which records the time since the last merger for each galaxy, provides an opportunity to determine the merger fraction in an analagous way to the observational morphology measurements. This requires the assumption of a timescale over which a galaxy that has recently undergone a merger would be visible as a merger remnant. In what follows I use a timescale of 0.5 Gyr, but note that there is approximately a factor of 2 uncertainty arising from this assumption, as discussed above.

In Fig. 3.2, I show the merger fraction determined from the mock catalogue in equal volume bins out to a redshift of 1.5. In this case it is the remnant galaxy that is in the given mass bin, rather than the one of the progenitors, as in the rate calculation above. The horizontal error bars show the redshift range of each bin. The vertical error bars give the binomial error $[f(1-f)/N]^{1/2}$, where f is the fraction of remnants and N is the total number of galaxies in the mass bin. In all mass bins, the fraction decreases from redshifts $\gtrsim 1$ to the present day. Low mass galaxies have the lowest merger fractions, ranging from 17% at $z = 1.45$ to 4% at $z = 0.3$. The evolution of the merger fraction is very similar for the two lowest mass bins, suggesting that galaxies with masses below $3 \times 10^{10}\mathrm{M}_{\odot}$ have similar merger histories. This can also be seen directly from Fig. 3.1 as the mass function is relatively flat over this range of masses. In the highest mass bin the fraction decreases from 23 to 14% over the same range in redshift. The number statistics for galaxies with $M_{\star} > 10^{11}\mathrm{M}_{\odot}$ are small, particularly at higher redshifts – there are only 60 galaxies in the $1.4 < z < 1.5$ bin, for example.

The major merger fraction varies from 1 to 8% in the lowest mass bins, 3 to 12% for galaxies with $10.5 < \log(M_{*}/\mathrm{M}_{\odot}) < 11$ and 5 to 18% for galaxies with $\log(M_{*}/\mathrm{M}_{\odot}) > 11$. The fraction for high mass galaxies seems high, but the low total number of galaxies in this bin should be borne in mind. The values for intermediate mass galaxies agree reasonably with estimates of the merger fraction for galaxies with $M > 5 \times 10^{10}\mathrm{M}_{\odot}$ from Bell et al. (2006b) (5% for Combo-17 galaxies at $0.4 < z < 0.8$) although the fraction is slightly higher than the value they found at low-z ($\sim 1\%$) based on the correlation function of SDSS galaxies at $z \sim 0.1$. These were also shown to agree well with other observational estimates, correcting for differences in method and selection as far as possible, and with the prediction from a previous version of the Somerville et al. model.

Power-law fits to the evolution of the merger fraction (Equation 3.1) are shown by the dotted lines for each mass bin in Fig. 3.2. The fit parameters are summarized in Table 3.1. The most massive galaxies seem to undergo less evolution than lower mass galaxies, although this is largely driven by the low-z data point, which lies above the extrapolation from higher redshifts. The slopes are similar for the lower three mass bins. For major mergers there is a factor of $\gtrsim 2$ difference in normalisation. The slopes steepen compared to the total merger fraction in the lowest and highest mass bin. There are greater fluctuations over the redshift range so the

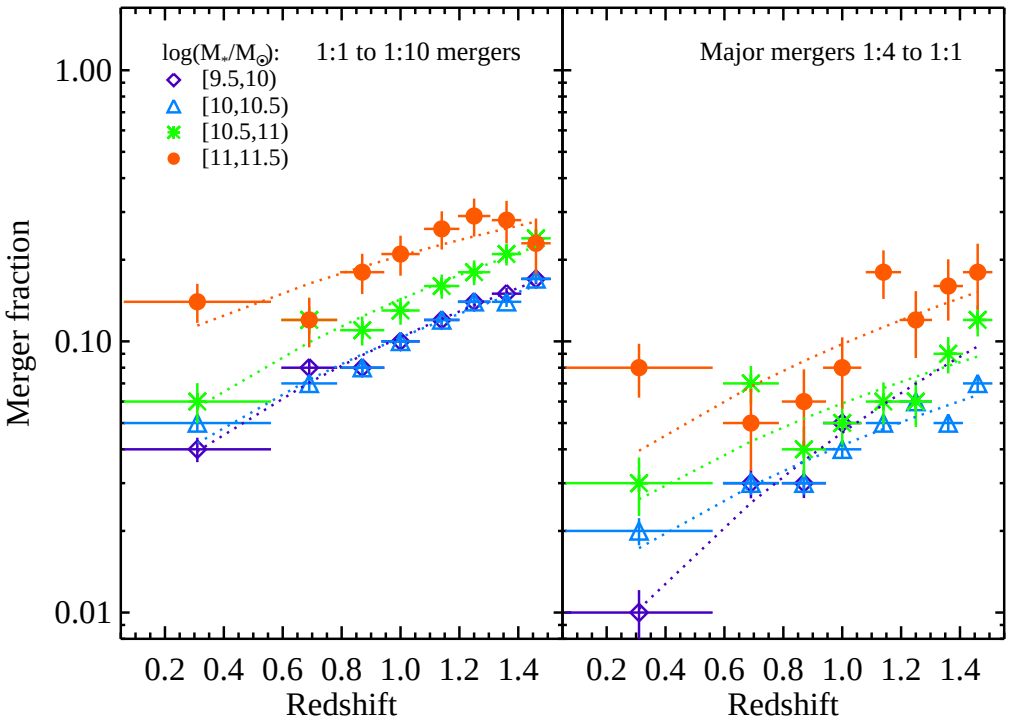

Figure 3.2: The fraction of remnant galaxies in 4 mass bins that have recently undergone a merger in the model, as a function of redshift. The left panel shows all mergers with mass ratios of 1:10 to 1:1, while the right panel shows the major merger fraction, with mass ratios of 1:4 to 1:1. The horizontal error bars show the redshift range of each bin. The vertical error bars represent the binomial term $[f(1-f)/N]^{1/2}$, where f is the fraction of remnants and N is the total number of galaxies in the mass bin. A power-law fit to the evolution in each mass bin is shown as a dotted line.

power-law does not provide an ideal fit.

Each of these fits is within the range encompassed by observations, but it is difficult to compare directly due to the different mass selections and methods used. Kartaltepe et al. (2007) summarize previous results in their Table 2, finding an average exponent of $m = 2.1$, and similar averages for both close pair and morphological methods. As they note, the evolution depends strongly on the redshift range included in the fit. Fitting the model results below $z = 1$ I find much slower evolution ($m \lesssim 1.5$) in all but the lowest mass bin. These fits, shown in the right hand columns of Table 3.1, illustrate how large an effect the redshift range can have. The evolution also depends on the type of galaxy, as shown by Lin et al. (2008) and discussed in the next section.

Table 3.1: The evolution of the merger fraction, parametrized as $f = f_0(1+z)^m$

	$0.1 < z < 1.5$				$0.1 < z < 1$			
	All mergers		Major mergers		All mergers		Major mergers	
$\log(M_*/\mathrm{M}_\odot)$	f_0	m	f_0	m	f_0	m	f_0	m
$[9.5, 10)$	0.021	2.29	0.006	2.88	0.024	2.02	0.004	3.54
$[10, 10.5)$	0.024	2.12	0.010	2.06	0.031	1.59	0.013	1.49
$[10.5, 11)$	0.032	2.16	0.016	1.92	0.041	1.68	0.027	0.96
$[11, 11.5)$	0.078	1.40	0.022	2.14	0.099	0.87	0.085	-0.53

Relative contributions from wet and dry mergers

The mass ratio and amount of gas present during a merger are thought to be the determining factors for the properties of the remnant. Gas is collisional and may shock or collapse to form new stars, whereas the purely gravitationally interacting dark matter and stars can be treated as collisionless fluids. During a dissipational (gas-rich or wet) merger, gas is funneled to the centre where it can contribute to new bursts of star formation or fuel the central supermassive black hole. Gas-poor or dry mergers do not result in enhanced star formation and maintain the relationships on which their progenitors lie (e.g. the fundamental plane, Nipoti et al. 2003; Ciotti et al. 2007).

The properties of merger remnants have been explored in depth using numerical simulations both with and without gas. Simulations with no gas have shown that boxy isophotes are produced from major mergers and disky isophotes from minor mergers (e.g., Naab et al. 1999; Naab & Burkert 2003). Including gas in the simulations has dramatic effects – even major mergers with gas may result in disky isophotal shapes (Barnes & Hernquist 1996; Bekki & Shioya 1997; Naab et al. 2006) and in both major and minor gas-dominated mergers disk galaxies may be produced (Robertson et al. 2006). The isophotal shapes of early-types are correlated with other properties – higher mass galaxies are more likely to have boxy isophotes, less rotational support, a core at the centre of their luminosity profile and be radio-loud (see, e.g., Pasquali et al. 2007, and references therein). More luminous ellipticals are also more likely to be found in denser environments and have rounder shapes (Hao et al. 2006; van der Wel et al. 2009). In a scenario where the most massive red sequence galaxies are built up through major mergers, with their most recent mergers dry, many of these correlations with mass would be naturally produced. Exploring the merger histories of galaxies as a function of gas content thus provides important insight into the galaxy formation process.

The colour of galaxies correlates strongly with the amount of gas they contain. Red sequence galaxies have low gas fraction, while blue cloud galaxies contain a high proportion of gas. Observationally, it is much easier to separate galaxies into classes based on their colours, whereas in the model, gas fractions are readily available. In Fig. 3.3 I show the colour–magnitude diagram for galaxies in the ΛCDM model at $z = 0$, colour-coded by the percentage of galaxies in each colour and magnitude bin that has a low gas fraction. I define a gas frac-

tion threshold of $M_{\rm cold}/(M_* + M_{\rm cold}) < 0.2$ to distinguish gas-poor and gas-rich galaxies. This choice is justified by the striking correspondence between the region dominated by gas-poor galaxies and the red sequence seen in the figure. The dashed line shows a typical colour-cut used to separate the red sequence and blue cloud. It is given by $u-r = -0.66-0.14M_r-0.25$, 0.25 mag below a straight-line fit to the red sequence means. This line is a very good indicator of where the fraction of gas-poor galaxies becomes higher than the fraction of gas-rich galaxies. At least at low-z, red galaxy mergers can be directly associated with dry mergers.

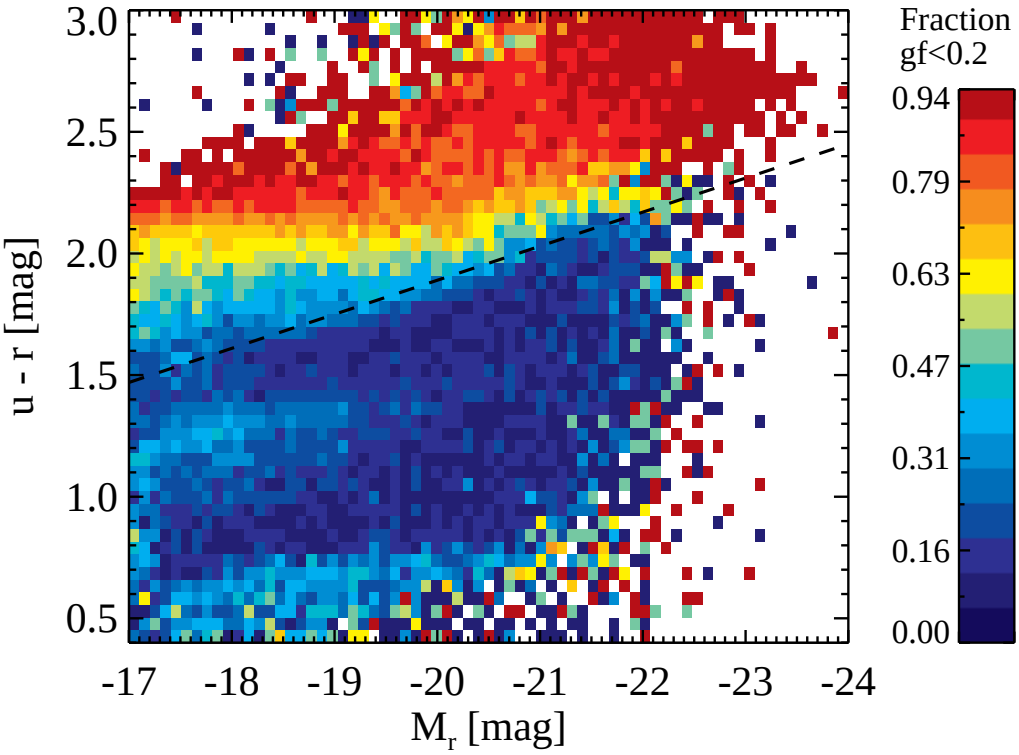

Figure 3.3: Model colour–magnitude diagram with colour-coding to show the fraction of galaxies in each bin that are gas-poor, where gas-poor is defined as a cold gas to total baryonic mass ratio of < 0.2. The dashed line indicates the separation between the red sequence and blue cloud, 0.25 mag below a fit to the red sequence. This corresponds closely to the transition from the region dominated by gas-poor galaxies to the region dominated by gas-rich galaxies.

In Fig. 3.4 I show the merger rate for progenitors of different gas fractions. A gas fraction threshold of 20% is used throughout. Mergers where both progenitors are gas-rich are termed "wet", mergers where one progenitor has a gas fraction lower than 20% are termed "mixed" and mergers where both progenitors are gas-poor are termed "dry". Galaxies of all masses have decreasing wet merger rates from $z \gtrsim 1.5$, with both the total and the major merger rate decreasing with similar slopes. There are very few major wet mergers for massive galaxies. The mixed merger rate is also decreasing with time, however the rate of decrease is slower, particularly for major mixed mergers. High mass galaxies have a fairly flat mixed merger rate

and have higher rates of mixed major mergers than wet major mergers. The number density of massive galaxies increases to low redshifts, thus a constant merger rate signifies an increase in the merger fraction for these galaxies. The dry merger rate is much lower than the wet merger rate at all redshifts and in all mass bins. It is roughly constant for low and intermediate mass galaxies and increases toward low redshifts for high mass galaxies. This reflects the build-up of massive galaxies on the red sequence through dry mergers at recent times. Low mass galaxies have low dry merger rates, despite their high number densities, as most of these galaxies lie in the blue cloud and have high gas fractions. Low mass galaxies on the red sequence are mostly satellite galaxies. Mergers between satellite galaxies are not accounted for in the model, as they are expected to be rare. The accretion of satellites onto higher mass central galaxies will be reflected in the total merger rate of higher mass bins.

These results agree qualitatively with the results presented by Lin et al. (2008) for dry, wet and mixed mergers from $0.2 < z < 1.2$ in the DEEP2 field, with other surveys used to supplement the data at low redshifts. Galaxies were selected to have evolution-corrected magnitudes in the range of $-21 < M_B^e < -19$ and a colour cut was used to separate red and blue galaxies, as a proxy for identifying gas-poor and gas-rich mergers. They note that selecting galaxies in this luminosity range results in different mass selections for blue and red galaxies, making it difficult to compare our results directly with theirs. The typical mass of a blue cloud galaxy is $2\times10^{10}\mathrm{M}_\odot$, while red galaxies with the same selection have typical masses of $\sim 10^{11}\mathrm{M}_\odot$. The merger fraction was estimated by counting kinematic close pairs. They find a declining total merger fraction with mild evolution and a more steeply declining wet merger fraction. Both the dry and mixed merger fractions increase over the redshift range under consideration. Wet mergers dominate at all redshifts, due to the higher number densities of blue cloud galaxies and lower mass range for blue cloud galaxies within their chosen magnitude limits. Comparing to the model results in the mass bins that include galaxies of their typical masses, I find similar trends in evolution. These results also agree with the relative contributions of different morphological types to the merger fraction as a function of mass and redshift found in other SAMs (Khochfar & Burkert 2003; Kang et al. 2007).

3.3 Major and minor mergers in GEMS

In this section I summarize the paper *"The history of galaxy interactions and their impact on star formation over the last 7 Gyr from GEMS"*, by Jogee, Miller, Penner, Skelton and the GEMS team (2009, ApJ 697, p. 1971), highlighting the comparison between the observations and the Somerville et al. (2008) model, which I contributed to the paper.

The paper explores the frequency of mergers out to $z \sim 0.8$ using data from the GEMS survey (Rix et al. 2004), an 800 arcmin^2 *HST* mosaic supplemented by multiwavelength data from Combo-17 (Wolf et al. 2004), the Spitzer infrared satellite (Rieke et al. 2004; Papovich et al. 2004) and the Chandra X-ray observatory (Alexander et al. 2003; Lehmer et al. 2005). The

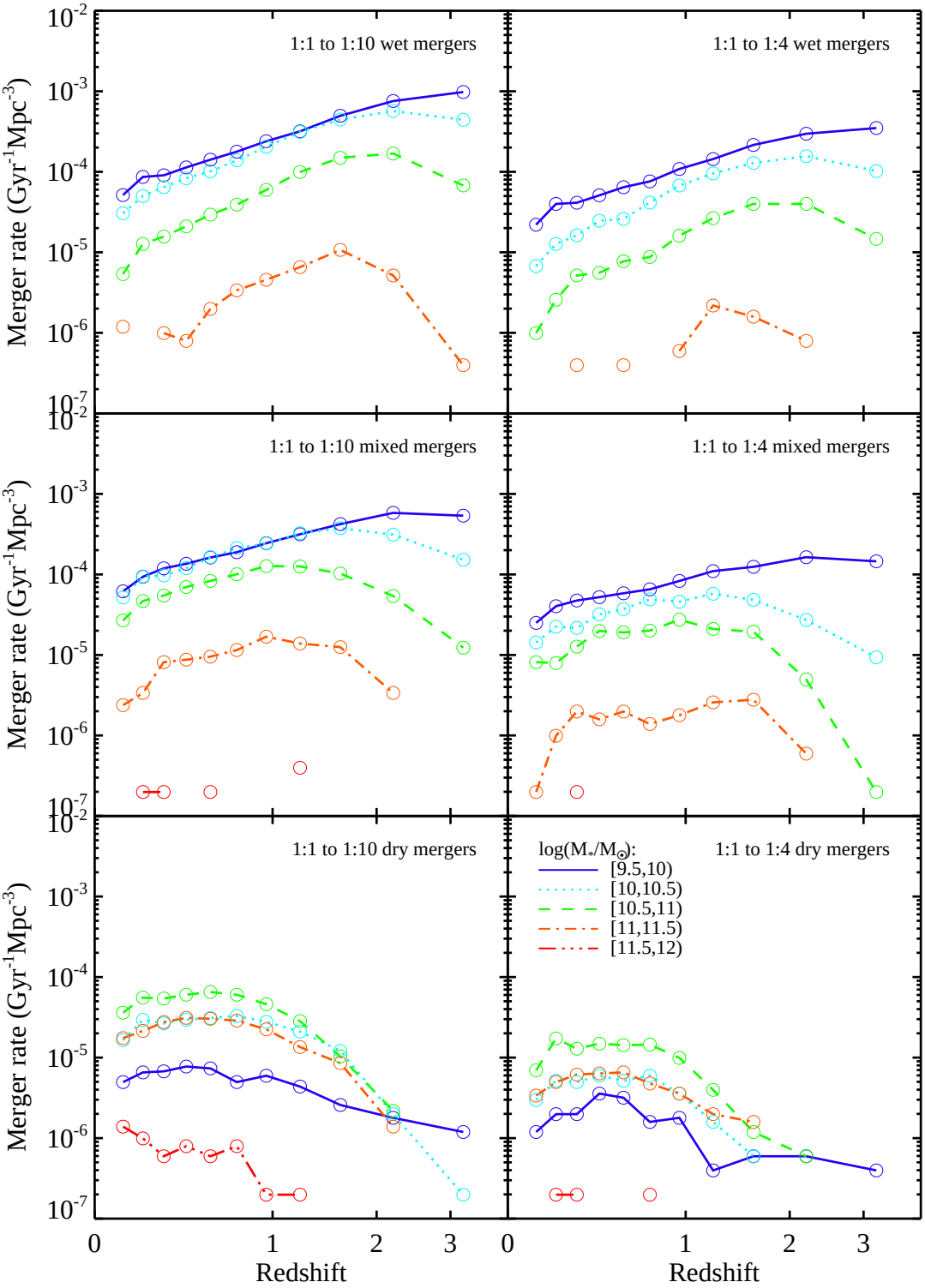

Figure 3.4: Model merger rates as function of z separated by the fraction of gas contained in each progenitor. If both galaxies have gas fraction < 0.2 the merger is described as dry, if one of the pair has a gas fraction < 0.2 it is mixed and if both have gas fractions higher than this it is wet.

merger fraction determined using visual classification is found to stay fairly constant, ranging from $9 \pm 5\%$ at $z = 0.8$ to $8 \pm 2\%$ at $z = 0.24$ for high mass galaxies ($M_\star \geq 2.5 \times 10^{10} \mathrm{M}_\odot$). Lower limits on the contributions from major and minor mergers over this redshift range are estimated to be 1.1 to 3.5% and 3.6 to 7.5%, respectively. Assuming a timescale of 0.5 Gyr, this translates into 68% of high mass galaxies having had a merger since $z \sim 0.8$, with a high proportion ($\sim$45%) of these likely to be minor mergers, 16% major and 7% ambiguous cases. The merger fraction and rate are compared to a number of different models of galaxy formation (halo occupation distribution, hydrodynamic SPH simulations and semi-analytic models). There is qualitative agreement between the observational results and model predictions but relatively large dispersion amongst the different models. The Somerville et al. (2008) model merger rates for all mergers and major mergers bracket the observed results.

3.3.1 Sample selection

Galaxies down to $R_{\mathrm{Vega}} \leq 24$ with *HST* ACS images in the F606W filter, spectrophotometric redshifts (Wolf et al. 2004) and stellar masses (Borch et al. 2006) from the Combo-17 project were selected from the GEMS field. Galaxy masses and photometric redshifts are based on the 17-band photometry from Combo-17. Simple dust-reddened single-burst spectral energy distribution (SED) templates (Wolf et al. 2004) were used to estimate an initial redshift. A more comprehensive library of template SEDs based on the Pégase stellar population synthesis models (Fioc & Rocca-Volmerange 1997) was then fitted to determine the mass-to-light ratio (Borch et al. 2006), assuming a Kroupa IMF (Kroupa et al. 1993). The stellar masses are consistent within 10% to those that would be derived using a Chabrier IMF. Borch et al. (2006) argue that the stellar masses have systematic errors of $\lesssim 0.1$ dex, with random errors from galaxy-to-galaxy of < 0.3 dex.

The F606W GEMS images were used for both the visual and automated classification, as they have higher signal-to-noise than the GEMS F850LP images, extending ~ 1.2 AB magnitudes deeper. Although galaxies are detected out to $z > 1$, the rest-frame wavelength of the F606W filter stays within the optical and near-UV below $z \sim 0.8$, making it possibly to classify the sample in a uniform way for $0.24 < z < 0.8$. Two samples of galaxies were considered. The high mass sample consists of ~ 800 galaxies with $M_\star \geq 2.5 \times 10^{10} \mathrm{M}_\odot$ and the intermediate mass sample of ~ 3700 galaxies with $M_\star \geq 1 \times 10^{9} \mathrm{M}_\odot$. The higher mass sample is complete for both blue cloud and red sequence out to $z = 0.8$. The lower mass sample misses red sequence galaxies in the high redshift bins, however.

3.3.2 Identification of mergers

Two classification schemes were used to identify galaxies as merging or interacting, non-interacting early-types and non-interacting late types. A visual classification was carried out by 3 of the authors independently (S. Jogee, S. Miller and K. Penner) and compared to the CAS

automated classification scheme (Conselice 2003). The CAS merger criterion were established using local samples and have not been thoroughly tested at high-z. It is thus important to compare the two methods for a large sample of galaxies out to high redshifts and establish how the merger fractions differ as a function of galaxy mass and redshift.

Visual classification The signatures of major and minor mergers seen in simulations were used to separate systems visually identified as mergers into finer divisions, providing the first observational estimate of the contribution of minor mergers to the total merger fraction. This is only possible using visual classifcation and is in most cases a subjective decision, as described below.

Major mergers are known to destroy stellar disks, transforming disk galaxies into spheroidal systems (e.g., Negroponte & White 1983; Barnes & Hernquist 1991; Mihos & Hernquist 1996; Naab & Burkert 2001). They typically produce extended tidal features such as bridges and tails, arcs, shells and ripples. Recent merger remnants often have asymmetric light distributions or double nuclei within a common envelope. Minor mergers, on the other hand, will not necessarily destroy the stellar disk of the more massive companion, but may excite perturbations such as warps, bars and spirals. These may lead to some of the tidal features described above, as well as rings or vertical heating of the disk (see the review by Jogee 2006, and references therein). Galaxies or very close pairs with these features were classified as major mergers (mass ratios 1:1 to 1:4), minor mergers (mass ratios 1:4 to 1:10) and ambiguous cases where the mass ratio could not be determined. In most cases the merging galaxies form a single distorted system that is unresolved by Combo-17 and thus has a single mass and redshift. The lower mass limit thus applies to the merger remnant, rather than progenitor galaxies. The classification as a major and minor merger in such cases is based on the appearance of the system, rather than mass estimates for each galaxy in a merging pair. In cases where the interacting galaxies are resolved, the measured mass ratio is used. Examples of some of the mergers are shown in Fig. 3.5.

Galaxies without large-scale distortions or very nearby companions are classified by their Hubble type (E–Sd) or as irregular. The non-interacting irregular class includes galaxies with asymmetries that seem to be internally triggered, by star formation for example. The scale of distortions in such galaxies is usually much smaller than in interacting galaxies (of the order of a few hundred pc rather than kpc). In automated classification methods, many of these are classed as mergers.

CAS classification The concentration, C, asymmetry, A, and clumpiness, S, were measured from the F606W image of each galaxy using the CAS code (Conselice 2003). The region demarcated by the cuts $A > 0.35$ and $A > S$ has been argued to capture merging galaxies, as it is dominated by galaxies with large asymmetries in the local optical data used for calibration (e.g, Conselice 2003, 2006). It may only be effective at recognising mergers over $\sim$ 1/3 of the merging period, however (Conselice 2006). We apply the same commonly-used criteria and

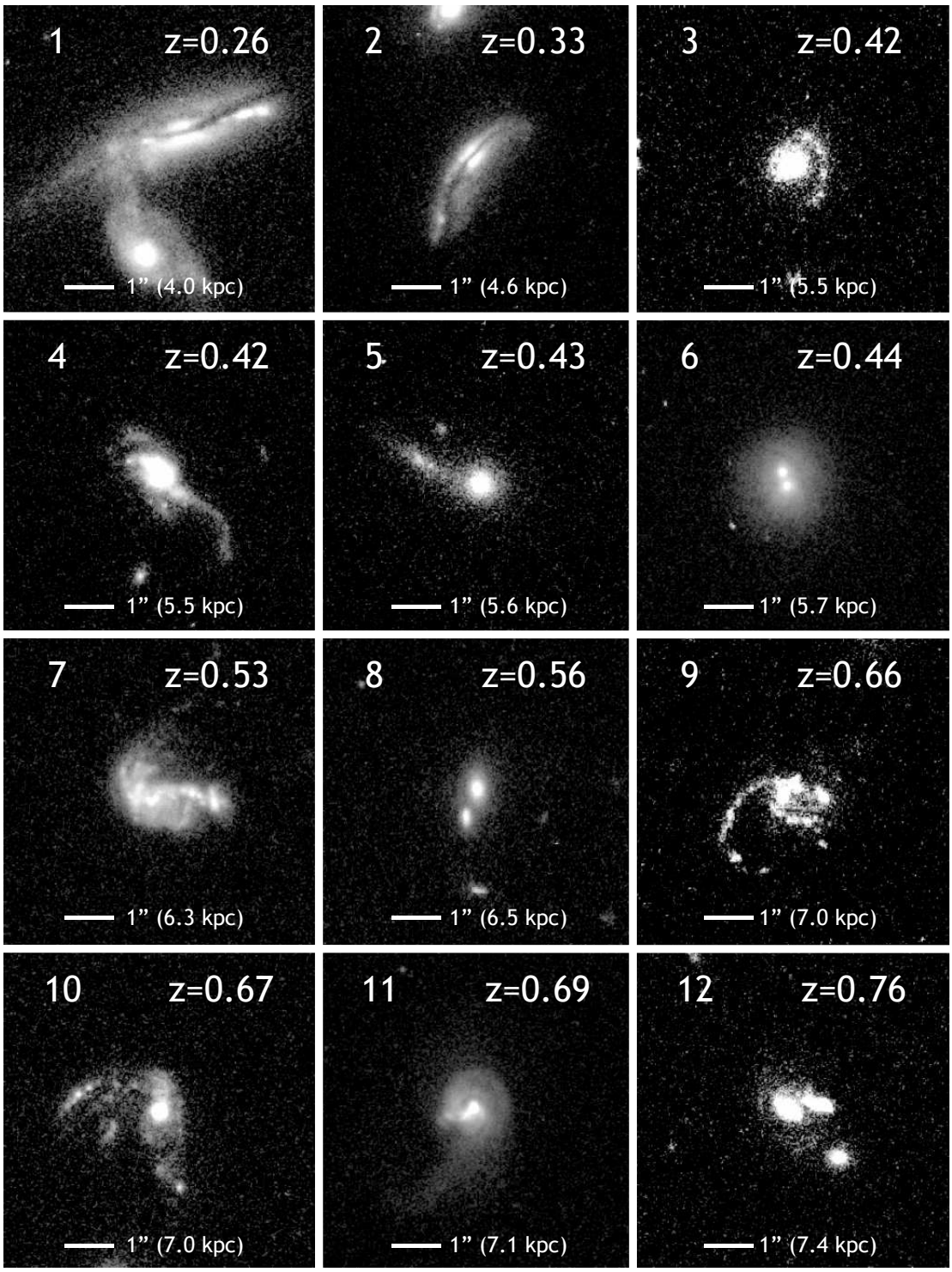

Figure 3.5: Examples of galaxies visually classified as mergers. Both advanced mergers (e.g. Panels 2, 3, 4, 5, 6, 7, 9 and 11) and young mergers (e.g. Panel 1) are included. Mergers are identified as major (Panels 1, 6, 12), Minor (Panels 2, 9) or ambiguous cases (Panels 3, 4, 5, 7, 8, 10, 11).

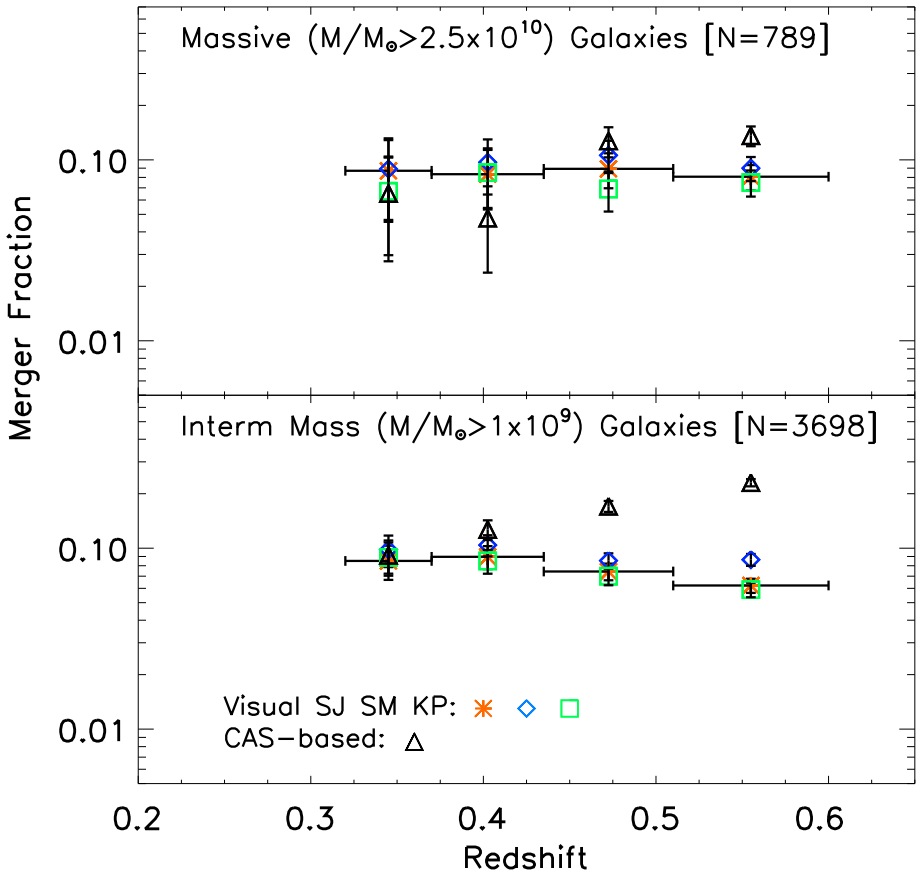

Figure 3.6: The merger fraction based on visual classification by three classifiers (SJ, SM, KP), compared to the fraction of mergers identified by the CAS method (triangles). The upper panel shows the merger fraction for high mass galaxies ($M_\star \geq 2.5 \times 10^{10}\mathrm{M}_\odot$). The lower panel shows the result for the intermediate mass sample ($M_\star \geq 1 \times 10^{9}\mathrm{M}_\odot$). The error bars represent only the binomial term $[f(1-f)/N]^{1/2}$ for each bin of size N.

compare the results to the visually identified mergers.

3.3.3 Results

Fig. 3.6 shows the resulting merger fraction for the high mass sample (upper panel) and intermediate mass sample (lower panel) for the three visual classifications and the CAS method. The error bar represents only the binomial term $[f(1-f)/N]^{1/2}$. The normalisation and trend agree amongst the three visual classifications. The dispersion between from classifier to classifier ranges from 15 to 26%. The latter value is combined in quadrature with the binomial term to represent the error in the fraction for the subsequent analysis. This is a conservative estimate of the error that should capture the uncertainties in the visual classification method.

For high mass galaxies, the fraction of merging galaxies captured by CAS agrees with the visual classification within a factor of 2. For the lower mass sample it is up to 3 times higher than the visual estimate in the high redshift bins, largely due to the inclusion of dusty, star-forming galaxies. In both mass bins the fraction of CAS mergers increases above the visual classification

for $z > 0.45$. In the high mass sample, approximately half of the visually classified mergers are also classified as mergers by CAS, while 66% of the intermediate mass sample are recovered. The recovery rate does not seem to depend strongly on redshift. The fractions of high mass galaxies classified as mergers by CAS but non-interacting visually are 34%, 75%, 72% and 67% in the four redshift bins. The corresponding fractions for the intermediate mass sample are 44%, 53%, 76% and 82%, indicating that the contamination rate is higher when lower mass galaxies are included, particularly at higher redshifts. These comparisons highlight that the two methods can return very different results, identifying different systems as mergers much of the time.

Redshift-dependent effects such as surface brightness dimming and bandpass shifting could contribute to the differences between the methods at high redshift. The results were tested for robustness against these effects using the deeper and redder F850LP images available for the GOODS field, which overlaps the central 20% of GEMS. The visual classification was repeated for $\sim$ 850 GOODS galaxies. The merger fraction for this sample increased marginally on average compared to the classification using GEMS images, with $\gtrsim 85\%$ of systems previously classified as mergers retaining this classification. The CAS parameters may change when deeper images are used, however (Conselice et al. 2008).

In what follows, we interpret the results only for the massive galaxy sample, due to the incompleteness of the red sequence for the lower mass sample. The fraction of high mass galaxies involved in mergers remains fairly constant, ranging from $9 \pm 5\%$ to $8 \pm 2\%$ in 1 Gyr bins from $z = 0.24$ to $z = 0.8$. The lower limits for major mergers are placed at 1.1 – 3.5% over this redshift range. The lower limits for minor mergers range from 3.6 – 7.5% and 1.2 – 2.0% are ambiguous cases.

The merger rate is calculated by transforming the fraction of galaxies that are involved in or have recently undergone a merger f via

$$R = \frac{N_{(M_\star \geq M_{\rm lim})}}{V} \frac{f}{t_{\rm vis}}, \tag{3.2}$$

where $N_{(M_\star \geq M_{\rm lim})}$ is the number of galaxies with a mass above the chosen mass limit ($M_{\rm lim} = 2.5 \times 10^{10} {\rm M}_\odot$), V is the comoving volume of the redshift bin and $t_{\rm vis}$ is the timescale over which a merger is recognizable. We assume that $t_{\rm vis} = 0.5$ Gyr but this has at least a factor of 2 uncertainty (see Section 3.1). This results in a fairly constant rate of $\sim 2 \times 10^{-4}$ Gyr^{-1} Mpc^{-3}. By integrating the merger rate, we find that $\sim 68\%$ of high mass galaxies have undergone a merger over the last 3 to 7 Gyr. Of these, $\sim$16, 45 and 7% are major, minor and ambiguous cases, respectively.

Comparison of observations and models

The merger fraction for high mass galaxies agrees well with a number of other observational studies, bearing in mind the different methods used and selection criteria. These are summarized

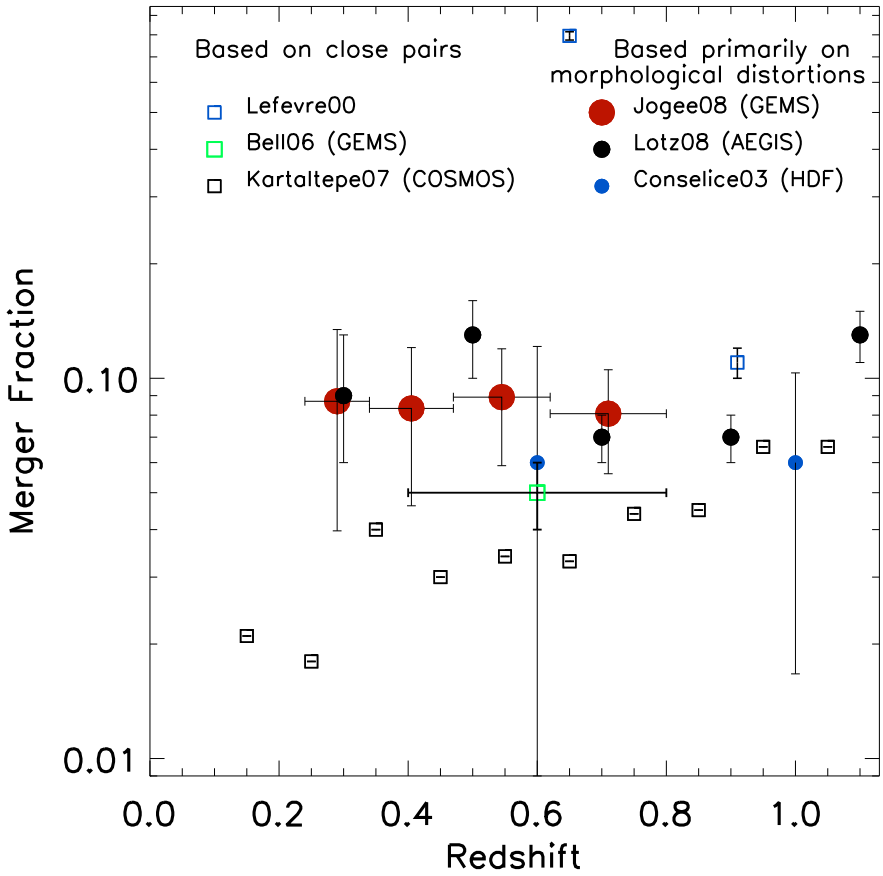

Figure 3.7: A comparison of the merger fraction for massive galaxies in GEMS and other observational studies, based on close pairs (squares, Le Fèvre et al. 2000; Bell et al. 2006b; Kartaltepe et al. 2007) or morphological classification (filled circles, Jogee et al. 2009; Lotz et al. 2008a; Conselice et al. 2003).

in Fig. 3.7. There is very good agreement with the morphological studies of Lotz et al. (2008a) for bright ($L_B > 0.4L^*$) galaxies in the Extended Groth Strip and Conselice et al. (2003) for the Hubble Deep Field (filled circles), although small number statistics limit the usefulness of the latter. Pairs of galaxies in the COSMOS field selected to have $L_V > 0.4L^*$ and projected separations of 5–20 kpc are shown by the black squares (Kartaltepe et al. 2007). In this case, the steeper evolution is largely driven by the low-z data, which are drawn from an SDSS Early Data release pair catalogue (Allam et al. 2004). The results of Bell et al. (2006b) and Le Fèvre et al. (2000) show better agreement. As discussed in the introduction, studies using close pairs tend to find slightly lower merger fractions, ranging from 2 – 6% out to $z \sim 1$. Most of these works use luminosity selections that capture only major mergers, whereas this determination includes minor mergers. This is likely to account for much of the difference. The lower limit for major mergers is in the range of the Kartaltepe et al. (2007) results, supporting this surmise.

Figure 3.8 shows a comparison of the observed merger fraction and merger rate with a number of theoretical models: halo occupation distribution (HOD) models (Hopkins et al. 2008), SAMs from Somerville et al. (2008), Bower et al. (2006) and Khochfar & Silk (2006), and a

cosmological smoothed particle hydrodynamics (SPH) simulation from Maller et al. (2006). Most of the models calculate the merger fraction by identifying mergers in simulation "snapshots", with the time between output redshifts approximately equal to the visibility timescale $t_{\rm vis}$. For the Somerville et al. (2008) model, I determine the merger fraction and rate from the mock catalogue introduced in Chapter 2. For each galaxy in the lightcone, which covers an area of approximately three GEMS fields, the times since the galaxy's last merger and major merger are recorded. The fraction of mergers is determined in an analagous way to the observations by dividing the number of galaxies in each redshift bin that have undergone a merger within $t_{\rm vis} = 0.5$ Gyr of their output redshift (assuming that they would be recognized as a merger remnant for this period of time) by the total number of galaxies above the mass limit. I use a mass limit of $M_{\rm lim} = 2.5 \times 10^{10}{\rm M}_{\odot}$, as for the observations. The merger rate is determined from the fraction using Equation 3.2.

We find that both the total (major+minor) merger fraction and the major merger fraction predicted by the Somerville et al. (2008) model agree well with the observations over much of the redshift range considered (as only a lower limit for the observed major merger fraction was obtained, these points are not shown in the figure). In the lowest redshift bin, the model fraction drops below the observations. This may be due to the small number statistics in this bin, which has the smallest volume, but this will affect both the model and observations. The major merger fraction for the model ranges from 1.5 to 4.5% between $z = 0.24$ and $z = 1$. The Khochfar & Silk (2006) and Somerville et al. (2008) models predict very similar total and major merger fractions. The Bower et al. (2006) model produces fewer minor mergers but approximately the same fraction of major mergers as the other SAMs. The HOD model predicts a higher total merger fraction, with the fraction of major mergers similar to the observed total fraction. Only a major merger fraction can be determined for the SPH model, which has limited dynamical range due to the huge amount of computational power required to simulate both dark matter and gas. SPH models are currently unable to match the galaxy mass function. The masses of galaxies at the knee of the mass function are too high, and there are too many galaxies of both high and low mass. The masses of galaxies from 2×10^{10} to $6 \times 10^{11}{\rm M}_{\odot}$ have been adjusted by a factor of 2.75 to account for this mismatch. With this correction, the SPH prediction lies in the same range as the major merger fraction of the HOD model.

There is reasonable agreement between the model merger rates and the observations. The Bower et al. (2006) SAM again produces a lower merger rate than the observations and other SAMs, while the HOD and SPH model results are higher than observed. The total and major merger rates in the Khochfar & Silk (2006) and Somerville et al. (2008) SAMs bracket the observed results. The main factor causing the model merger fraction and rate to differ relative to the observations is likely to be the difference between the mass functions out to $z = 0.80$ (see Section 2.3.1). The visibility timescale will also play a role – if mergers are observable for longer than 0.5 Gyr, the merger fraction in the models will be underestimated compared to observations even if the rates agree well.

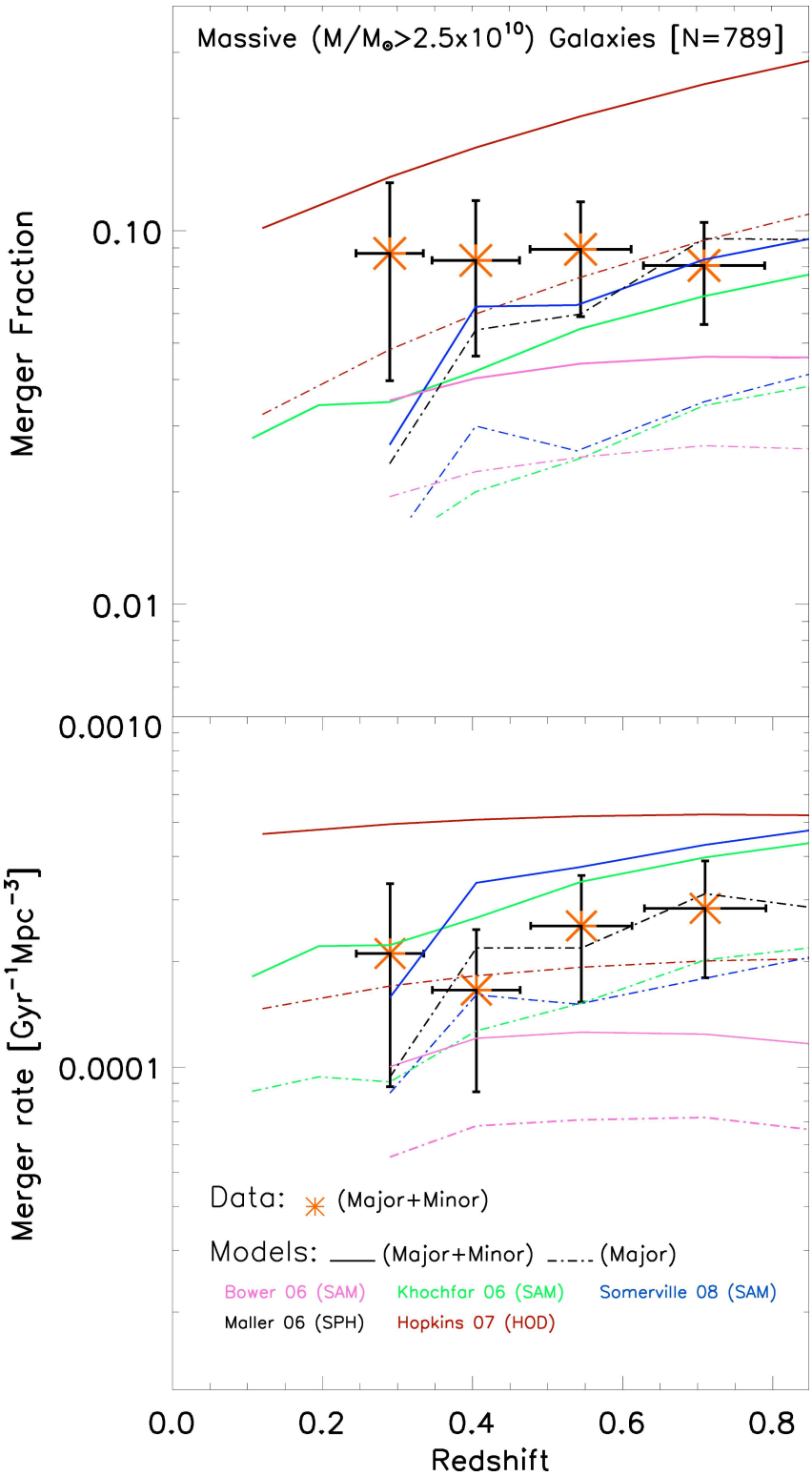

Figure 3.8: The observed total merger fraction (upper panel) and rate (lower panel) for massive galaxies in GEMS (data points with error bars) compared to different ΛCDM models: HOD models (Hopkins et al. 2008), SAMs (Somerville et al. 2008; Bower et al. 2006; Khochfar & Silk 2006) and an SPH simulation (Maller et al. 2006). Solid lines represent the total (major+minor) merger fraction/rate. Dash-dot lines show the major merger fraction/rate.

3.3.4 Summary

Using a large sample of massive galaxies ($M_\star \geq 2.5\times10^{10}\mathrm{M}_\odot$) in the GEMS field, we find that the fraction of galaxies classified visually as major or minor mergers ranges from $9\pm5\%$ at $z = 0.24$ to $8\pm2\%$ at $z = 0.8$. This corresponds to merger rate of $\sim 2-3\times10^{-4}$ Gyr^{-1} Mpc^{-3}. The CAS classification system identifies higher numbers of mergers at $z > 0.5$, with the difference enhanced when lower mass galaxies are included in the sample. The galaxies falsely classified as mergers are usually asymmetric as a result of star formation. There are fairly substantial differences between the two methods. The observed merger fraction agrees well with other morphological estimates and is higher than the estimates based on close pairs, likely as a result of including minor mergers. The lower limit for major mergers was found to be 1.1 – 3.5% from $z = 0.24 - 0.8$. We predict a total merger fraction ranging from 10 to 3% over the same redshift interval in the Somerville et al. (2008) model and a major merger fraction of 1.5 to 4.5%. These predictions agree well with the observational results over most of the redshift range considered, with the total merger fraction dropping to a lower value at $z < 0.4$. We find qualitative agreement between the observational results and a number of other models, but fairly large dispersion amongst the models.

3.4 Massive galaxy mergers in COSMOS and Combo-17

I present the results of the paper *"The merger-driven evolution of massive, red galaxies"* by Robaina, Bell, van der Wel, Skelton, Somerville, McIntosh, Meisenheimer and Wolf (2009, ApJ submitted). Here again, I contributed the results of the Somerville et al. (2008) SAM for comparison to the observations.

The merger histories of massive galaxies ($M_\star > 5\times10^{10}\mathrm{M}_\odot$) are explored using very large sample of galaxies selected from the COSMOS (Scoville et al. 2007) and Combo-17 surveys (Wolf et al. 2004). The two-point correlation function was used to determine the fraction of galaxies in pairs with separations of less than 30 kpc out to $z = 1.2$, with a low-redshift pair fraction calculated from the correlation function of SDSS galaxies used as a local benchmark. The observed fraction of galaxies in pairs varies between 1.5% and 3.15% between $z = 0.15$ and $z = 1.2$. This evolution can be parametrized as $f_m(z) = (0.0135 \pm 0.004)(1 + z)^{1.12\pm0.2}$. The model merger fraction is found to vary between 2.8 and 3.3% between $z = 0.2$ and $z = 1.2$, resulting in slower evolution given by $f_m(z) = 0.014(1 + z)^{0.27}$.

3.4.1 Observational method

The sample is drawn from the ∼2 square degree COSMOS survey (Scoville et al. 2007), supplemented by data from three widely separated Combo-17 fields, each of ~ 0.25 square degrees. The inclusion of the Combo-17 fields reduces the effects of cosmic variance by ∼30% (estimated from the results of Moster et al. 2009). The masses of COSMOS galaxies are estimated

from the broad-band photometry using a non-evolving template library derived from the Pégase stellar population synthesis model (Fioc & Rocca-Volmerange 1997) with a Chabrier IMF. The determination of stellar masses for Combo-17 galaxies, described briefly above, is detailed in Borch et al. (2006). Galaxies with masses $\geq 5 \times 10^{10} \mathrm{M}_{\odot}$ are selected from the COSMOS field for $0.2 < z < 1.2$ and in the Combo-17 fields out to $z < 0.8$, as beyond this redshift Combo-17 is no longer complete down to the mass limit. This results in a sample of ∼18000 galaxies.

The fraction of galaxies above the mass limit with separations of < 30 kpc is determined using the projected two-point correlation function (Davis & Peebles 1983), as the redshift errors translate into large line-of-sight distance uncertainties ($\sim 50 - 100$ Mpc). The correlation function gives the excess probability that galaxies are found at a particular distance compared to a randomly distributed sample (see Bell et al. 2006b; Robaina et al. 2009a, for more details). The real-space correlation function $\xi(r)$ is related to the projected correlation function via

$$w(r_p) = \int_{-\infty}^{\infty} \xi[r_p^2 + \pi^2]^{1/2} \, d\pi \, ,$$

where r_p is the projected distance between the galaxies and π is the line-of-sight separation. Assuming the real-space correlation function can be described as a power-law with exponent γ and normalisation r_0, the projected correlation function is given by

$$w(r_p) = C r_0^{\gamma} r_0^{1-\gamma}$$

with $C = \sqrt{\pi}\Gamma[(\gamma - 1)/2]/\Gamma(\gamma/2)$ (e.g., Bell et al. 2006b). This power-law is fitted to the data to obtain the values of γ and r_0. The results are corrected for the fraction of galaxies scattered beyond the maximum redshift difference allowed for each pair assuming the redshift error follows a Gaussian distribution, as shown by Wolf et al. (2003, 2004). The fraction of galaxies in close pairs (within a distance r_f of another galaxy) is then given by

$$P(r \leq r_f) = \frac{4\pi n}{3 - \gamma} r_0^{\gamma} r_f^{3-\gamma} \, , \tag{3.3}$$

where n is the number density (Bell et al. 2006b; Patton et al. 2000; Masjedi et al. 2006).

The fraction of galaxies in close pairs at low-z is calculated from Equation 3.3 using the correlation function parameters of SDSS galaxies from Li et al. (2006), adjusted by 5% to account for the difference in mass limit. The number density is taken from the g-band stellar mass function of SDSS galaxies (Bell et al. 2003), corrected for the different IMF and H_0.

3.4.2 Results and model comparison

The resulting fraction of galaxies in close pairs ($r < 30$ kpc) is given in Table 3.2 and shown in Fig. 3.9. Here the filled points show the results for the full sample, including both COSMOS and Combo-17 galaxies. The empty diamonds show the fractions obtained if only COSMOS

galaxies are used. The star shows the fraction of galaxies in close pairs obtained from the SDSS data. An error-weighted least squares fit of Equation 3.1 to the filled points is shown as a solid line. The resulting fit parameters are $f_0 = (0.0135 \pm 0.004)$ and $m = 1.12 \pm 0.2$.

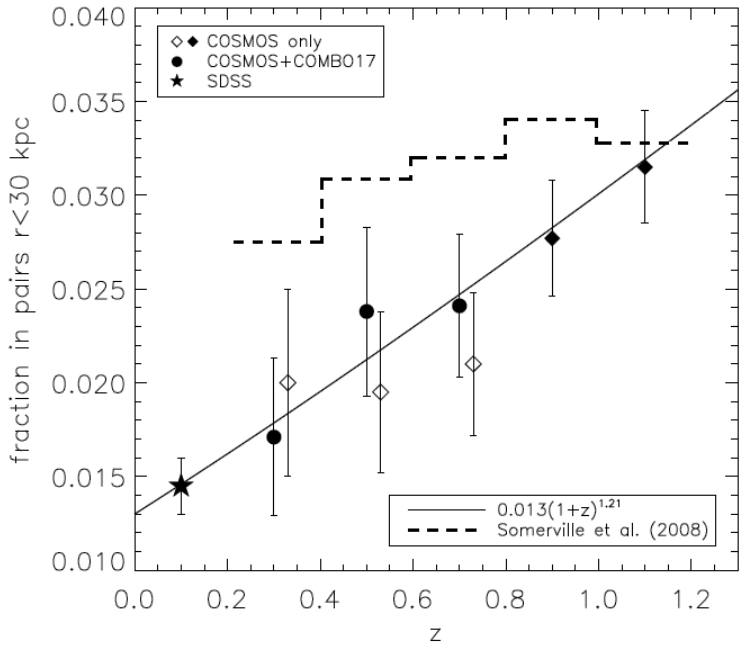

Figure 3.9: The fraction of galaxies with $M_\star \geq 5 \times 10^{10} \mathrm{M}_\odot$ in close pairs ($r < 30$ kpc) in the COSMOS and Combo-17 fields compared to the fraction of galaxies involved in mergers in the Somerville et al. (2008) SAM. The diamonds indicate the results for COSMOS alone (offset slightly and shown as empty diamonds in the range where Combo-17 data is available). The filled circles include the Combo-17 data. The star shows the pair fraction from the SDSS. The dashed line shows the predicted fraction of galaxies involved in merger in the model. A power-law fit to the data is shown as a solid line.

Table 3.2 and Fig. 3.9 also include the fraction of merging galaxies determined from the Somerville et al. (2008) SAM. The model result was calculated by counting the number of mergers in the box simulation where both galaxies have stellar masses of $M_\star \geq 5 \times 10^{10} \mathrm{M}_\odot$, giving a merger rate for galaxies above the mass limit in the volume of the simulation. The merger rate is converted to a fraction using Equation 3.2 with the number density of galaxies in the same mass and redshift range determined from the mock catalogue. This is then multiplied by two to obtain the fraction of galaxies in interacting pairs. The volume of the lowest redshift bins in the mock catalogue is small, resulting in less reliable estimates of the merger fraction.

The fraction of pairs in the model is slightly higher in all but the last redshift bin. Given the differences in mass function, which affect the number densities used to covert the model merger rate to a fraction, the agreement is encouraging. As for the observations, the evolution can be parametrized by $f_m(z) = 0.014(1+z)^{0.27}$. The overall normalization is in very good agreement with the observed fraction, but the evolution is slower. The difference in evolution may be the result of the small number statistics at low redshifts in the mock. In both the model

Table 3.2: The fraction of galaxies in close pairs from the COSMOS and Combo-17 fields compared to the Somerville et al. 2008 SAM

z	Observations $f_{\rm pair}(< 30{\rm kpc})$	Model $f_{\rm merge}$
$0.2 < z < 0.4$	0.0171 ± 0.0050	0.0275
$0.4 < z < 0.6$	0.0238 ± 0.0043	0.0309
$0.6 < z < 0.8$	0.0241 ± 0.0038	0.0322
$0.8 < z < 1.0$	0.0277 ± 0.0031	0.0337
$1.0 < z < 1.2$	0.0315 ± 0.0030	0.0325

and the data, most of the mergers are found to be major (ie. with a mass ratio between 1:1 and 1:4), even though no selection on mass ratio is made.

I find stronger evolution ($m = 1.64$) for the fraction of remnant galaxies with $M_\star \geq 10^{11}{\rm M}_\odot$ that have recently undergone a merger than the fraction of progenitor galaxies with $M_\star \geq 5 \times 10^{10}{\rm M}_\odot$ shown in Fig 3.9. This accounts for much of the difference between the slow evolution found here and the results in Section 3.2. This is likely to be due to the inclusion of other combinations of masses with mass ratios between 1:1 and 1:4 that will lead to such a remnant. Galaxies with stellar masses of $4 \times 10^{10}{\rm M}_\odot$ and $6 \times 10^{10}{\rm M}_\odot$, for example, will be included in the remnant fraction but not in progenitor fraction. The different redshift range and choice of bins also contributes to the slower evolution. There is reassuring agreement in the determinations of the merger fraction using the mock catalogue with a timescale of 0.5 Gyr and converting the merger rate from the box into a fraction as described above.

The observational and model results agree well with the fraction of 2.8% found by Bell et al. (2006b) for galaxies with masses above $3 \times 10^{10}{\rm M}_\odot$ in close major pairs ($r < 30$ kpc) between $z = 0.4$ and 0.8. The values are slightly lower than the 5% found in the same study by auto-correlating galaxies with $M_\star > 2.5 \times 10^{10}{\rm M}_\odot$. This difference can largely be attributed to an increase in the number of minor mergers included by lowering the mass limit. A pair fraction of $\sim$5% is found by repeating the analysis with the COSMOS data using a mass limit of $2.5 \times 10^{10}{\rm M}_\odot$. These results also in good agreement with the results of Jogee et al. (2009) described in Section 3.3, bracketed by the major and total merger fractions.

The low redshift fraction agrees with the estimate for SDSS from the Bell et al. (2006b) study, as well as the fraction found by McIntosh et al. (2008) for galaxies in dense environments. The pair fraction found by Xu et al. (2004) using 2MASS and the 2dFGRS is brought into agreement with the other results by correcting the fraction down by 30% to account for projections along the line of sight (see Bell et al. 2006b).

3.5 Conclusions

I have investigated the merger rate and fraction of galaxies in the Somerville et al. (2008) SAM as a function of mass and redshift. I find that rate is decreasing at $z < 1$ for all but the most

massive galaxies. The evolution depends on the mass range under consideration. Parametrizing the evolution of the merger fraction at $z < 1$ as $f \propto (1+z)^m$, I find values of m for the total merger fraction ranging from 2.29 for low mass galaxies ($M_\star < 10^{10}\mathrm{M}_\odot$) to 1.40 for the most massive galaxies ($M_\star \geq 10^{11}\mathrm{M}_\odot$). The slope of the evolution is similar in all mass bins with $M_\star < 10^{11}\mathrm{M}_\odot$. For major mergers, m varies between 1.92 and 2.88, with the strongest evolution for low masses, driven largely by the low-z bin. The evolution is slower when only redshifts below one are considered. The normalisation of the merger fraction increases with mass.

A gas-fraction threshold of 20%, corresponding closely to the transition from red sequence to blue cloud, is used to separate wet, mixed and dry mergers. The merger rate of gas-rich galaxies decreases from $z \sim 2$ to the present day. It follows the total merger rate closely, particularly in the lower mass bins which are dominated by blue cloud galaxies. Both the mixed and dry merger rates evolve more slowly. The dry merger rate is almost flat for $z \lesssim 1$ even for low mass galaxies, and increases with time for high mass galaxies. The increasing contribution from dry mergers over time reflects the depletion of gas and global decline in star formation rate since $z \sim 1$ (Lilly et al. 1996; Madau et al. 1996; Hopkins 2004; Le Floc'h et al. 2005). These results are in good qualitative agreement with the observed evolution and relative contributions of blue, mixed and red galaxy mergers found by Lin et al. (2008) for galaxies in the DEEP2 field and morphological mix of merging galaxies in other SAMs (Khochfar & Burkert 2003; Kang et al. 2007).

I have presented two studies where the merger fraction from the SAM was compared to the observed merger fraction. Care was taken to determine the model merger fraction in as analogous a way as possible to the observations, with the same redshift binning and mass selection. In the first (Jogee et al. 2009), the merger fraction for GEMS galaxies with masses above $2.5 \times 10^{10}\mathrm{M}_\odot$ was estimated using visual and automated morphological classification. The resultant merger fraction was found to be approximately constant, ranging from $9 \pm 5\%$ at $z = 0.24$ to $8 \pm 2\%$ at $z = 0.8$. The lower limit for the contribution from major mergers ranges from 1.1 to 3.5%. Both the normalization and slow evolution of the merger rate, as well as the contribution from major mergers, are reproduced by the model. The second study (Robaina et al. 2009b) used the galaxy correlation function on small scales to determine the fraction of COSMOS and Combo-17 galaxies with $M_\star > 5 \times 10^{10}\mathrm{M}_\odot$ in close pairs ($r < 30$ kpc). The fraction ranges from 1.5 – 3.2% from $z = 0.1$ to $z = 1.2$, agreeing well with the major merger estimate above. The fraction of merging galaxies in the model is slightly higher than the observations at low redshift, possibly due to the small volume of the low-z bins, but shows good agreement at $z \sim 1$. The model predicts milder evolution than the observations due to the higher fraction at low-z. The differences in evolution require more investigation.

The reasonably satisfying agreement between the model predictions and a range of observations that use different mass selections and means of identifying mergers gives some degree of confidence in the model merger histories. This qualitative agreement suggests that the merger

histories will be useful in building intuition on how galaxies are affected by mergers. Having found that the galaxy merger trees are fairly robust, I use them as the basis for further modelling to explore the effects of merging on the galaxy population in Chapters 4 and 5.

Chapter 4

The effect of dry mergers on the colour-magnitude relation

Abstract

I investigate the effect of dry merging on the colour–magnitude relation (CMR) of galaxies and find that the amount of merging predicted by a hierarchical model results in a red sequence that compares well with the observed low-redshift relation. A sample of $\sim$29, 000 early-type galaxies selected from the Sloan Digital Sky Survey Data Release 6 shows that the bright end of the CMR has a shallower slope and smaller scatter than the faint end. This magnitude dependence is predicted by a simple toy model in which gas-rich mergers move galaxies onto a "creation red sequence" (CRS) by quenching their star formation, and subsequent mergers between red, gas-poor galaxies (so-called "dry" mergers) move galaxies along the relation. I use galaxy merger trees from a semi-analytic model of galaxy formation to test the amplitude of this effect and find a change in slope at the bright end that brackets the observations, using gas fraction thresholds of 10 – 30% to separate wet and dry mergers. A more realistic model that includes scatter in the CRS shows that dry merging decreases the scatter at the bright end. Contrary to previous claims, the small scatter in the observed CMR thus cannot be used to constrain the amount of dry merging.

4.1 Introduction

Galaxies are found to occupy two distinct regions in colour–magnitude space, known as the red sequence and blue cloud (Strateva et al. 2001; Blanton et al. 2003). The blue cloud, made up mostly of star-forming late-type galaxies, is a broad distribution with large scatter in colour at all magnitudes. The red sequence is made up mostly of early-type galaxies with little continuing star formation. These galaxies lie along a tight colour–magnitude relation (CMR), which results primarily from the relation between mass and metallicity (e.g., Faber 1973; Larson 1974;

Kodama & Arimoto 1997; Gallazzi et al. 2006), in the sense that the most massive galaxies are the most metal rich and consequently redder.

The amount of stellar mass in the red galaxy population has approximately doubled since $z = 1$ (e.g., Bell et al. 2004; Brown et al. 2007; Faber et al. 2007); yet these galaxies have low levels of star formation which cannot account for the increase in mass. In contrast, the amount of stellar mass in blue galaxies remains approximately constant over the same time period, although these galaxies are actively forming stars. Much of the growth of the red sequence population can be accounted for by the truncation of star formation in $< L^*$ galaxies (Bell et al. 2007). There are relatively few galaxies found in the so-called "green valley" between the two populations, suggesting that the process that transforms the colours and morphologies of these galaxies, moving them from the blue cloud onto the red sequence, is fairly rapid. One such mechanism is the merging of galaxies, a natural consequence of hierarchical structure growth. The link between merging galaxies and the transformation of morphology was proposed as early as the 1940s, with Holmberg's classical paper on the clustering of "nebulae" (Holmberg 1940). This discussion was followed by the first N-body simulation of a galaxy interaction, in which he used light-bulbs to simulate the gravitational properties of two disk galaxies in close passage. He showed that tidal forces between two stellar systems could lead to the capture and subsequent merging of the two galaxies in certain cases (Holmberg 1941). The era of more sophisticated computer simulations began with the Toomre & Toomre (1972) paper on the tidal features of interacting galaxies. They were able to recreate the bridge and tail structures observed in a number of interacting galaxy pairs, as shown in Fig. 1.1. It was speculated that early-type galaxies may be the end-result of the merging process (see also Toomre 1977). A number of simulations since then have shown that this is the case – merging is a violent relaxation process that randomizes the orbital motions. Gas is furthermore funneled toward the centre and used up in a burst of star formation, resulting in remnants that are reddened and spheroidal in shape (e.g., Barnes & Hernquist 1996; Cox et al. 2006). Mergers are thus thought to play an important role in the quenching of star formation and movement of galaxies from the blue cloud onto the red sequence, particularly at intermediate masses.

The most massive $> L^*$ galaxies on the CMR are thought to form through mergers of galaxies that already lie on the red sequence and contain little gas. Models of galaxy formation predict that these dry mergers are important and they have been observed from their morphological signatures (van Dokkum 2005; Bell et al. 2006a; McIntosh et al. 2008) but concensus has not yet been reached on the observed merger rate and resulting growth of mass since $z \sim 1$. Merger rates based on close-pair counts indicate significant merger activity between $\sim L^*$ early-type galaxies (e.g., van Dokkum 2005; Bell et al. 2006a; McIntosh et al. 2008) with major dry mergers playing an increasing role towards lower redshifts and for more massive galaxies (e.g., Lin et al. 2008; Bundy et al. 2009). A key uncertainty in this approach is the assignment of a merging timescale. As described in Chapter 3, this uncertainty is considerable, exceeding a factor of 2. Other observations can indirectly constrain the dry merger rate; e.g., the evolution of

the stellar mass–size relation (McIntosh et al. 2005; van der Wel et al. 2008) and number density of the most massive early-type galaxies since $z \sim 1$ (e.g., Scarlata et al. 2007; Cimatti et al. 2006; Wake et al. 2006; Cool et al. 2008; Faber et al. 2007). The latter will be discussed in depth in Chapter 5.

The CMR provides another promising avenue to explore. Both the slope and scatter of the relation place constraints on the formation histories of early-type galaxies. The CMR is generally assumed to be linear; however, there is some debate whether there is a change of slope with magnitude. This is evident in the CMRs of some clusters (e.g., Metcalfe et al. 1994; Ferrarese et al. 2006) but a number of other determinations show no particular evidence for a break with magnitude (e.g., Terlevich et al. 2001; McIntosh et al. 2005). In the field, Baldry et al. (2004) used careful fitting of double Gaussians to the colour distribution of low-redshift red sequence of SDSS (York et al. 2000) galaxies to measure the mean colours of the red sequence and blue cloud as a function of magnitude. These relations were found to be well-described by a tanh function plus a straight line. The scatter in the CMR ranges from as little as 0.04 mag for the Coma and Virgo clusters (Bower et al. 1992; Terlevich et al. 2001) to 0.1 mag in other clusters and the field (Schweizer & Seitzer 1992; McIntosh et al. 2005; Ruhland et al. 2009). The intrinsic scatter limits the spread in age of the stellar populations (Bower et al. 1992, 1998, BKT98 hereafter). This was seen as evidence that elliptical galaxies formed at high redshifts, evolving passively thereafter; however, recent work shows that this scatter is consistent with a model for the constant growth of the red sequence through the quenching of star formation in blue cloud galaxies (Harker et al. 2006; Ruhland et al. 2009). BKT98 used a simple model to argue that dry merging would cause a decrease in slope and increase in the scatter of the relation. The tightness of the relation in clusters such as Coma would thus limit the amount of mass growth due to dry mergers to a factor of 2–3 at most since the majority of stars were formed.

Overview of this chapter

The core of the work presented in this chapter was originally published as a letter in the Astrophysical Journal (Skelton et al. 2009). In this chapter I reconsider the effect of dry mergers on the bright end of the CMR. As noted by Bernardi et al. (2007), colour is not expected to change during such mergers since there is no associated star formation; thus galaxies move horizontally as the mass of the system increases. In addition, the shape of the mass function suggests that a bright galaxy will preferentially merge with one of the more numerous fainter galaxies. These galaxies lie further down the CMR and are bluer; thus dry mergers cause a tilt toward bluer colours at the bright end. I show that this is indeed observed in the local CMR averaged over all environments, using data from the SDSS (Section 4.2). In the same spirit as BKT98, I use a simple toy model to investigate the consequences of dry merging, using galaxy merger histories from the Somerville et al. (2008) SAM set in a ΛCDM hierarchical universe (Section 4.3). I show that when scatter is included in the initial CMR, dry merging causes a

decrease in the slope and a tightening of the CMR at the bright end. Although dry merging does affect the evolution of the CMR, the predicted effect does not conflict with the observed relation. As throughout this thesis, I have adopted a cosmology with $\Omega_M = 0.3$, $\Omega_\Lambda = 0.7$, and $H_0 = 100h$ km s^{-1} Mpc^{-1} with $h = 0.7$.

4.2 The observed red sequence

I use a subsample of galaxies from the SDSS Data Release 6 (DR6; Adelman-McCarthy et al. 2008) selected from the New York University Value-Added Galaxy Catalog (NYU-VAGC; Blanton et al. 2005). I select galaxies in a thin redshift slice ($0.0375 < z < 0.0625$) with Galactic extinction corrected (Schlegel et al. 1998) Petrosian magnitudes $m_r < 17.77$, resulting in a sample of 72,646 objects. This range in redshift provides a significant number of bright galaxies but is narrow enough to avoid the need for volume and evolution corrections. The Sérsic magnitudes provided in the NYU-VAGC are used as an estimate of total magnitude, since Petrosian magnitudes are known to underestimate the total flux, particularly for early-type galaxies (Graham et al. 2005). The photometry of bright galaxies in the SDSS is also affected by the overestimation of the sky background, which leads to underestimated magnitudes (see, e.g., Bernardi et al. 2007). The change in slope seen at the bright end of the CMR would be enhanced by a systematic brightening of the magnitudes of the most massive galaxies; thus I expect the result to be robust to these photometric errors. `kcorrect_v4_1` (Blanton & Roweis 2007) is used to k-correct to rest-frame $z = 0.1$ bandpasses. The most reliable estimate of galaxy colour uses SDSS model magnitudes, where the r-band image is used to determine the best-fit (exponential or de Vaucoleurs) profile and only the amplitude of the fit adjusted in other bands. An equivalent aperture is thus used in both bands, resulting in an unbiased and high S/N estimator of colour in the absence of gradients across the galaxy. All methods using the same aperture in different bands (fiber magnitudes, model magnitudes or Sérsic magnitudes defined using the i-band Sérsic model as a convolution kernel for the other bands), as well as Petrosian magnitudes, give a very similar result. Sérsic models fit to each band separately give much greater scatter, and qualitatively similar curvature, compared to the higher S/N model magnitudes used here.

I have chosen to show the CMD in $g-r$ colour and r-band magnitude space because both the bimodality and a change in slope are obvious features; however, it was verified that these are also visible in other combinations of colour and magnitude. Concentration, given by $C = R_{90}/R_{50}$ where R_{90} and R_{50} are the radii enclosing 90% and 50% of the Petrosian flux, respectively, has been shown to correlate with galaxy morphology (Strateva et al. 2001; Shimasaku et al. 2001). I apply a cut of $C \geq 2.6$, a criterion that has been used to broadly select early-type galaxies in previous work using SDSS data (e.g., Bell et al. 2003; Kauffmann et al. 2003), to isolate the red sequence. This ensures that a Gaussian fit to the CMR is not pulled down by late-type galaxies at the faint end, where the separation between the two populations is less distinct. The remaining sample contains 29,017 galaxies and is complete for $M_r \lesssim -18.3$ mag.

The CMD for these galaxies is shown in the upper left panel of Figure 4.1. In each magnitude bin of 0.25 mag along the red sequence, I fit a single Gaussian function to the distribution of colours. Fitting a double Gaussian to account for residual blue cloud galaxies does not affect the position of the means along the red sequence. The mean and width of the Gaussians are shown as diamonds and bars in the figure. It is clear that the slope of the relation changes with magnitude, flattening at the bright end. Straight lines fitted to the means above and below $M_r = -21$ mag are shown as dashed lines in all panels to facilitate comparison with the model. The faint-end fit, given by

$$^{0.1}(g-r) = 0.10 - 0.04^{0.1}M_r\,, \tag{4.1}$$

is used as the input creation red sequence (CRS) for the model, as described below.

4.3 Modeling the effect of merging along the red sequence

I would like to isolate the effect of dry merging on the colours of galaxies on the red sequence through a simple toy model. This approach is similar to previous work by BKT98; however, I use galaxy merger histories from an up-to-date model of galaxy formation and make different assumptions about the formation of the red sequence. I suppose that quenching of star formation – either through merging between gas-rich galaxies ("wet" mergers) or dwindling gas supply – places galaxies on a CRS, whereas the BKT98 model assumes that the relation is in place at some formation epoch. Galaxy merger trees and information on the masses and gas fractions of merging galaxies are extracted from the Somerville et al. (2008) SAM. The full SAM, which incorporates star formation and feedback effects, produces a bimodal colour distribution in broad qualitative agreement with observations, as shown in Section 2.3.1. Simple assumptions are made to determine the magnitudes and colours of galaxies on the red sequence after merging events rather than using the luminosities given by the full model, however. In this way the effects can be directly attributed to merging rather than trying to disentangle the complex mix of baryonic processes included in the SAM, and the differences between the observed and model luminosity evolution are avoided.

Dark matter (DM) merger histories are constructed using the extended Press–Schechter formalism, as described in Somerville & Kolatt (1999) but with the modifications described in Somerville et al. (2008), which lead to better agreement with N-body simulations. Galaxies within the merged DM halos lose angular momentum through dynamical friction and fall toward the center, merging some time later (see Somerville et al. 2008, and Chapter 2 for details). I follow the merger histories of galaxies within all halos with $\log_{10}[\mathrm{M_{halo}}/\mathrm{M_\odot}] > 11.7$, rather than just cluster-sized halos as BKT98 did. I consider mergers with mass ratios between 1:1 and 1:10, where the mass used is the DM mass within twice the characteristic NFW scale radius plus the total baryonic mass; however, only major mergers (mass ratios between 1:1 and 1:4) are assumed to be sufficient at quenching star formation resulting in a remnant on the CRS. The magnitude of the remnant galaxy is found from the total stellar mass of the

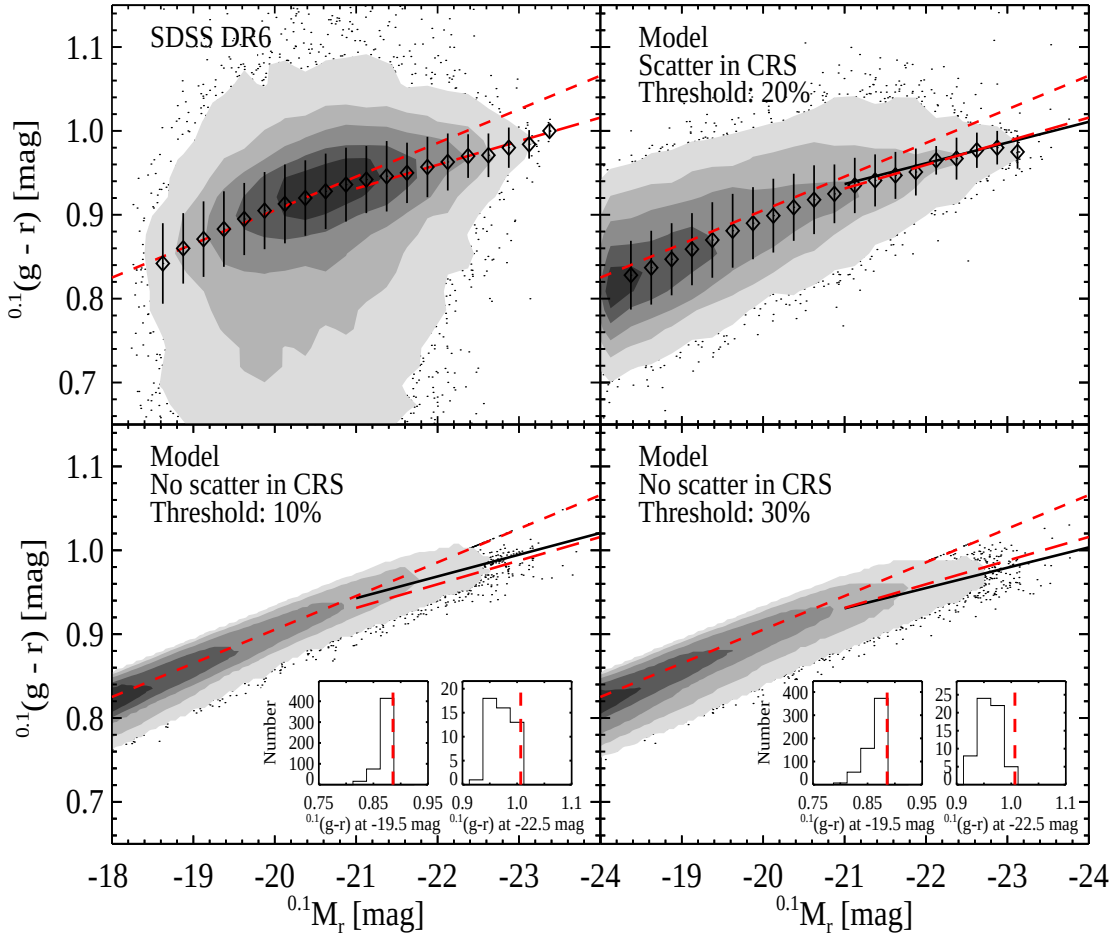

Figure 4.1: Red sequence from SDSS observations compared to a toy model for dry merging. The upper left panel shows the CMD of galaxies with concentrations of $C \geq 2.6$ from the SDSS DR6. The upper right panel shows the red sequence for a model which includes scatter in the CRS, with a gas fraction threshold of 20%. The contours enclose 2, 10, 25, 50 and 75% of the maximum value. The mean and scatter of the distribution binned in magnitude are shown as diamonds and bars in the upper panels. The short dashed lines in all panels show the fit to the observed means for magnitudes fainter than $M_r = -21$ mag, extended over the whole magnitude range to illustrate the change in slope at the bright end. Long dashed lines show the fit to the bright end ($M_r < -21$ mag) of the observed relation while fits to the model distributions are shown as solid lines. The lower panels show the model red sequence using gas fraction thresholds of 10 and 30% with no scatter in the initial relation. The inset histograms show the distribution of colours in two magnitude bins 0.1 mag wide, centered on ${}^{0.1}M_r = -19.5$ and ${}^{0.1}M_r = -22.5$ mag. In the faint bin, most galaxies still lie on the CRS (dashed lines), while in the bright bin most galaxies have undergone dry mergers and moved off the initial relation.

two progenitors using the M/L ratio of low-redshift red sequence galaxies produced by the SAM (${}^{0.1}M_r = 2.87 - 2.22\log_{10}[\mathrm{M}_*/\mathrm{M}_\odot]$). For each of the progenitor galaxies, I determine the fraction of baryonic mass contained in cold gas. If either galaxy has a gas fraction above some threshold, the merger is assumed to be wet and produces a remnant galaxy on the CRS. In order to compare directly with observations I have used the measured faint-end slope and zeropoint of the observed red sequence to specify the remnant's colour. The CRS is thus given by Equation 4.1, as described in Section 4.2 and shown by the short dashed lines in all panels of Figure 4.1. In so choosing, I assume that all gas-poor galaxies appear on the CRS at the epoch of interest, and evolve passively (and identically) thereafter. Accordingly, one can parameterize a galaxy completely by the $z = 0.1$ colour and magnitude. Subsequent dry merging, where the gas fraction is below the chosen threshold, produces remnant galaxies with colours and magnitudes determined by the simple combination of the progenitor colours and magnitudes. In cases where a galaxy's recorded merger history has no major wet mergers, the first gas-poor progenitors to merge are assigned colours on the CRS and the remnant's properties are determined as above.

In Figure 4.1 I compare the observed red sequence (upper left panel) with the CMR of remnant galaxies in the model, using gas fraction thresholds ranging from 10 to 30%. A linear regression to the bright end ($M_r < -21$ mag) of the model distribution is shown as a solid line in each case. There is a clear tilt toward a shallower slope for bright galaxies produced by merging, with the slope and break point sensitive to the chosen gas fraction threshold. The observed bright-end slope is bracketed by models with thresholds of 10% and 30% (lower panels). Using a lower threshold, more mergers are defined as wet, with remnants placed directly onto the CRS, and thus there are fewer remnants of dry mergers with bluer colours than the initial relation. This can also be seen in the inset histograms in the lower panels, which show the distribution of colours in magnitude bins of 0.1 mag centered at ${}^{0.1}M_r = -19.5$ and ${}^{0.1}M_r = -22.5$ mag. In the faint bin, the distribution peaks on the CRS (dashed line) showing that most of the faint galaxies have not had dry mergers. In contrast, most of the galaxies in the bright bin have undergone dry mergers and are predicted to lie significantly blueward of the CRS at the present day. The shift away from the CRS is smaller when the gas fraction threshold is lower; furthermore, the slope at the bright end changes less dramatically and the break from the CRS occurs at brighter magnitudes.

The upper right panel of Figure 4.1 shows the effect of including scatter in the initial relation, with a gas fraction threshold of 20%. I assume that galaxies produced by wet mergers are normally distributed about the CRS, with the width of the distribution given by the average observed scatter for galaxies with $M_r > -21$ mag (0.046 mag). I fit a Gaussian to the colour distribution in each magnitude bin of 0.25 mag, in the same way as for the observations. The means and widths of these Gaussians are shown as diamonds and bars in the figure. The slope at the bright end decreases as expected from the models without scatter, while the relation becomes tighter, with decreasing scatter toward the bright end. The means of the Gaussians are offset

slightly from the observed relation due to the small fraction of dry mergers taking place at all magnitudes. Applying a small zeropoint offset (~ 0.01 mag) to the CRS with a corresponding change in gas fraction threshold would account for this difference without affecting the result. The scatter around the mean in the most luminous bins is slightly smaller in the observations; however, note that there are very few galaxies in the brightest bins and thus the Gaussian fits are more tentative.

4.4 Discussion and conclusions

The existence of a tight CMR over a wide range in magnitude has been used to argue against the importance of dry mergers for the growth of red galaxies, since they were expected to flatten the relation and increase the scatter (BKT98); yet there seem to be few plausible alternative mechanisms for the creation of the most massive galaxies on the red sequence. I revisit this apparent conflict, showing that the red sequence for local field galaxies from the SDSS has a change in slope at the bright end and that a toy model for dry merging in a hierarchical universe produces a red sequence that is consistent with these observations.

In the simplest model, remnants of wet mergers are placed on a CRS with no scatter. Subsequent dry merging results in a tilt toward bluer colours at the bright end and an increase in the width of the relation as remnants move off the initial line. A change in the slope of the CMR was predicted by the model of BKT98; they assumed that the initial red sequence formed at a given *time* and that subsequent merging at all stellar masses was dry, shifting the entire population to bluer colours. In contrast, I find that the relation will flatten only at the bright end. The formation of the red sequence is associated with an *event* (a gas-rich merger). This leads to little change at the faint end (most mergers there are gas-rich) and a stronger change at the bright end (most mergers there are dry). The change in slope and magnitude at which the break occurs depend strongly on the assumption of a gas fraction threshold below which mergers are assumed to be dry. I find that gas fraction thresholds of 10% and 30% bracket the observed relation. The brightest galaxies in all environments (halo masses) experience growth through dry mergers thus I do not find an offset for brightest cluster galaxies compared to the rest of the population at the same luminosity. This seems to agree well with the work of Bernardi et al. (2007) where the CMR for BCGs is compared to a sample of early-types.

A model including scatter in the CRS shows a similar change in slope to the models without scatter, as well as a reduction in scatter at the bright end as a consequence of the central limit theorem. The width of the relation is thus only increased by dry merging when the initial relation is assumed to have no scatter. The scatter in the observed relation is slightly smaller than in the model; however, in this simple model differences in the age or metallicity of the galaxies involved in mergers have not been accounted for. I have assumed the CRS has the same scatter as the faint end of the observed red sequence of local galaxies, which has a contribution from the aging of the stellar populations (Gallazzi et al. 2006). If dry mergers occur soon after galaxies

arrive on the red sequence, the difference in colour between merging galaxies will be smaller than the scatter of the total population and thus the scatter in colour of dry merger remnants will be even smaller than predicted.

Chapter 5

The evolution of early-types in a hierarchical universe

Abstract

I explore the evolution of early-type galaxies by incorporating stellar population synthesis modelling into the hierarchical merging model developed in the previous chapter. A realistic red sequence galaxy population at $z \sim 1$ can be produced through the passive aging and merging of galaxies that formed all their stars at relatively recent times ($z \sim 2$) or through recent quenching of more continuous star formation in galaxies that began forming early ($z \sim 4$). The change in colour and magnitude thereafter depend on the star formation history, but also have a strong dependence on whether mergers and star formation continue after $z = 1$. A model with no merging after $z = 1$ predicts too much evolution in luminosity at a fixed space density compared to observations. For such a model, the change in colour and magnitude at a fixed mass resemble that of a passively evolving population that formed at $z \sim 2$. Recent dry mergers result in less rapid evolution in luminosity and colour, while the recent addition of young stellar populations in galaxies that have their star formation quenched after $z = 1$ reduces the changes even further. The resultant evolution is much slower, resembling the passive evolution of a population that formed at high redshift ($z \sim 3 - 5$). The slow observed evolution of early-type galaxies, usually assumed to be the passive evolution of an old population, can thus be explained as the result of hierarchical growth.

5.1 Introduction

There have been two competing views for the formation of early-type galaxies, dating back to the 1970s (Eggen et al. 1962; Larson 1975). In the first, known as monolithic collapse, spheroidal galaxies form early through the collapse of clouds of gas into stars, with the majority of stars forming within a relatively brief period of time. In the second, now standard view, all

galaxies form in a hierarchical process. The stars in an individual galaxy may originate from a number of smaller galaxies that formed at different times and subsequently merged, following the mergers of the dark matter halos in which they are embedded. Despite the strong evidence that we live in a hierarchical universe, the colours and magnitudes of early-type galaxies have evolved little over the last half of the Universe's history and are consistent with that of an old population of stars formed at high redshift (e.g., Tinsley 1968; Ellis et al. 1997; Bower et al. 1998; Wake et al. 2006; Cool et al. 2008). This argues for little recent evolution from mergers and when naively interpreted, lends support to the first picture. How can we reconcile the observed evolution of the early-type population with the standard view of galaxy formation?

The majority of early-type galaxies are red in colour and lie on a tight colour-mass (or magitude) relation (CMR) known as the red sequence. This relation can largely be attributed to an increase of metallicity with mass, with more metal rich galaxies having redder colours (Kodama & Arimoto 1997; Gallazzi et al. 2006). Most star-forming galaxies have disk morphologies and lie in a region of colour–magnitude space called the blue cloud. The total mass of galaxies on the red sequence has grown by a factor of 2 since a redshift of 1 (Bell et al. 2004; Faber et al. 2007), although most new stars form in the blue cloud. At intermediate masses, this growth can be accounted for by an influx of blue cloud galaxies that have had their star formation shut down (Harker et al. 2006; Bell et al. 2007; Ruhland et al. 2009), with merging being a likely mechansism for rapid morphological and colour transformation. The growth in mass on the red sequence has been well measured only for galaxies near the knee of the luminosity function ($\sim L^*$); consensus has not been reached on whether the number density of massive galaxies has evolved since $z = 1$. It has been argued that there is less evolution at the massive end than for lower masses (e.g., Brown et al. 2007)

If growth does occur at the bright end of the red sequence, it must take place through the merging of gas-poor galaxies that already lie on the red sequence, since their colours are such that they cannot have formed through the recent monolithic collapse of gas into stars and there are no brighter disk galaxies that could have faded and reddened to form them. Dry mergers do occur in the local Universe (van Dokkum 2005; Bell et al. 2006a; Tal et al. 2009), and a non-negligible fraction of massive galaxies are found to occur in close pairs that are likely to merge (Bell et al. 2006b; Robaina et al. 2009b, although see Masjedi et al. 2006, who measures very low merger rates for luminous red galaxies). Recent measurements place the fraction of $M_* > 5 \times 10^{10}\mathrm{M}_\odot$ galaxies in close pairs at 1 to 3% out to $z = 1$, implying that such galaxies undergo 0.7 mergers on average since this time (Robaina et al. 2009b, see Chapter 3). The interpretation of merger rate measurements in terms of red sequence growth requires a number of assumptions. A particularly large uncertainty is the determination of the timescale over which dry mergers can be identified, either as close pairs or through morphological signatures. The merger fraction described above seems to be sufficient to explain the growth of the red sequence above $\sim 10^{11}\mathrm{M}_\odot$ since $z = 1$.

To determine how the massive end of the red sequence evolves, one would ideally want to

measure the mass function; however, this requires combining the measured luminosity function (LF) with knowledge of the mass-to-light ratio, which also evolves. Stellar population synthesis models are usually used to estimate the mass-to-light ratio, requiring assumptions on the age and star formation histories of the galaxies. To measure these quantities, the evolution must be known – this circularity is one of the reasons that passive evolution is often assumed for early-types. The number density of massive galaxies will increase through merging but at the same time, the stellar populations of the galaxies evolve, becoming fainter and redder with time because there is little new star formation. The evolution of the luminosity function thus incorporates these two counteracting effects. Recent work on the evolution of the LF of massive red galaxies since $z \sim 1$ found changes in number density consistent with the purely passive fading of an old population (Wake et al. 2006; Brown et al. 2007; Cool et al. 2008; Banerji et al. 2009), suggesting that there is little room for merging over the last 8 bilion years.[1]

There are two further effects related to dry mergers that influence the evolution of the LF. In Skelton et al. (2009, see Chapter 4) we showed that dry mergers lead to a change in slope at the bright end of the CMR. Bright galaxies thus have slightly bluer colours than expected from extrapolating the faint end of the relation. In addition, it is likely that the red sequence is built up through both the quenching of disk galaxies and dry merging (Faber et al. 2007's "mixed quenching and dry merging scenario"). Galaxies that have recently had their star formation suppressed and moved onto the red sequence will have relatively young populations with bluer colours. Subsequent dry mergers involving these galaxies will produce remnants that evolve faster than if all their stars formed at high redshifts. To determine the growth of the red sequence, these blue progenitors should also be taken into account. This is known as the progenitor bias (van Dokkum & Franx 2001).

Overview of this chapter

In this chapter, I caution against the interpretation that massive early-types formed at high redshift and underwent purely passive evolution, with no room for merging. Using a suite of simple models that incorporate the evolution of stellar populations into a hierarchical merging framework, I show that at fixed mass, dry merging and recent quenching decrease the change in colour and luminosity since $z = 1$. The resultant evolution is consistent with that of a population that formed early and evolved passively, *even though there has been significant merging activity*. In Section 5.2 I describe the expected evolution of passively aging galaxies that formed at high redshift and lay the foundation for modelling changes in the galaxy population with stellar population synthesis models. Section 5.3 describes the models used to investigate the evolution of a galaxy population assembled hierarchically, building on the simple toy model presented

[1] Perhaps contrary to expectation, one of the largest difficulties in this analysis is determining the bright end of the LF at low redshift to high precision. Bright galaxies in the local Universe have extended outer envelopes (perhaps due to dry merging) making it difficult to estimate the total magnitude and accurately subtract the background (e.g., Bernardi et al. 2007; Lauer et al. 2007). Small photometric errors translate into a large error in number density because of the exponential drop of the LF toward the bright end.

in Chapter 4. Section 5.4 compares the resultant evolution of colour and luminosity from the passive evolution and merging models. In Section 5.5 I discuss the results. The conclusions that can be drawn on early-type evolution are summarized in Section 5.6.

5.2 Passive evolution models

The evolution of an early-type galaxy that formed at high redshift and has not undergone merging or had stellar mass added at recent times is often described as the evolution of a simple population of stars that formed within a short time with a single metallicity. As initially argued by Gunn (1978) and presented in Longair (1998), the rate of evolution for such a population at late times is determined largely by the rate at which stars evolve off the main sequence. This results in the fading of the stellar population with $L \propto 1 + z$ in the standard cosmology. Galaxies are thus approximately twice as luminous at redshift one than at the present day. Various pieces of observational evidence justify the use of passive evolution models for early-type galaxy evolution. The near-infrared and optical luminosity function undergo only mild evolution since $z = 1$, suggesting that much of the mass was built up before this time (e.g., Cowie et al. 1996). The observed colours and magnitudes of present day early-types are also consistent with that of a relatively uniform stellar population that formed early and is passively fading (see for e.g. Ellis et al. 1997; Bower et al. 1998). Massive, passive galaxies have been found out to high redshifts (Kriek et al. 2006; McGrath et al. 2007), suggesting that the stars in at least some present-day massive ellipticals were already in place at high redshift.

I use the Bruzual & Charlot (2003, BC03 hereafter) stellar population synthesis models to follow the evolution of a simple stellar population (SSP) formed at redshifts of 2, 3, 4 and 5, with a Chabrier IMF and the Padova 1994 libraries of stellar evolution. The Chabrier IMF has a power-law slope of -1.3 between $1\mathrm{M}_{\odot}$ and $100\mathrm{M}_{\odot}$ and a log-normal distribution below this mass, centered on $0.08\mathrm{M}_{\odot}$ with a width of 0.69 (Chabrier 2003). The stars are assumed to form instantaneously in a single burst at each of the formation redshifts and evolve passively thereafter, with no additional mass added. The evolutionary tracks in the $U - V$ colour and B-band magnitude for a solar metallicity ($Z = 0.02$) population are shown in Fig. 5.1. For each of these formation redshifts, the difference in magnitude and colour from $z = 1$ to $z = 0$ is given in Table 5.1.

A more realistic model for the passive aging of a population should include galaxies with a range of stellar masses, and therefore a range of metallicities. Since the evolution of a stellar population depends on its metallicity, different mass galaxies will evolve at different rates. As a simple approximation to the mass-metallicity relation, I fit a straight line through the median metallicity as a function of stellar mass from Gallazzi et al. (2005), obtaining the relation

$$Z = -0.085 + 0.0098 \log \left(\frac{M_*}{\mathrm{M}_{\odot}} \right) \tag{5.1}$$

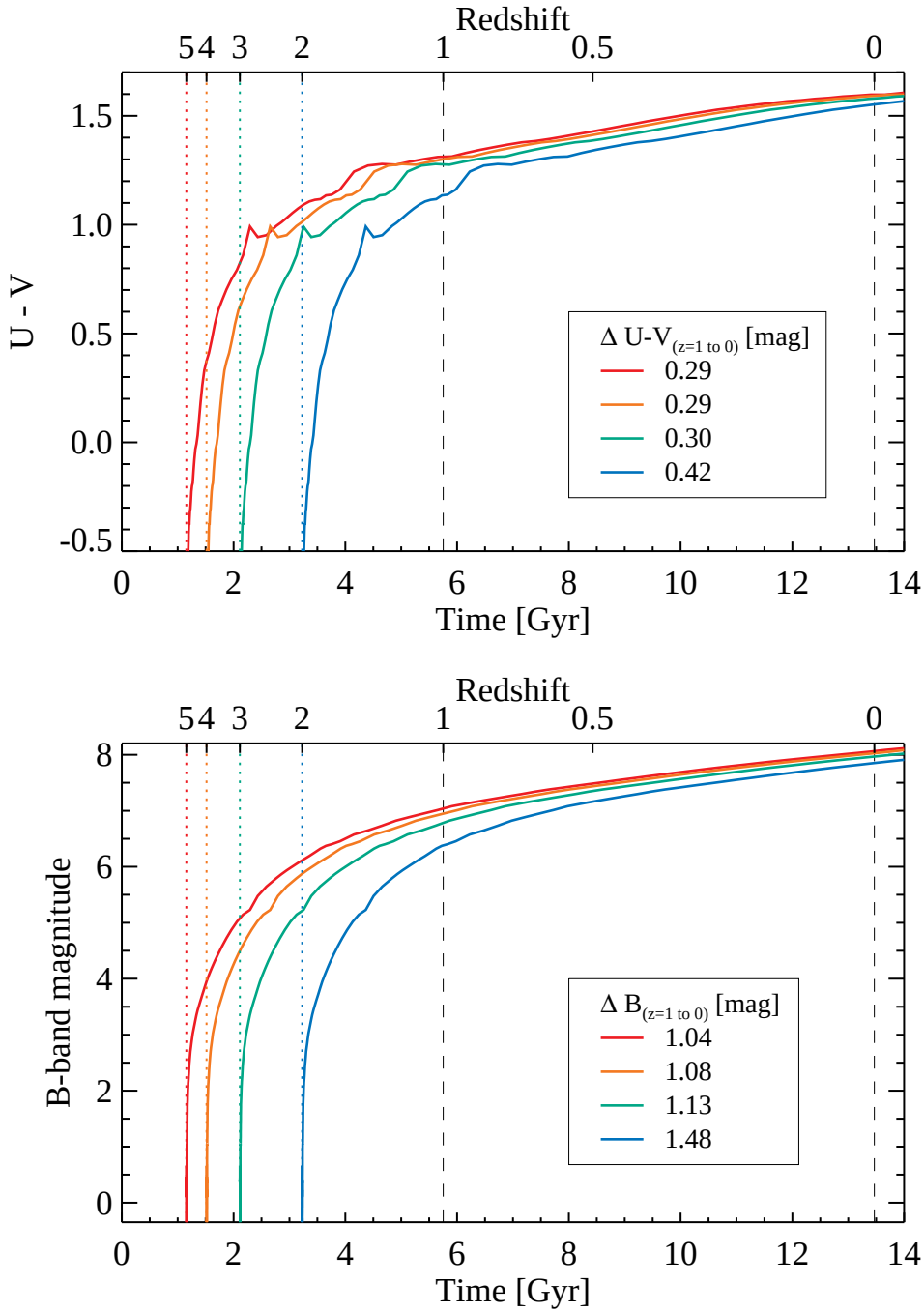

Figure 5.1: Evolutionary tracks in $U - V$ colour (top panel) and B-band magnitude (bottom panel) for a simple stellar population with solar metallicity from the Bruzual & Charlot (2003) models, assuming formation redshifts of 5, 4, 3 and 2. The changes in colour and magnitude from $z = 1$ to $z = 0$ for each formation redshift are given in the boxes.

Table 5.1: Passive evolution since $z = 1$

	SSP		Variable metallicities			
	$1Z_\odot$		$\log_{10}\left(\frac{M}{M_\odot}\right) = (10.7, 11]$		$\log_{10}\left(\frac{M}{M_\odot}\right) = (11, 11.5]$	
z_f	$\Delta(U-V)$	ΔB	$\Delta(U-V)$	ΔB	$\Delta(U-V)$	ΔB
5	0.29	1.04	0.29	0.96	0.29	0.96
4	0.29	1.08	0.29	1.01	0.30	1.02
3	0.30	1.13	0.30	1.11	0.31	1.12
2	0.42	1.48	0.41	1.37	0.42	1.39

Using Equation 5.1, I assign 1000 model galaxies with a range of masses above $M_* = 5 \times 10^{10}\mathrm{M}_\odot$ a metallicity. This minimum mass corresponds approximately to solar metallicity. Evolutionary tracks for an SSP that formed instantaneously at $t = 0$ are available from the BC03 models for 6 metallicities, ranging from $Z = 0.0001$ to $Z = 0.05$. By interpolating between these metallicities at each time interval, I obtain the magnitude and colour evolution for each model galaxy. Assuming a single formation redshift, I measure the average change in magnitude and colour for galaxies within a small mass range, accounting for the relative numbers of galaxies as a function of mass (this is important only at the massive end, where the change in number density with mass is very rapid). Each galaxy is assigned a weight based on the Schechter function fit to the observed mass function of red galaxies from the SDSS (Bell et al. 2003), with parameters $\phi^* = 0.0107/h^3 Mpc^{-3} \log_{10} M^{-1}$, $\log_{10}\left(\frac{M^* h^2}{M_\odot}\right) = 10.50$ and $\alpha = -0.70$. This has been converted to a Chabrier IMF by subtracting 0.1 dex from the mass. I present the change in colour and magnitude from $z = 1$ to $z = 0$ for galaxies in two mass ranges, $\log_{10}\left(\frac{M}{M_\odot}\right) = (10.7, 11]$ and $\log_{10}\left(\frac{M}{M_\odot}\right) = (11, 11.5]$, with four choices of formation redshift, $z_f = \{2, 3, 4, 5\}$, in Table 5.1. There is very little difference in the amount of evolution expected for the two mass selections. The colour evolution is approximately that of a solar metallicity SSP, but there is less evolution in the B-band, as expected for higher metallicity SSPs. These estimates for the evolution of passively evolving galaxies are used as a benchmark for comparison to models set in a hiearchical merging framework in Section 5.5.

5.3 Models with quenching and merging

In order to investigate how the colours and magnitudes of galaxies *evolve* in a hierarchical universe, I incorporate the evolution of stellar populations of different metallicities into the toy model for merging developed in Chapter 4. I use the galaxy merger histories from the Somerville et al. (2008) SAM, as well as the masses and gas fractions of merging galaxies given by the SAM. I use Equation 5.1 to assign each galaxy a metallicity, based on its mass at the time of the merger. This assumes that the mass-metallicity relation does not evolve and the metallicity of each galaxy remains the same for the duration of its star formation. Although

these are clearly simplifications, they are defensible choices in the light of this model framework. To determine the luminosities and colours of merging galaxies, and their evolution after the merger, I assume a star formation history for each galaxy and use the BC03 models, with a Chabrier IMF and the Padova 1994 stellar libraries, to determine how the flux changes with time for each population of stars that form. I interpolate between the six available SSP evolutionary tracks to determine the appropriate evolution given each galaxy's metallicity. To determine a galaxy's luminosity at the time of observation, I integrate the flux remaining from each unit of stars formed. I use the Johnson U, B and V filters, rather than the SDSS bands used in the previous chapter, in order to compare directly with observations out to $z = 1$.

In the model presented in Chapter 4, I assumed that major gas-rich mergers move galaxies from the blue cloud onto the red sequence, placing them onto a "creation red sequence" that relates their colour and magnitude. In the model presented here, galaxy colours are determined by their star formation history. I assume that galaxies form stars continuously from some formation redshift z_f up to a "truncation" time, after which no stars form. The truncation time is assumed to be a fixed period after star formation begins, unless a major wet merger occurs before this. The assumption that such mergers are effective in quenching star formation is thus maintained. As before, a major merger is defined to be one where the ratio of the masses of the two galaxies is between 1:1 and 1:4, using the total baryonic and dark matter mass within NFW scale radius. To distinguish between wet and dry mergers, I use a gas fraction threshold of 20%, the value that produced the best match to the observed red sequence in the previous model. If either of the galaxies has a gas fraction above this, the merger is classified as wet. Minor wet mergers have no effect.

To maintain the simplicity of the model, I have chosen a constant star formation history up until the time of truncation, although in principle, any star formation history could be used. An exponentially declining function is a common choice, for example (see for e.g., Ruhland et al. 2009). The normalisation is determined by the mass at the time of the merger. It has been shown that during mergers star formation is only mildly enhanced with respect to normal star-forming galaxies (Robaina et al. 2009a; Jogee et al. 2009); thus we do not incorporate merger-induced bursts of star formation into the models.

To investigate plausible evolutionary scenarios I have chosen three possibilities for the maximum length of time over which stars can form. The same galaxy merger histories and model parameters are used in all cases, and unless stated otherwise, I assume that star formation starts at $z_f = 4$. In the first model, termed "early quenching", I assume that the stars in all galaxies in the merger tree form instantaneously in a single burst, by halting star formation directly at the time of formation. In the second, star formation can proceed for up to 4 Gyr after the time of formation (this corresponds to $z \approx 1$ for a formation redshift of 4). Major wet mergers occurring before this time are effective at quenching star formation, but regardless of the mechanism, all remaining star formation stops after 4 Gyr. To investigate whether mergers continue to play an important role at recent times, I consider a variation of this model with no mergers occuring

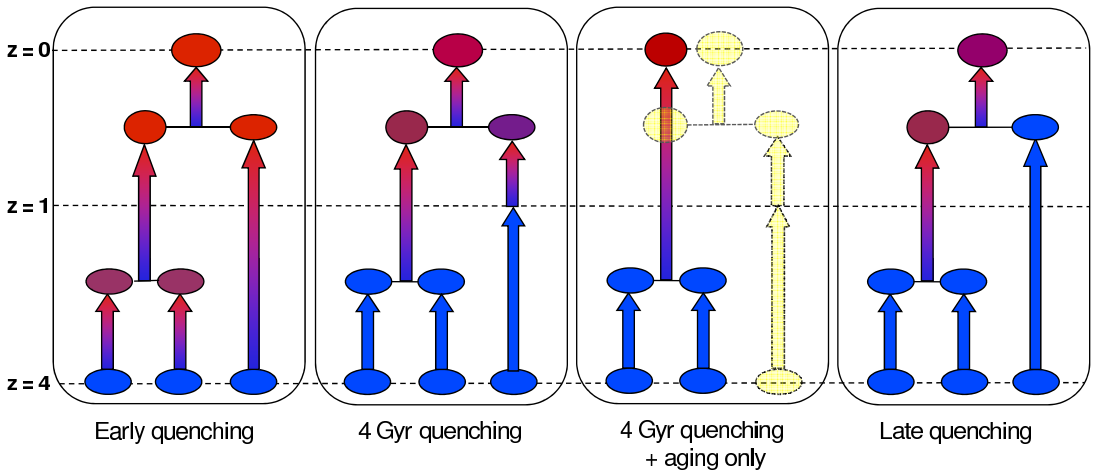

Figure 5.2: A cartoon illustrating the evolution of a galaxy that has undergone a major merger at high redshift and a second major merger at $z < 1$ in the four models. Arrows with a colour gradient indicate passive evolution. Continuing star formation is indicated by the blue arrows. In the early quenching model, galaxies undergo passive evolution from the time of formation. In the other three models, star formation stops at the time of the first major merger. Galaxies that do not undergo a merger before $z = 1$ start to fade passively at this time in the 4 Gyr model but continue to form stars in the late quenching model. Galaxies that only merge after $z = 1$ are not included in the 4 Gyr+aging only model, as shown by the shaded path.

after $z = 1$. I refer to this model as "4 Gyr + aging only", as after $z = 1$ the only evolution is the passive aging of galaxies that are already on the red sequence. In the third scenario, star formation is allowed to continue until the present day, so that major mergers are the only available mechanism for quenching star formation at any time. This is termed "late quenching". The four models are illustrated by the cartoon in Fig. 5.2.

5.4 Resultant colour and magnitude evolution

In the early quenching model, the red sequence begins forming at high redshifts. From its time of formation, each galaxy undergoes the passive evolution described in Section 5.2, but also experiences dry mergers. This model confirms the expecations of the simple toy model of Chapter 4, reproducing the low-z result while including the passive evolution of the stellar populations. We find a change in slope and a decrease in scatter at the bright end of the red sequence, as can be seen in Fig. 5.3. Both the normalisation and slope depend somewhat on the choice of mass-metallicity (M-Z) relation. A shallower M-Z relation results in a shallower CMR at all redshifts, limiting the amount of curvature that can be caused by merging. Using Equation 5.1, the red sequences produced in the 4 Gyr and late quenching models agree well with the observed relation, thus I have chosen to use this M-Z relation in all the models.

I compare the evolution predicted by the model to the observed evolution of red sequence

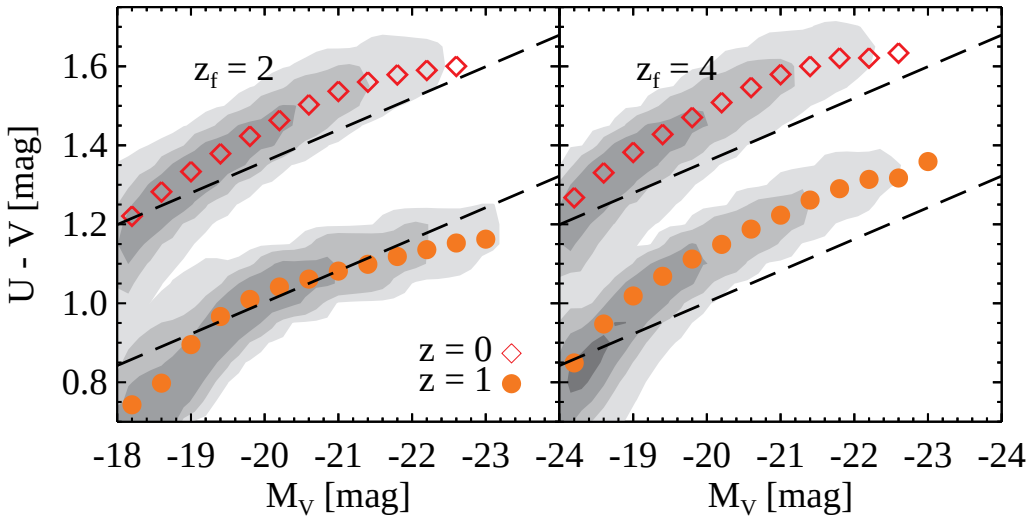

Figure 5.3: The evolution of the red sequence in the early quenching model, in which the stars form instantaneously at the formation redshift and evolve passively with dry merging. In the left panel, stars form at $z_f = 2$, while in the right panel they form at $z_f = 4$. The lower contours represent the red sequence at $z = 1$, with filled circles indicating the median values in magnitude bins of 0.4 mag. The upper contours and diamonds represent the $z = 0$ red sequence and its median values. The observed relations from Brown et al. (2007) are shown as dashed lines.

galaxies in the Bootes field from Brown et al. (2007). This is described by

$$U - V = 1.4 - 0.08(M_V - 5\log_{10}(h) + 20) - 0.42(z - 0.05) + 0.07(z - 0.05)^2, \quad (5.2)$$

and is very similar to the evolution found by Bell et al. (2004) for galaxies in the Combo-17 survey. In the model, a narrow colour–magnitude relation has formed by a redshift of one, as shown in Fig. 5.3. With a formation redshift of 4, the CMR is already redder than the observed relation by $z = 1$ (right panel). The red sequence is thus redder than observed at $z = 0$ although the change in zeropoint is approximately the same as the difference between the observed zeropoints over this period. An M-Z relation based on the relationship between the colours and metallicities of a population of a fixed age in the BC03 models similarly results in too red a relation at $z = 0$. Assuming a lower formation redshift ($z_f = 2$, left panel) brings the CMR at $z = 1$ into better agreement with the observations, but still results in too red a relation at $z = 0$, as the more recently formed population evolves faster.

In both the second and third models, star formation continues to $z = 1$ unless it is shut down by a major wet merger event. The red sequences for these models therefore only diverge after $z = 1$. Thereafter, all galaxies stop forming stars and fade passively in the second model but continue to form stars in the third model, so that new galaxies with young populations are added to the red sequence until the $z = 0$. In the "aging only" variation, no mergers occur

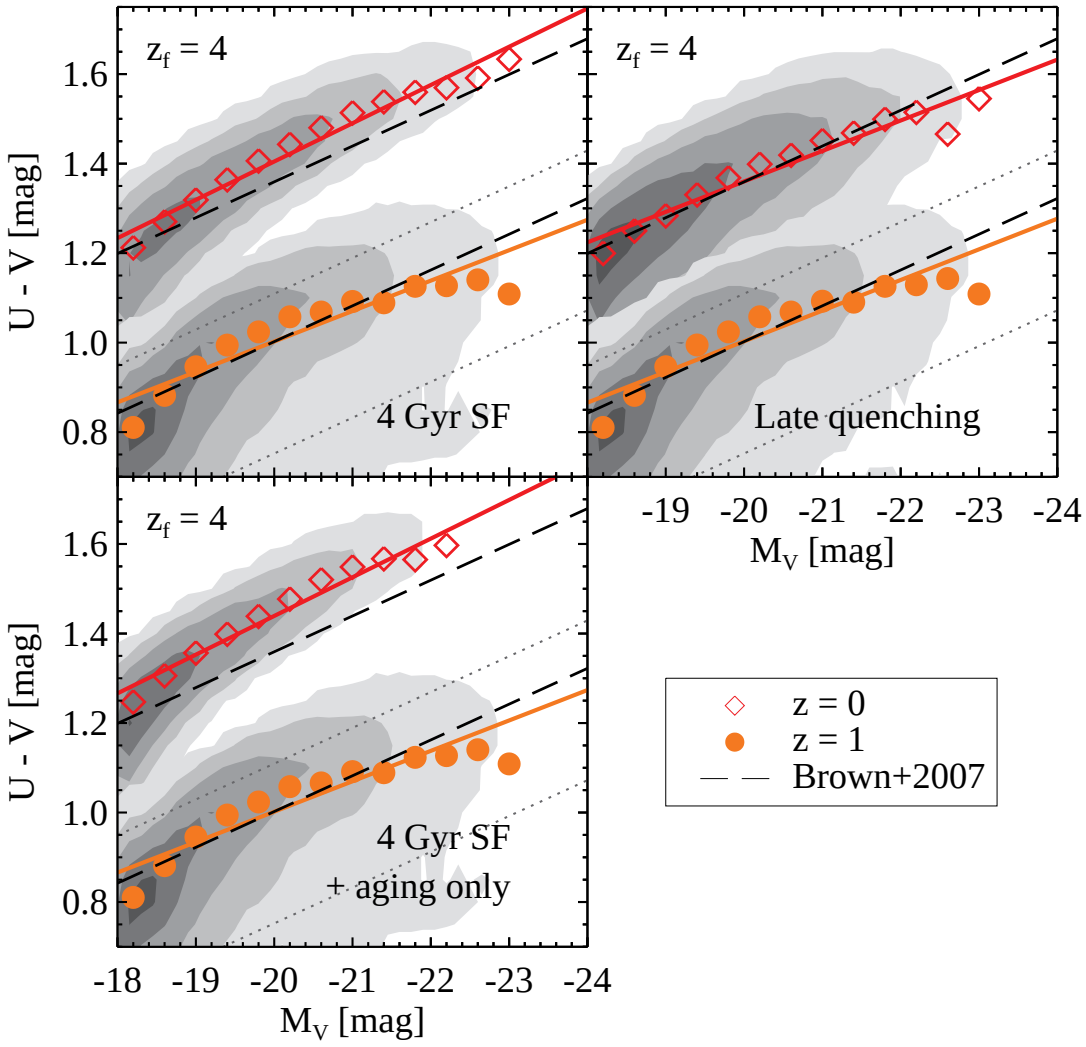

Figure 5.4: The evolution of the red sequence from $z = 1$ to $z = 0$ in the three models with extended star formation periods. In the top left panel, galaxies on the red sequence stop forming new stars at $z = 1$ (4 Gyr after formation) and evolve passively, with mergers. The 4 Gyr+aging only model, which has the same truncation time but no mergers occuring after $z = 1$, is shown in the bottom left panel. The late quenching model, where star formation can continue until $z = 0$, is shown on the right. In each case the lower contours represent the red sequence at $z = 1$ and the upper contours the red sequence at $z = 0$. The medians of the distribution binned in magnitude are shown as filled circles and diamonds. The observed relations from Brown et al. (2007) are shown as dashed lines. The dotted lines 0.25 mag below the observed relation are used as a lower limit to select galaxies on the red sequence.

after $z = 1$, so the number density of galaxies as a function of mass does not change but those galaxies already on the red sequence fade passively. This gives an upper limit for the amount of luminosity evolution, as in reality there are also likely to be galaxies that deplete their gas and move onto the red sequence without undergoing mergers.

The distributions of galaxies in colour–magnitude space at $z = 1$ and $z = 0$ are shown in Fig. 5.4 for these three models. I isolate the red sequence at each redshift by applying a colour cut 0.25 mag below the observed relation given in Equation 5.2 (dotted lines). This is comparable to the method used by both Brown et al. (2007) and Bell et al. (2004). The cut only removes a few galaxies – those that have had their star formation shut down very recently – but does affect the position of the medians, particularly at the bright end where the numbers are low. The median colour in magnitude bins of 0.4 mag are shown as filled circles ($z = 1$) and diamonds ($z = 0$) in the figure. Although the relations are clearly not linear, I have fitted straight lines through the medians to compare to the observed CMR. At $z = 1$ the model CMR matches both the zeropoint and slope of the observed relation from Brown et al. (2007) reasonably well, as shown in Fig. 5.4. The change in colour with redshift in the late quenching model produces a relation that agrees well with the observed red sequence at $z = 0$. Both the 4 Gyr and 4 Gyr+aging only models lie redward of the observed relation at $z = 0$, indicating that the galaxy population has undergone more evolution in colour than expected from observations.

The continuation of mergers after $z = 1$ has a strong effect on the number of galaxies, particularly at the bright end. This can be seen by comparing the mass function (MF) and luminosity function (LF) evolution in the three models (Fig. 5.5). Both functions are the same for all the models at $z = 1$ but evolve differently thereafter. The 4 Gyr+aging only model has no change in the distribution of mass after $z = 1$. The only evolution is the passive fading of the stars in the galaxies already on the red sequence. This results in too few bright galaxies at $z = 0$, clearly seen in both the CMR and LF. The number density of bright, massive galaxies is increased through mergers, thus both the 4 Gyr and late quenching models show evolution in the MF and LF. The fading and reddening of the stellar populations is compensated by the addition of mass from mergers, as well as recent additions to the red sequence, in the late quenching case.

5.5 Discussion

In the previous section I showed that the observed colour–magnitude distribution at $z = 1$ can be reproduced by models where star formation begins relatively early ($z_f = 4$) and is gradually quenched through major mergers. Taking only passive fading of the stellar populations into account, a realistic red sequence population in place at $z = 1$ will undergo very rapid evolution in colour and luminosity, resulting in too red a relation at $z = 0$. The evolution is slowed by including merging between red sequence galaxies after $z = 1$. The addition of young stellar populations onto the red sequence through the quenching of star formation in blue cloud

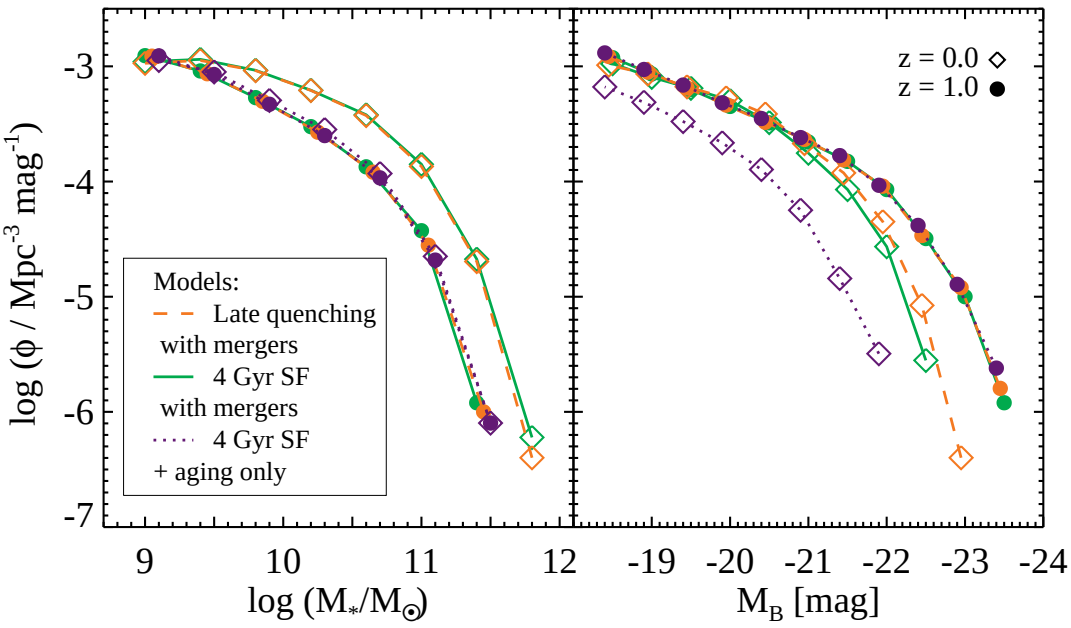

Figure 5.5: The evolution of the red sequence mass function (left panel) and luminosity function (right panel) from $z = 1$ (filled circles) to $z = 0$ (diamonds). With only passive evolution and no change in mass, there is a dramatic change in luminosity (4 Gyr+aging only, dotted blue line). The luminosity evolution is reduced by including mergers (4 Gyr model, solid green line) and newly formed stars (late quenching model, dashed orange line)

galaxies reduces the evolution even further. The predicted changes in colour since $z = 1$ for this range of possible scenarios are consistent with those of ancient simple stellar populations that formed between redshifts of 3 and 5, and similar to the observed CMR evolution.

The number densities of bright and faint galaxies produced by the models that include mergers after redshift one are approximately equivalent to the observed number densities at low redshift. There is a shortage of intermediate mass galaxies, making the shape of both the MF and LF differ from the observations in detail. For this reason, I do not compare the predicted MF and LF evolution in the different models directly to the observed distributions, but rather consider the relative changes at a fixed mass and space density.

The changes in colour and magnitude for model galaxies in the range of $10.7 < \log(M/\mathrm{M}_\odot) \leq 11$ are shown in Fig. 5.6. I compare the predicted evolution of the models with the average changes in colour and magnitude for passively evolving galaxies in the same mass range from Table 5.1. Both the early quenching models have approximately the evolution expected for a passively evolving galaxy formed at the same redshift, although the change in colour for the $z_f = 2$ model is slightly smaller than in the purely passive case, as can be seen in the figure. This is likely to be the result of dry mergers (cf. Chapter 4), although there is no obvious blueward offset for the $z_f = 4$ model. In the 4 Gyr+aging only model, the galaxies in this

fixed mass range are exactly the same population at both redshifts, whereas in the other models, galaxies can move into this mass range as their masses are increased through merging. The mass selection thus results in a much smaller sample at $z = 0$ in the 4 Gyr+aging only model. The continuation of merging produces a bluer and brighter population at $z = 0$, with recent additions to the red sequence after $z = 1$ enhancing the effect. The relatively small resulting changes in colour and magnitude resemble those of a passively evolving population that formed at higher redshift, as can be seen from the similarity in the position of the late quenching model point and the passive evolution vectors with z_f between 3 and 5. The change in colour and magnitude for the 4 Gyr+aging only model replicates that of a more recently formed, passively fading population, because there is no merging or additional star formation that can compensate for the rapid luminosity and colour evolution.

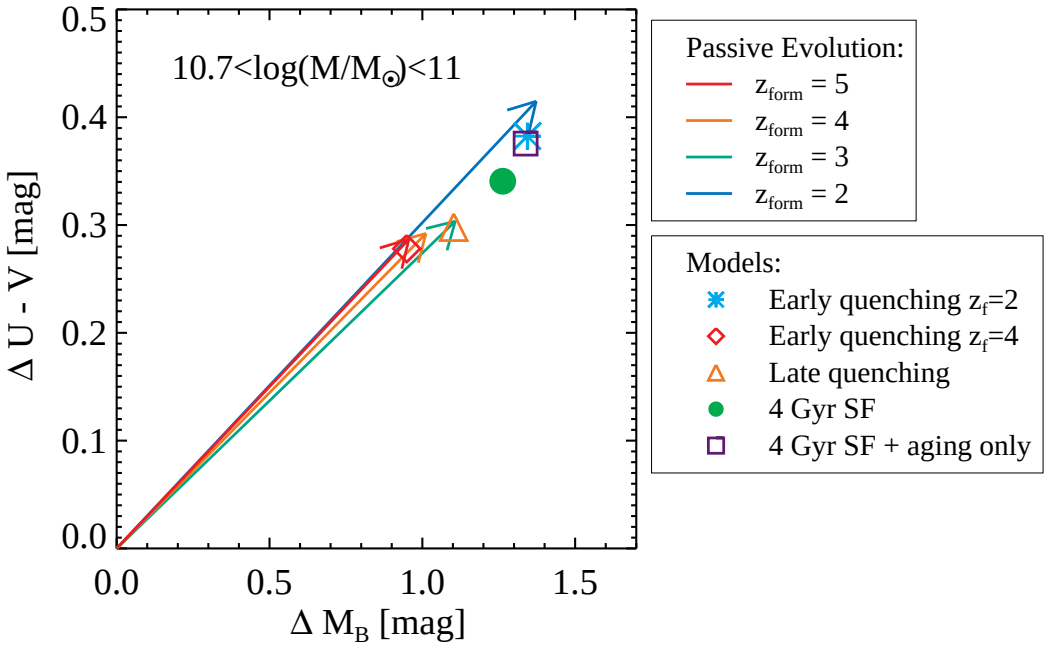

Figure 5.6: The change in colour and magnitude from $z = 1$ to $z = 0$ for galaxies in the given mass range in the hierarchical models compared to the expected changes for passively evolving SSPs formed at redshifts from 2 to 5 (arrows). The $z_f = 4$ and $z_f = 2$ early quenching models are shown by a diamond and star, respectively. The late quenching, 4 Gyr and 4 Gyr+aging only models are shown by the triangle, filled circle and square, respectively.

Observational measurements of the change in M/L_B and $U - V$ for *cluster* galaxies with $\log(M_\star/\mathrm{M}_\odot) > 11$ lie in the range of 1.3 – 1.52 mag and 0.24 – 0.34 mag, respectively (van Dokkum & van der Marel 2007; van Dokkum 2008, van der Wel 2009, private communication). These measurements were made with the same data, using different estimates of the mass (dynamical mass, stellar mass and velocity dispersion). The large differences between the different determinations can partly be attributed to the uncertainty in the k-correction for Coma

cluster galaxies (van der Wel 2009, private communication). It should also be noted that this is an extrapolation between a single cluster at high z (MS 1054-03 at $z = 0.83$) and the Coma cluster at $z = 0.022$. Given the uncertainties in the data, it is reassuring that the values of the observed luminosity and colour evolution lie in the predicted range. The observed magnitude changes would suggest a better match to the $z_f = 2$ early quenching and 4 Gyr+aging only models, however the colour changes are more consistent with a higher formation redshift and the late quenching model. The difference between the observed evolution and the evolution predicted by passive models was used to argue for an evolving IMF (van Dokkum 2008); my models show that dry merging and new additions to the red sequence need to be taken into account before such a conclusion can be drawn. More work is needed to pin down the observed evolution for a larger sample of field galaxies.

5.5.1 The luminosity function evolution

A fairly straight-forward way of measuring the evolution of the LF (provided that a Schechter function or other analytic form fits the LF reasonably well) is by determining the change in magnitude at a fixed space density (e.g., Brown et al. 2007). This has the advantage that it is relatively insensitive to the details of red galaxy selection and avoids the use of a magnitude threshold that is sensitive to the exact shape of the LF at the bright end. The Schechter function (Schechter 1976) is often used to represent the LF, as it captures the observed power-law slope at the faint end and exponential drop-off at the bright end. It is given by

$$\phi(M)dM = \phi^* 10^{0.4(\alpha+1)(M^*-M)} e^{-10^{0.4(M^*-M)}} dM, \tag{5.3}$$

where α is the faint-end slope, M^* is the characteristic magnitude at the knee of the curve and ϕ^* is a normalisation.

In Fig. 5.7 I show the change in magnitude for the 5 models at 3 space densities, overlaid on the observed LFs from the Bootes field (NOAO Deep Wide-Field Survey, Brown et al. 2007) at $z = 0.9$ and the 2 degree Field Galaxy Redshift Survey (2dFGRS, Madgwick et al. 2002) at $z = 0.1$. The evolution vectors are determined by subtracting the magnitudes at which a Schechter function fitted to each model reaches the specified space density at the two redshifts.

There are a number of caveats to note in interpreting this figure:

- Although the number statistics at $z = 0.1$ are good, the magnitudes in this case are measured from scanned photographic plates (with updated CCD calibrations) and are thus subject to large errors (rms $\sim \pm 0.15$ mag). The difficulties in determining the background accurately and estimating the total light for extended nearby galaxies limit the usefulness of current estimates of the low-z LF at the bright end. The low-z LF shown in the figure should thus be viewed as a guideline, with large uncertainties.

- The predicted magnitude changes for the models depend on the shape of the LF, thus the differences between the observed and model LFs should be borne in mind. In particular,

there is a lack of intermediate luminosity galaxies, reducing the normalisation and changing the slope of the model LF compared the the observed LF. The difference between the model and observed LFs at $z = 0.9$ could be as large as 0.5 mag at a space density of $\phi = 10^{-4}\mathrm{Mpc}^{-3}\mathrm{mag}^{-1}$, greater than the predicted evolution for most of the models. Note that the $z = 0.9$ LF measured by Brown et al. (2007) has higher space densities than measured with Combo-17 and DEEP2 (Bell et al. 2004; Faber et al. 2007), however these are still approximately a factor 2 greater than the models.

- There is a noticeable difference between the predicted evolution taken from $z = 0.9$ and that taken from $z = 1$ for a passively evolving population formed at $z_f = 2$. The reason for this can be seen in the SSP evolutionary tracks shown in Fig. 5.1. In the $z_f = 2$ SSP there is a "bump" in the colour track just after $z = 1$, resulting in a much smaller change in colour measured from $z = 0.9$ to $z = 0.1$ than measured from $z = 1$ to $z = 0.1$. The bump falls at higher redshifts for populations that formed earlier, thus it does not affect the measurements of their evolution. It will have some effect on the models with extended periods of star formation, however. The reason for this sudden jump in colour is not clear but a similar feature is also seen in the Pégase stellar population synthesis model (Fioc & Rocca-Volmerange 1997), suggesting that it is generic.

The top two arrows in Fig. 5.7 show the evolution of early quenching models, where stars form at z_f and the population ages and dry merges until the present. In these models, a population that formed at high redshifts ($z_f = 4$, red line) undergoes very little evolution while a similar population that formed more recently ($z_f = 2$, cyan line) evolves faster, with the evolution vectors at fixed space density extending beyond the observed low-z LF. Fig. 5.7 shows that a red sequence galaxy population with a realistic mix of stellar populations at $z = 1$ will undergo very rapid evolution in magnitude at fixed space density if there is no growth in mass (purple line). The evolution is dramatically slowed by growing the red sequence population through dry mergers between already-existing early-type galaxies to larger masses (green line), and slowed further by the addition of new red sequence galaxies from the quenching of star formation in recent wet mergers (orange line). This "late quenching" model is reasonably consistent with the observations at all space densities.

5.6 Conclusions

I have used stellar population synthesis models to incorporate realistic star formation histories into a hierarchical merging framework, in order to explore the colour and magnitude evolution of red sequence galaxies. I use the galaxy merger trees from the Somerville et al. (2008) SAM combined with stellar evolutionary tracks from the Bruzual & Charlot (2003) model, making simple assumptions on the relation of mass to metallicity and the redshift at which galaxy formation begins. I assume that major wet mergers are effective at quenching star formation but

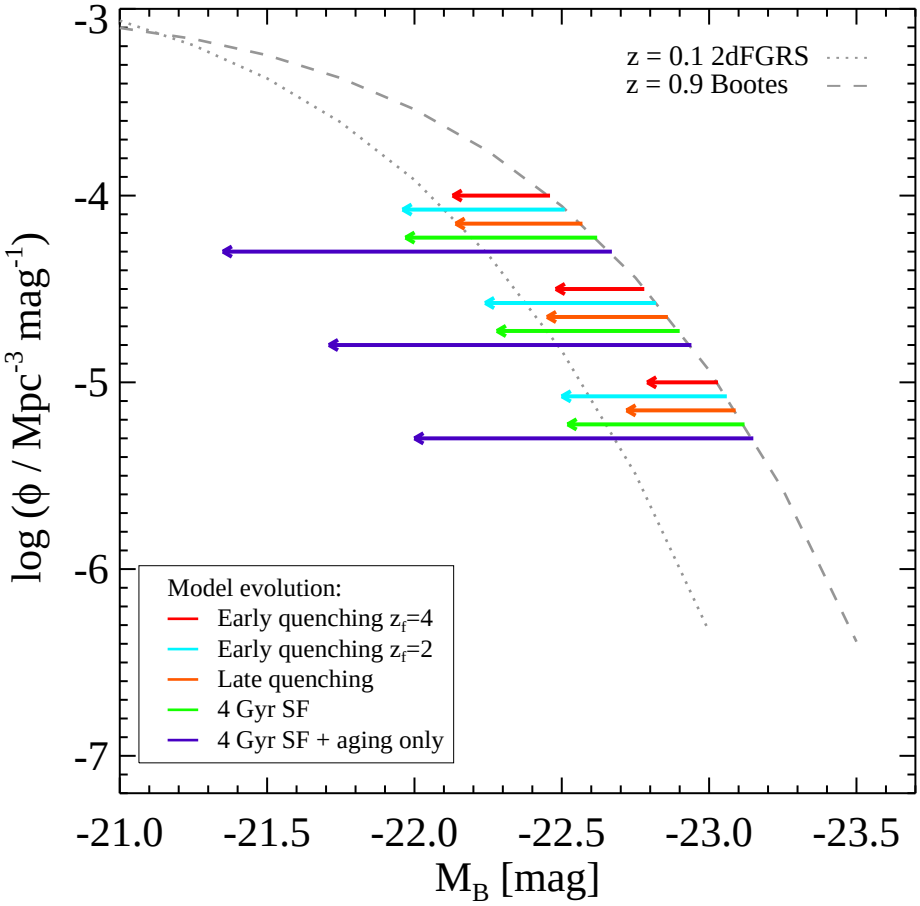

Figure 5.7: The change in magnitude from $z = 0.9$ to $z = 0.1$ at fixed space densities in the models, compared to the observed evolution of the LF. The low-z LF is from the 2dFGRS (Madgwick et al. 2002), while the high-z LF is for galaxies in the Bootes field from Brown et al. (2007).

that star formation may also shut down after a period of time, independently of mergers. With this model setup, I examine the role of recent mergers and the effect of adding younger populations to the red sequence at late times.

A realistic red sequence population at $z = 1$ can be formed through the passive fading of galaxies that form in a single burst relatively recently ($z_f \sim 2$) or through more extended star formation, shut down by major mergers at different times, in galaxies that began forming earlier ($z_f \sim 4$). Galaxies that form all their stars at high redshifts have colours that are too red by $z = 1$, but the slow reddening they experience thereafter gives approximately the observed amplitude of colour evolution.

A population with approximately the correct colour at $z = 1$ evolves very rapidly over the last half of cosmic history if no further mergers occur and there is no new mass added to the red sequence. This results in a colour–magnitude relation that is too red at low redshift, with too

few bright red galaxies and too much luminosity evolution at fixed space density compared to observations. At a fixed mass, the change in colour and magnitude predicted by such a model are approximately the same as the changes predicted for a purely passively evolving population that formed at $z_f \sim 2$.

Dry mergers occuring between $z = 1$ and $z = 0$ slow down the evolution, producing a slightly bluer CMR at $z = 0$ that is closer to the observed relation, and more realistic evolution of the LF. By allowing star formation to continue after $z = 1$, the changes in a population's colour and luminosity are reduced even further, through the addition of young stellar populations to the red sequence. Both the CMR and the LF evolution of this "late quenching" model are consistent with the observed evolution. The smaller changes in colour and magnitude at a fixed mass replicate the behavior of a passively evolving population that formed at high redshift ($z_f = 3 - 5$). The observed evolution of the red sequence galaxy population can therefore be interpreted either as the evolution of an old passively-evolving population or as the cosmologically-motivated hierarchical growth of an evolving population. The evolution of the CMR and the LF cannot clearly discriminate between these scenarios, at least using this simple model. Although they predict very similar evolution, the implications of the two for the growth of stellar mass are very different.

Chapter 6

Summary and future outlook

To explore how mergers affect the evolution of early-type galaxies, I developed a simple toy model that makes use of the galaxy merger trees from a semi-analytic model of galaxy formation. Including stellar population syntheis models into this framework allow me to follow the evolution of the galaxy population. With these tools, I have addressed two outstanding questions on the evolution of early-type galaxies:

- Does dry merging violate the slope and small scatter of the observed colour–magnitude relation?
- Does the observed slow evolution of early-type galaxies leave any room for hierarchical growth through mergers?

I use the output of the Somerville et al. (2008) SAM to obtain the merger trees that form this basis of this modelling. The model has been extensively described in Somerville & Primack (1999); Somerville & Kolatt (1999); Somerville et al. (2001, 2008) and is summarized in Chapter 2.

In the same chapter, I analysed the distributions of galaxy masses, luminosities and colours produced by the SAM. The model luminosities are strongly affected by recent star formation, metallicity and dust. A dust-correction (see Gilmore et al. 2009, for details) is necessary to reproduce both the LF and the observed CMD of galaxies. At low redshift, there is good agreement between the observed mass function and optical luminosity function in the r-band from the SDSS (Bell et al. 2003) and the model distributions of mass and luminosity. With the dust correction applied, there is also qualitative agreement between the $z = 0$ model CMD and the distribution of $\sim 72,000$ galaxies in a thin redshift slice selected from the SDSS DR6. In both the observations and the model there is a bimodal galaxy distribution that can be described by the superposition of two Gaussian functions in magnitude bins along the relation. The red sequence has curvature, and can be fitted with the combination of a tanh function plus a straight line, as Baldry et al. (2004) showed using an earlier release of SDSS data.

I examined the properties of the model galaxies out to $z \sim 1$ using a mock catalogue with three times the volume of the GEMS survey. The model red sequence is less well-defined

at higher redshifts, and has two peaks of galaxies – one at intermediate magnitudes and one at the faint end. This second peak is not observed in either the Combo-17 (Bell et al. 2004) or NOAO Deep Wide-Field Survey (Brown et al. 2007) red sequences in the $0.2 < z < 0.4$ redshift bin where the data is complete to low enough magnitudes to compare. The separation of the red sequence into these two regions is likely to be caused by the feedback mechanisms implemented at different mass scales in the model. Most faint red galaxies are satellites, which undergo strangulation as they enter a larger halo, while massive galaxies are reddened through the evacuation of gas by AGN feedback. The red sequence of the model between $0.2 < z < 1.0$ is too blue compared to the colour evolution found in both the Combo-17 survey and NOAO Deep Wide-Field Survey. There are too few bright galaxies in the model, with the difference between the model and observed B-band LFs increasing to higher redshifts. Contrary to what is observed, there is very little evolution in the number density of red galaxies. The model mass function provides a reasonable match to the data at the bright end, but exceeds the observations at stellar masses of $\lesssim 6 \times 10^{10}\mathrm{M}_{\odot}$ in all redshift bins. Faint and intermediate mass galaxies seem to be produced too early in the model, resulting in almost no evolution in the mass function since $z \sim 1$. This is a serious problem, which has also been found to affect other SAMs, as discussed by (Fontanot et al. 2009).

I determined the evolution of the merger rate and fraction in the SAM as a function of mass and gas fraction. For all but the most massive galaxies, mergers occurred more regularly at high redshifts, with the merger rate reaching a peak at redshifts > 1 and decreasing toward $z = 0$. The merger rate of very massive galaxies increases to the present day as the number density grows. The fraction of galaxies in a given mass bin involved in mergers decreases from $z = 1.5$ to $z = 0$ in all mass bins, with the normalisation increasing from low to high mass. The evolution of the merger fraction can be represented by a power law $f_m(z) = f_0(1+z)^m$, with $1.40 < m < 2.29$ for all mergers and $1.92 < m < 2.88$ for major mergers. I use the fraction of baryonic mass in cold gas in each galaxy to distinguish wet, mixed and dry mergers, with a gas fraction threshold of 20% separating the galaxies into different types. The red sequence is dominated by galaxies with gas fractions smaller than this threshold. The merger rate of gas-rich galaxies is similar to the total merger rate, particularly in the lower mass bins which contain mostly blue cloud galaxies. The mixed and dry merger rates evolve more slowly, with very flat major merger rates in all mass bins. High mass galaxies ($M_{\star} \geq 10^{11}\mathrm{M}_{\odot}$) are mostly gas-poor early-types on the red sequence. As a result, they have higher dry merger rates than mixed and wet merger rates. The rate of dry merging for massive galaxies continues to rise to the present day, as the mass on the red sequence increases.

I compared the merger fraction predicted by the model to two observational studies that determine the merger fraction using different techniques. In the first, Jogee et al. (2009) use visual morphological classification to identify mergers in the GEMS survey (Rix et al. 2004). The merger fraction for galaxies with stellar masses greater than $2.5 \times 10^{10}\mathrm{M}_{\odot}$ is found to be approximately constant, ranging from $9 \pm 5\%$ at $z = 0.24$ to $8 \pm 2\%$ at $z = 0.8$. There is good

agreement between this study and the merger fraction found in other works using morphological classifications (Lotz et al. 2008b; Conselice et al. 2003). Studies using close pairs find slightly lower merger fractions at intermediate redshifts and stronger evolution in the merger fraction (Kartaltepe et al. 2007; Bell et al. 2006b) but these results are generally for major mergers. The lower limit for the contribution from major mergers was found to vary between 1.1% and 3.5% over the same redshift range. Using the mock catalogue to select galaxies that have had a merger within 0.5 Gyr of the output redshift, I find a merger fraction of 3 to 10%. This agrees with the observational estimate over most of the redshift range considered, dropping to a lower value at $z \sim 0.3$. The major merger fraction ranges from 1.5 to 4.5% from $z = 0.24$ to $z = 1$, consistent with the observational lower limit.

The second study uses the correlation function to determine the fraction of massive galaxies ($M_\star > 5 \times 10^{10}\mathrm{M}_\odot$) in close pairs ($< 30$ kpc) from COSMOS and Combo-17 data (Robaina et al. 2009b). The fraction is found to increase from 1.7% to 3.2% between $z = 0.2$ and $z = 1.2$. The low-z fraction found using published values for the correlation function parameters and number density of SDSS galaxies is 1.4%. Combining these results, the evolution can be described by $f_m(z) = (0.0135 \pm 0.004)(1 + z)^{1.12\pm0.2}$. In the SAM box simulation, the fraction of galaxies with $M_\star > 5 \times 10^{10}\mathrm{M}_\odot$ involved in mergers ranges from 2.8 to 3.3% for $0.2 < z < 1.2$. The overall normalisation is similar to the observations but the evolution is slower ($m = 0.27$). The agreement between the merger fraction predicted by the SAM and the observations is satisfactory, given the difficulties in measuring and interpreting close pairs and remnants observationally, as well as the uncertainty in timescale and differences in methodology for the model and observations.

To overcome the discrepancies between the model and observed luminosity evolution and to be able to interpret changes in the galaxy population caused by merging, I used only the merger histories, masses and gas fractions of the SAM galaxies in further modelling. The differences between the observed and model mass function will impact on these models through the galaxy masses recorded at the time of each merger, but the galaxy merger trees themselves seem to be fairly robust, insofar as they can be tested against observations. In Section 6.1 I consider how the models can be improved in the future by minimizing the impact of an incorrect mass function.

Motivated by the first question above, I revisited the observed colour–magnitude relation. A sample of $\sim 29,000$ galaxies from the SDSS DR6 was selected using high concentration as a criterion to capture early-type galaxies. The red sequence formed by these galaxies narrows and changes slope with magnitude, with smaller scatter and a shallower slope measured at the bright end. I used a simple toy model for merging, in the same spirit as previous work by Bower et al. (1998), to test whether dry merging could produce these characteristics. The model assumes that major gas-rich mergers are effective at quenching star formation, moving galaxies from the blue cloud onto a "creation red sequence". Subsequent dry mergers move galaxies along the relation by increasing their masses. As there is no change in colour induced

by such mergers, the remnant galaxies lie slightly blueward of the initial relation. Most mergers between faint galaxies are gas-rich, while more massive galaxies experience higher numbers of dry mergers. This leads to a change in slope, bending the relation blueward at the bright end. The magnitude of the break point and change of slope depend on the choice of gas fraction threshold separating wet and dry mergers. Thresholds of 10 and 30% bracket the observed relation. Including scatter in the initial relation results in a decrease in scatter at the bright end as a consequence of averaging the colours of the merging galaxies. The amount of merging predicted by a hiearchical model produces a colour–magnitude relation that matches well with observations. The slope and small scatter of the observed CMR cannot be used to argue against substantial growth of early-type galaxies through dry merging.

In Chapter 5 I revisited the apparent conflict between the slow observed evolution of early-type galaxies and the hierarchical model. I expanded the toy model to take into account different star formation histories and metallicities using stellar population synthesis models. This allowed me to explore changes in the red sequence population over time. A red sequence that matches reasonably well with observations at $z = 1$ can be produced from the passive evolution and merging of galaxies that formed relatively recently ($z_f = 2$) or from more recent quenching of star formation through mergers, in galaxies that started forming stars earlier ($z_f \sim 4$). The changes in colour and magnitude from $z = 1$ to $z = 0$ depend strongly on whether the red sequence continues to grow through mergers and the addition of recently quenched blue cloud galaxies. In a model with no mergers occuring after $z = 1$, the galaxies on the red sequence fade passively, with no change in number density. This results in dramatic evolution in luminosity at a fixed space density, and large changes in colour and magnitude at a fixed mass. The evolution of the population is slowed down by dry mergers occurring after $z = 1$. The amount of evolution is reduced even further by adding galaxies that have their star formation quenched through major wet mergers after $z = 1$ to the red sequence. This addition of younger populations onto the red sequence at recent times moves the red sequence slightly blueward, bringing it into good agreement with the observed CMR. In a model where both dry merging and star formation quenching continue to recent times, the changes in colour and magnitude at a fixed mass are similar to the changes for an old single-burst population that formed at high redshift ($z_f \sim 3 - 5$). Early-type galaxies can appear to have evolved passively even though significant merging activity continues to occur to recent times. It is therefore not necessary to invoke an anti-hierarchical account of early-type galaxy formation.

6.1 Future outlook

The work presented in this thesis resolves two difficulties for the standard hierarchical model of galaxy formation, but naturally raises many more questions. There are a number of directions in which further exploration would be useful and necessary.

Future work on calibrating the timescales for the different methods of identifying mergers

using numerical simulations (see e.g., Lotz et al. 2008b) will improve both the observed and model estimates of the merger fraction. The SAM can be used to better understand the relation between the fraction of galaxies of a particular mass that will merge (a subset of the observed close pair fraction) and the remnant population of higher mass (observed as morphologically disturbed galaxies). This may help to resolve the difference in evolution found using the two methods.

The halo occupation distribution (HOD) framework can be used to overcome the dependence of the merging model presented in Chapter 5 on the details of mass function evolution in the SAM. In HOD models, dark matter halos are populated with galaxies such that the clustering, mass, luminosity and colour distributions match the observed distributions at a particular redshift. By creating a galaxy population at $z = 1$ that matches the observed distribution by design, and evolving it to low redshift using similar techniques to those used here, I will be able to directly interpret differences with the observed distributions at low-z in terms of the chosen galaxy merger and star formation histories.

I would also like to devote attention to the observational side of early-type galaxy evolution discussed in the last chapter. The model predictions presented here require observational verification or contradiction. There are two approaches, suggested by Figures 5.6 and 5.7, where further work is required observationally:

- A precise determination of the low-z LF is required to differentiate between different model scenarios. I have done a preliminary investigation into whether the SDSS photometry of bright galaxies can be improved. I find that there are substantial differences between the existing Petrosian, Model and Sersic magnitude estimates for bright nearby galaxies. The use of aperture photometry within a fixed physical radius with a global estimate of the background will substantially reduce the systematic uncertainties at the bright end of the LF. Consistent techniques should be used for a high-z sample, from the DEEP2 survey, for example, to determine the LF evolution.

- As pointed out in the discussion, there are currently few reliable estimates of the change in colour and mass-to-light ratio (M/L) of massive ellipticals from $z \sim 1$ with which to compare. To date, measurements of the change in M/L from the fundamental plane have been made for a handful of high-z clusters (van Dokkum & Franx 1996; Bender et al. 1998; van Dokkum & Stanford 2003; Fritz et al. 2005; Jørgensen et al. 2006). Samples of early-type field galaxies with mass estimates from kinematics or strong lensing are generally small and limited by cosmic variance (van der Wel et al. 2005; di Serego Alighieri et al. 2005; Fritz et al. 2009; van de Ven et al. 2003; Rusin & Kochanek 2005). Treu et al. (2005) found faster evolution in M/L for field galaxies than is observed in clusters, using the largest sample to date, consisting of 226 spheroidal galaxies in the GOODS North field. They found that the evolution depends on stellar mass, with galaxies of $M_\star > 10^{11}\mathrm{M}_\odot$ evolving more slowly than less massive galaxies. Extended star formation periods or a

contribution from young stellar populations are required to account for the observed evolution. Although these results suggest that late quenching does play an important role, as predicted by the model, it will be important to consolidate the existing measurements and quantitatively compare the changes in both colour and M/L with the model predictions. Extending the sample size and redshift range with future spectroscopic observations will further improve our understanding of early-type galaxy evolution.

It will also be interesting to compare the expectations of the model for the field and cluster to observations and interpret the differences in terms of the merger histories. In the model, cluster galaxies can be selected using halo mass as a proxy for environment. A preliminary check indicates that the CMR for clusters is slightly redder and has smaller scatter than the CMR averaged over all environments, even in the "late quenching" model. This suggests that fewer galaxies in clusters have undergone recent quenching and the stellar populations are on average older than the field. This is consistent with the recent results of Roche et al. (2009) using SDSS data at low-z. A comprehensive comparison can be made by producing the model output in the same g- and r-bands as the data.

Another interesting application of the model could be to test the assumption that major wet mergers are instrumental in transforming star forming galaxies into red spheroids. If this accounts for most of the growth of the red sequence, changes in the model luminosity function at $\sim L^*$ should reflect this. Comparing the number densities of blue spheroids and post-starburst galaxies to the number of recently quenched galaxies will also give insight into this process. I would like to determine whether the fraction of disky and boxy early-types on the red sequence can be related to the gas fraction of the most recent merger (see, e.g., Pasquali et al. 2007; Kang et al. 2007), and explore whether age and metallicity scatter in the red sequence are related to the amount of dry merging, an idea proposed by Faber et al. (2007).

Bibliography

Abazajian, K. N., Adelman-McCarthy, J. K., Agüeros, M. A., et al. 2009, ApJS, 182, 543

Abraham, R. G., van den Bergh, S., & Nair, P. 2003, ApJ, 588, 218

Adelman-McCarthy, J. K., Agüeros, M. A., Allam, S. S., et al. 2008, ApJS, 175, 297

Alexander, D. M., Bauer, F. E., Brandt, W. N., et al. 2003, AJ, 126, 539

Allam, S. S., Tucker, D. L., Smith, J. A., et al. 2004, AJ, 127, 1883

Astier, P., Guy, J., Regnault, N., et al. 2006, A&A, 447, 31

Baldry, I. K., Glazebrook, K., Brinkmann, J., et al. 2004, ApJ, 600, 681

Banerji, M., Ferreras, I., Abdalla, F. B., Hewett, P., & Lahav, O. 2009, ArXiv e-prints

Barnes, J. E. & Hernquist, L. 1996, ApJ, 471, 115

Barnes, J. E. & Hernquist, L. E. 1991, ApJL, 370, L65

Baugh, C. M. 2006, Reports on Progress in Physics, 69, 3101

Bekki, K. 2009, MNRAS, 399, 2221

Bekki, K. & Shioya, Y. 1997, ApJL, 478, L17

Bell, E. F., McIntosh, D. H., Katz, N., & Weinberg, M. D. 2003, ApJS, 149, 289

Bell, E. F., Naab, T., McIntosh, D. H., et al. 2006a, ApJ, 640, 241

Bell, E. F., Phleps, S., Somerville, R. S., et al. 2006b, ApJ, 652, 270

Bell, E. F., Wolf, C., Meisenheimer, K., et al. 2004, ApJ, 608, 752

Bell, E. F., Zheng, X. Z., Papovich, C., et al. 2007, ApJ, 663, 834

Bender, R., Saglia, R. P., Ziegler, B., et al. 1998, ApJ, 493, 529

Bennett, C. L., Banday, A. J., Gorski, K. M., et al. 1996, ApJL, 464, L1

Bernardi, M., Hyde, J. B., Sheth, R. K., Miller, C. J., & Nichol, R. C. 2007, AJ, 133, 1741

Bernardi, M., Sheth, R. K., Annis, J., et al. 2003, AJ, 125, 1882

Berrier, J. C., Bullock, J. S., Barton, E. J., et al. 2006, ApJ, 652, 56

Bershady, M. A., Jangren, A., & Conselice, C. J. 2000, AJ, 119, 2645

Binney, J. & Tremaine, S. 1987, Galactic dynamics, ed. J. . T. S. Binney

Blanton, M. R., Hogg, D. W., Bahcall, N. A., et al. 2003, ApJ, 594, 186

Blanton, M. R. & Roweis, S. 2007, AJ, 133, 734

Blanton, M. R., Schlegel, D. J., Strauss, M. A., et al. 2005, AJ, 129, 2562

Bond, J. R., Cole, S., Efstathiou, G., & Kaiser, N. 1991, ApJ, 379, 440

Borch, A., Meisenheimer, K., Bell, E. F., et al. 2006, A&A, 453, 869

Bower, R. G. 1991, MNRAS, 248, 332

Bower, R. G., Benson, A. J., Malbon, R., et al. 2006, MNRAS, 370, 645

Bower, R. G., Kodama, T., & Terlevich, A. 1998, MNRAS, 299, 1193

Bower, R. G., Lucey, J. R., & Ellis, R. S. 1992, MNRAS, 254, 601

Boylan-Kolchin, M., Ma, C.-P., & Quataert, E. 2008, MNRAS, 383, 93

Brown, M. J. I., Dey, A., Jannuzi, B. T., et al. 2007, ApJ, 654, 858

Bruzual, G. & Charlot, S. 2003, MNRAS, 344, 1000

Bullock, J. S., Kolatt, T. S., Sigad, Y., et al. 2001, MNRAS, 321, 559

Bundy, K., Fukugita, M., Ellis, R. S., et al. 2009, ArXiv e-prints

Cassata, P., Cimatti, A., Franceschini, A., et al. 2005, MNRAS, 357, 903

Chabrier, G. 2003, PASP, 115, 763

Chandrasekhar, S. 1943, ApJ, 97, 255

Charlot, S. & Fall, S. M. 2000, ApJ, 539, 718

Cimatti, A., Daddi, E., & Renzini, A. 2006, A&A, 453, L29

Ciotti, L., Lanzoni, B., & Volonteri, M. 2007, ApJ, 658, 65

Conselice, C. J. 2003, ApJS, 147, 1

Conselice, C. J. 2006, ApJ, 638, 686

Conselice, C. J., Bershady, M. A., Dickinson, M., & Papovich, C. 2003, AJ, 126, 1183

Conselice, C. J., Bershady, M. A., & Jangren, A. 2000, ApJ, 529, 886

Conselice, C. J., Rajgor, S., & Myers, R. 2008, MNRAS, 386, 909

Cool, R. J., Eisenstein, D. J., Fan, X., et al. 2008, ApJ, 682, 919

Cowie, L. L., Songaila, A., Hu, E. M., & Cohen, J. G. 1996, AJ, 112, 839

Cox, T. J., Dutta, S. N., Di Matteo, T., et al. 2006, ApJ, 650, 791

Cox, T. J., Jonsson, P., Somerville, R. S., Primack, J. R., & Dekel, A. 2008, MNRAS, 384, 386

Croton, D. J., Springel, V., White, S. D. M., et al. 2006, MNRAS, 365, 11

Davis, M., Faber, S. M., Newman, J., et al. 2003, in Society of Photo-Optical Instrumentation Engineers (SPIE) Conference Series, ed. P. Guhathakurta, Vol. 4834, 161–172

Davis, M. & Peebles, P. J. E. 1983, ApJ, 267, 465

De Propris, R., Conselice, C. J., Liske, J., et al. 2007, ApJ, 666, 212

De Propris, R., Liske, J., Driver, S. P., Allen, P. D., & Cross, N. J. G. 2005, AJ, 130, 1516

Dekel, A., Birnboim, Y., Engel, G., et al. 2009, Nature, 457, 451

Di Matteo, T., Springel, V., & Hernquist, L. 2005, Nature, 433, 604

di Serego Alighieri, S., Vernet, J., Cimatti, A., et al. 2005, A&A, 442, 125

Dreyer, J. L. E. 1888, MEMRAS, 49, 1

Efstathiou, G. 1992, MNRAS, 256, 43P

Eggen, O. J., Lynden-Bell, D., & Sandage, A. R. 1962, ApJ, 136, 748

Eisenstein, D. J., Zehavi, I., Hogg, D. W., et al. 2005, ApJ, 633, 560

Ellis, R. S., Smail, I., Dressler, A., et al. 1997, ApJ, 483, 582

Faber, S. M. 1973, ApJ, 179, 731

Faber, S. M., Willmer, C. N. A., Wolf, C., et al. 2007, ApJ, 665, 265

Ferrarese, L., Côté, P., Jordán, A., et al. 2006, ApJS, 164, 334

Fioc, M. & Rocca-Volmerange, B. 1997, A&A, 326, 950

Fixsen, D. J., Cheng, E. S., Gales, J. M., et al. 1996, ApJ, 473, 576

Fontanot, F., De Lucia, G., Monaco, P., Somerville, R. S., & Santini, P. 2009, MNRAS, 397, 1776

Freedman, W. L., Madore, B. F., Gibson, B. K., et al. 2001, ApJ, 553, 47

Friedman, A. 1922, Zeitschrift fur Physik, 10, 377

Friedman, A. 1924, Zeitschrift fur Physik, 21, 326

Frieman, J. A., Turner, M. S., & Huterer, D. 2008, ARA&A, 46, 385

Fritz, A., Böhm, A., & Ziegler, B. L. 2009, MNRAS, 393, 1467

Fritz, A., Ziegler, B. L., Bower, R. G., Smail, I., & Davies, R. L. 2005, MNRAS, 358, 233

Gallazzi, A., Charlot, S., Brinchmann, J., & White, S. D. M. 2006, MNRAS, 370, 1106

Gallazzi, A., Charlot, S., Brinchmann, J., White, S. D. M., & Tremonti, C. A. 2005, MNRAS, 362, 41

Geller, M. J. & Huchra, J. P. 1989, Science, 246, 897

Gilmore, R. C., Madau, P., Primack, J. R., Somerville, R. S., & Haardt, F. 2009, MNRAS, 1287

Gott, I. J. R., Dickinson, M., & Melott, A. L. 1986, ApJ, 306, 341

Gottlöber, S., Klypin, A., , & Kravtsov, A. V. 2001, ApJ, 546, 223

Governato, F., Gardner, J. P., Stadel, J., et al. 1999, AJ, 117, 1651

Graham, A. W., Driver, S. P., Petrosian, V., et al. 2005, AJ, 130, 1535

Gunn, J. E. 1978, in Saas-Fee Advanced Course 8: Observational Cosmology Advanced Course, ed. A. Maeder, L. Martinet, & G. Tammann

Gunn, J. E. & Gott, J. R. I. 1972, ApJ, 176

Guo, Q. & White, S. D. M. 2008, MNRAS, 384, 2

Hao, C. N., Mao, S., Deng, Z. G., Xia, X. Y., & Wu, H. 2006, MNRAS, 370, 1339

Häring, N. & Rix, H. 2004, ApJL, 604, L89

Harker, J. J., Schiavon, R. P., Weiner, B. J., & Faber, S. M. 2006, ApJL, 647, L103

Herschel, J. F. W. 1864, Royal Society of London Philosophical Transactions Series I, 154, 1

Heymans, C., Bell, E. F., Rix, H., et al. 2006, MNRAS, 371, L60

Holmberg, E. 1940, ApJ, 92, 200

Holmberg, E. 1941, ApJ, 94, 385

Hopkins, A. M. 2004, ApJ, 615, 209

Hopkins, P. F., Hernquist, L., Cox, T. J., et al. 2005, ApJ, 630, 705

Hopkins, P. F., Hernquist, L., Cox, T. J., et al. 2006a, ApJS, 163, 1

Hopkins, P. F., Hernquist, L., Cox, T. J., & Kereš, D. 2008, ApJS, 175, 356

Hopkins, P. F., Hernquist, L., Cox, T. J., Robertson, B., & Springel, V. 2006b, ApJS, 163, 50

Hoyle, F. & Tayler, R. J. 1964, Nature, 203, 1108

Hubble, E. 1929, Proceedings of the National Academy of Science, 15, 168

Hubble, E. & Humason, M. L. 1931, ApJ, 74, 43

Hubble, E. P. 1925, The Observatory, 48, 139

Jarrett, T. 2004, Publications of the Astronomical Society of Australia, 21, 396

Jogee, S. 2006, in Lecture Notes in Physics, Berlin Springer Verlag, Vol. 693, Physics of Active Galactic Nuclei at all Scales, ed. D. Alloin, 143

Jogee, S., Miller, S. H., Penner, K., et al. 2009, ApJ, 697, 1971

Jørgensen, I., Chiboucas, K., Flint, K., et al. 2006, ApJL, 639, L9

Kang, X., van den Bosch, F. C., & Pasquali, A. 2007, MNRAS, 381, 389

Kartaltepe, J. S., Sanders, D. B., Scoville, N. Z., et al. 2007, ApJS, 172, 320

Kauffmann, G., Heckman, T. M., White, S. D. M., et al. 2003, MNRAS, 341, 33

Kauffmann, G. & White, S. D. M. 1993, MNRAS, 261, 921

Kauffmann, G., White, S. D. M., & Guiderdoni, B. 1993, MNRAS, 264, 201

Khochfar, S. & Burkert, A. 2003, ApJL, 597, L117

Khochfar, S. & Silk, J. 2006, MNRAS, 370, 902

Kimm, T., Somerville, R. S., Yi, S. K., et al. 2009, MNRAS, 394, 1131

Kitzbichler, M. G. & White, S. D. M. 2008, MNRAS, 391, 1489

Kodama, T. & Arimoto, N. 1997, A&A, 320, 41

Komatsu, E., Dunkley, J., Nolta, M. R., et al. 2009, ApJS, 180, 330

Kormendy, J., Fisher, D. B., Cornell, M. E., & Bender, R. 2009, ApJS, 182, 216

Kormendy, J. & Richstone, D. 1995, ARA&A, 33, 581

Kriek, M., van Dokkum, P. G., Franx, M., et al. 2006, ApJL, 649, L71

Kroupa, P., Tout, C. A., & Gilmore, G. 1993, MNRAS, 262, 545

Lacey, C. & Cole, S. 1993, MNRAS, 262, 627

Larson, R. B. 1974, MNRAS, 169, 229

Larson, R. B. 1975, MNRAS, 173, 671

Lauer, T. R., Faber, S. M., Richstone, D., et al. 2007, ApJ, 662, 808

Le Fèvre, O., Abraham, R., Lilly, S. J., et al. 2000, MNRAS, 311, 565

Le Floc'h, E., Papovich, C., Dole, H., et al. 2005, ApJ, 632, 169

Lehmer, B. D., Brandt, W. N., Alexander, D. M., et al. 2005, ApJS, 161, 21

Lemaître, G. 1927, Annales de la Societe Scietifique de Bruxelles, 47, 49

Li, C., Kauffmann, G., Heckman, T. M., Jing, Y. P., & White, S. D. M. 2008, MNRAS, 385, 1903

Li, C., Kauffmann, G., Jing, Y. P., et al. 2006, MNRAS, 368, 21

Lilly, S. J., Le Fèvre, O., Hammer, F., & Crampton, D. 1996, ApJL, 460, L1

Lin, L., Koo, D. C., Willmer, C. N. A., et al. 2004, ApJL, 617, L9

Lin, L., Patton, D. R., Koo, D. C., et al. 2008, ApJ, 681, 232

Longair, M. S. 1998, Galaxy formation, Astronomy and Astrophysics library (Springer-Verlag Berlin Heidelberg)

Lotz, J. M., Davis, M., Faber, S. M., et al. 2008a, ApJ, 672, 177

Lotz, J. M., Jonsson, P., Cox, T. J., & Primack, J. R. 2008b, MNRAS, 391, 1137

Lotz, J. M., Primack, J., & Madau, P. 2004, AJ, 128, 163

Macciò, A. V., Kang, X., & Moore, B. 2009, ApJL, 692, L109

Madau, P., Ferguson, H. C., Dickinson, M. E., et al. 1996, MNRAS, 283, 1388

Madgwick, D. S., Lahav, O., Baldry, I. K., et al. 2002, MNRAS, 333, 133

Maller, A. H., Katz, N., Kereš, D., Davé, R., & Weinberg, D. H. 2006, ApJ, 647, 763

Marconi, A. & Hunt, L. K. 2003, ApJL, 589, L21

Masjedi, M., Hogg, D. W., Cool, R. J., et al. 2006, ApJ, 644, 54

Mather, J. C., Cheng, E. S., Eplee, J. R. E., et al. 1990, ApJL, 354, L37

McGrath, E. J., Stockton, A., & Canalizo, G. 2007, ApJ, 669, 241

McIntosh, D. H., Bell, E. F., Rix, H.-W., et al. 2005, ApJ, 632, 191

McIntosh, D. H., Guo, Y., Hertzberg, J., et al. 2008, MNRAS, 388, 1537

Merritt, D. 1987, ApJ, 313, 121

Metcalfe, N., Godwin, J. G., & Peach, J. V. 1994, MNRAS, 267, 431

Mihos, J. C. & Hernquist, L. 1994, ApJL, 425, L13

Mihos, J. C. & Hernquist, L. 1996, ApJ, 464, 641

Moster, B. P., Somerville, R. S., Maulbetsch, C., et al. 2009, ArXiv e-prints

Naab, T. & Burkert, A. 2001, ApJL, 555, L91

Naab, T. & Burkert, A. 2003, ApJ, 597, 893

Naab, T., Burkert, A., & Hernquist, L. 1999, ApJL, 523, L133

Naab, T., Jesseit, R., & Burkert, A. 2006, MNRAS, 372, 839

Navarro, J. F., Frenk, C. S., & White, S. D. M. 1997, ApJ, 490, 493

Negroponte, J. & White, S. D. M. 1983, MNRAS, 205, 1009

Nipoti, C., Londrillo, P., & Ciotti, L. 2003, MNRAS, 342, 501

Panter, B., Jimenez, R., Heavens, A. F., & Charlot, S. 2007, MNRAS, 378, 1550

Papovich, C., Dole, H., Egami, E., et al. 2004, ApJS, 154, 70

Pasquali, A., van den Bosch, F. C., & Rix, H. 2007, ApJ, 664, 738

Patton, D. R. & Atfield, J. E. 2008, ApJ, 685, 235

Patton, D. R., Carlberg, R. G., Marzke, R. O., et al. 2000, ApJ, 536, 153

Patton, D. R., Pritchet, C. J., Carlberg, R. G., et al. 2002, ApJ, 565, 208

Peebles, P. J. E. 1969, ApJ, 155, 393

Penzias, A. A. & Wilson, R. W. 1965, ApJ, 142, 419

Percival, W. J., Cole, S., Eisenstein, D. J., et al. 2007, MNRAS, 381, 1053

Perlmutter, S., Aldering, G., Goldhaber, G., et al. 1999, ApJ, 517, 565

Press, W. H. & Schechter, P. 1974, ApJ, 187, 425

Rieke, G. H., Young, E. T., Engelbracht, C. W., et al. 2004, ApJS, 154, 25

Riess, A. G., Filippenko, A. V., Challis, P., et al. 1998, AJ, 116, 1009

Riess, A. G., Strolger, L.-G., Casertano, S., et al. 2007, ApJ, 659, 98

Rix, H.-W., Barden, M., Beckwith, S. V. W., et al. 2004, ApJS, 152, 163

Robaina, A. R., Bell, E. F., Skelton, R. E., et al. 2009a, ApJ, 704, 324

Robaina, A. R., Bell, E. F., van der Wel, et al. 2009b, ApJ submitted

Robertson, B., Cox, T. J., L.Hernquist, et al. 2006, ApJ, 641, 21

Roche, N., Bernardi, M., & Hyde, J. 2009, ArXiv e-prints

Ruhland, C., Bell, E. F., Häußler, B., et al. 2009, ApJ, 695, 1058

Rusin, D. & Kochanek, C. S. 2005, ApJ, 623, 666

Scarlata, C., Carollo, C. M., Lilly, S. J., et al. 2007, ApJS, 172, 494

Schawinski, K., Khochfar, S., Kaviraj, S., et al. 2006, Nature, 442, 888

Schechter, P. 1976, ApJ, 203, 297

Schlegel, D. J., Finkbeiner, D. P., & Davis, M. 1998, ApJ, 500, 525

Schweizer, F. & Seitzer, P. 1992, AJ, 104, 1039

Scoville, N., Abraham, R. G., Aussel, H., et al. 2007, ApJS, 172, 38

Sheth, R. K. & Tormen, G. 1999, MNRAS, 308, 119

Shimasaku, K., Fukugita, M., Doi, M., et al. 2001, AJ, 122, 1238

Skelton, R. E., Bell, E. F., & Somerville, R. S. 2009, ApJL, 699, L9

Skibba, R., Sheth, R. K., Connolly, A. J., & Scranton, R. 2006, MNRAS, 369, 68

Smoot, G. F., Bennett, C. L., Kogut, A., et al. 1992, ApJL, 396, L1

Somerville, R. S. 2002, ApJL, 572, L23

Somerville, R. S., Hopkins, P. F., Cox, T. J., Robertson, B. E., & Hernquist, L. 2008, MNRAS, 391, 481

Somerville, R. S. & Kolatt, T. S. 1999, MNRAS, 305, 1

Somerville, R. S. & Primack, J. R. 1999, MNRAS, 310, 1087

Somerville, R. S., Primack, J. R., & Faber, S. M. 2001, MNRAS, 320, 504

Springel, V., Di Matteo, T., & Hernquist, L. 2005a, MNRAS, 361, 776

Springel, V., White, S. D. M., Jenkins, A., et al. 2005b, Nature, 435, 629

Strateva, I., Ivezić, Ž., Knapp, G. R., et al. 2001, AJ, 122, 1861

Tal, T., van Dokkum, P. G., Nelan, J., & Bezanson, R. 2009, AJ, 138, 1417

Terlevich, A. I., Caldwell, N., & Bower, R. G. 2001, MNRAS, 326, 1547

Tinsley, B. M. 1968, ApJ, 151, 547

Toomre, A. 1977, in Evolution of Galaxies and Stellar Populations, ed. B. M. Tinsley & R. B. Larson, 401

Toomre, A. & Toomre, J. 1972, ApJ, 178, 623

Treu, T., Ellis, R. S., Liao, T. X., et al. 2005, ApJ, 633, 174

van de Ven, G., van Dokkum, P. G., & Franx, M. 2003, MNRAS, 344, 924

van der Wel, A., Franx, M., van Dokkum, P. G., et al. 2005, ApJ, 631, 145

van der Wel, A., Holden, B. P., Zirm, A. W., et al. 2008, ApJ, 688, 48

van der Wel, A., Rix, H., Holden, B. P., Bell, E. F., & Robaina, A. R. 2009, ApJL, 706, L120

van Dokkum, P. G. 2005, AJ, 130, 2647

van Dokkum, P. G. 2008, ApJ, 674, 29

van Dokkum, P. G. & Franx, M. 1996, MNRAS, 281, 985

van Dokkum, P. G. & Franx, M. 2001, ApJ, 553, 90

van Dokkum, P. G. & Stanford, S. A. 2003, ApJ, 585, 78

van Dokkum, P. G. & van der Marel, R. P. 2007, ApJ, 655, 30

Wake, D. A., Nichol, R. C., Eisenstein, D. J., et al. 2006, MNRAS, 372, 537

Weinmann, S. M., van den Bosch, F. C., Yang, X., et al. 2006, MNRAS, 372, 1161

White, S. D. M. 1978, MNRAS, 184, 185

Wolf, C., Meisenheimer, K., Kleinheinrich, M., et al. 2004, A&A, 421, 913

Wolf, C., Meisenheimer, K., Rix, H.-W., et al. 2003, A&A, 401, 73

Xu, C. K., Sun, Y. C., & He, X. T. 2004, ApJL, 603, L73

York, D. G., Adelman, J., Anderson, J. J. E., et al. 2000, AJ, 120, 1579

Zibetti, S., White, S. D. M., Schneider, D. P., & Brinkmann, J. 2005, MNRAS, 358, 949

Acknowledgements

My heartfelt thanks go to my supervisor, Eric Bell. His expertise, creativity, enthusiasm and love of Astronomy make learning from him and working with him a very valuable and enjoyable experience. I really appreciate his constant support and guidance. I'd also like to thank Hans-Walter Rix for his support and his advice as a member of my thesis committee, for refereeing this thesis and being on the examination committee. I am grateful to Rachel Somerville for generously providing me with her model output and allowing me to use aspects of her model throughout this thesis, as well as giving helpful comments. Thanks too, to Ralf Klessen, the third member of my thesis committee. I also appreciate Arjen van der Wel's willingness to help wherever he could, and many useful conversations with my officemate and colleague, Aday Robaina. I appreciate Christine Ruhland's company and patience during a very work-intense visit to Michigan, and Eric and his family's hospitality in hosting us. Warm thanks to Christian Fendt for all his help and support all the way through.

I am incredibly grateful to my parents for their constant support in all my career decisions, interest in what I do and faith in my abilities, which played a huge role in getting me this far. To them and to my sisters, for all their love, generosity and innumerable other things - thank you!

A huge thanks to Chris for his love and support. I really appreciate your patience and care, the advice and help you gave me along the way, your company on many (many) long days and nights of work over the last few months, and all the time we've shared.

Heidelberg would not have been the same without my dearest friends, Cassie, Marcello and Surhud. Thanks for giving me an "office away from the office", sharing so many experiences and tea breaks, all the laughter and fun. Thanks to Surhud for fixing up my computer at a crucial time and always being willing to help, whether it be with Theoretical Astrophysics homework, back at the beginning, a spontaneous MCMC class or watering my plants. Marcello, I value your friendship very highly and have appreciated your support and advice many times over the last three years. Cassie, you have been a spark of light. I love your fun approach and joy in life. You and Thomas helped me settle into Heidelberg and have given me many unforgettable experiences since then. Thanks for all the pancakes, döners and concerts and for welcoming me to join you on numerous adventures, near and far. I wish the best for you all and hope you'll visit me in South Africa one of these days!

I am very glad to have become friends with Giovanna, Bagmeet and Swapna, Anu and Lisa, Giulia and Claudia, Ramin, Kris, Kelly and many other wonderful people during my time

in Heidelberg. Thanks too, to Martin, for sharing the role of student representative with me, greatly broadening my involvement in institute life. Thanks to the student representatives of all the generations I overlapped with. I am very happy to have been a part of the International Max Planck Research School (IMPRS) and really enjoyed getting to know all the IMPRS and MPIA students over the years.